Understanding the Pleckstrin Homology (PH) Domain Peculiar Mechanism in Akt Translocation, Phosphorylation, and Activation

by

Jackson Weako

A Dissertation Submitted to the Graduate School of Sciences and Engineering in Partial Fulfillment of the Requirements for the Degree of

Doctor of Philosophy

in

Computational Science and Engineering

KOÇ ÜNİVERSİTESİ

December 23, 2021

Understanding the Pleckstrin Homology (PH) Domain Peculiar Mechanism in Akt Translocation, Phosphorylation, and Activation.

Koç University

Graduate School of Sciences and Engineering

This is to certify that I have examined this copy of a doctoral dissertation by

Jackson Weako

and have found that it is complete and satisfactory in all respects, and that any, and all revisions required by the final examining committee have been made.

Committee Members:

_____

Prof. Ozlem K. Ozkaya (Advisor)

_____

Prof. Attila Gürsoy [Co-Advisor]

_____

Prof. E. Demet Akten Akdoğan

_____

Assoc. Prof. I. Halil Kavakli

_____

Assoc. Prof. Mehmet Sayar

_____

Dr. Ruth Nussinov

Date: _____

To my parents: Mr. Moses K. Weako & Mrs. Quita A. Tokpah
Thank you for the enormous supports and unwavering love.

ABSTRACT

The protein kinase B (PKB, also designated Akt), is unarguably a crucial player in cell proliferation, survival, metabolism, angiogenesis, and apoptosis. Akt plays a pivotal role in the Ras-PI3K-Akt-mTOR signaling pathway. Akt recruitment to the plasma membrane is enabled by its Pleckstrin homology (PH) domain, which interacts with signaling membrane lipid, PIP_3, or PIP_2. The interplay between the PH domain and PIP_3 results in conformational changes that facilitate phosphorylations of Thr308 in the kinase domain, and Ser473 in the C-terminal regulatory domain by PDK1 and mTORC2 complex, respectively. Enormous Akt activation mechanisms have been proposed by various studies, which all seem to result in PH domain peculiar role in translocating Akt to the plasma membrane, and to implication of Calmodulin (CaM) intermolecularly interacting with the PH domain in breast cancer as established by previous NMR studies. However, the exact mechanism of how CaM interacts with the PH domain at the atomic level remains unclear. Also, in Akt autoinhibition state or a "PH-in" conformer, the PH domain intramolecularly interact with the kinase domain to prevent phosphorylation of a functional residue in the kinase domain. Several residues in the PH-kinase allosteric interface maintain the PH-kinase domain autoinhibition, and mutations of critical residues in the PH-kinase domain interface have the proclivity to disrupt the interface, resulting in a "PH-out" conformer state. A "PH-out" conformer of Akt is required for the PH domain to interact with membrane lipids, an event critical for Akt activation. Furthermore, phosphorylation of Ser473 in the C-terminal tail that forms electrostatic interaction with Arg 144 in the PH-kinase linker leads to conformational rearrangements in the PH domain activating Akt. However, the structure of full-length Akt autoinhibited state is yet to be crystalized to understand the PH and kinase domain autoinhibition. Here, this dissertation purpose is two-fold: using modeling and molecular dynamics (MD) simulations to figure out how CaM interacts with the PH domain to recruit Akt to the plasma membrane and how the PH domain intramolecularly interact with the kinase domain at the atomic level with emphasis on the interfacial residues that play a crucial role in the PH-kinase domain autoinhibition.

In the dissertation's first part, CaM-PH domain complexes were modeled and subjected to all atoms MD simulations. The simulation results show that CaM-PH domain interactions are thermodynamically stable and involve a **β**-strand, rather than an **α**-helix interaction, both agreeing with the NMR data and that electrostatic and hydrophobic interactions are critical to maintaining CaM-PH complex. The PH domain interacts with CaM lobes; however, multiple modes are possible, and the involvement of IP_4, polar head of PIP_3 attenuates CaM-PH domain interaction, implicating the release mechanism at the plasma membrane. In the second part of the dissertation,

we modeled full-length Akt (480 residues) in the inactive state to explore the intramolecular interaction between the PH and kinase domains and identify crucial interfacial residues that maintain the PH-kinase intact interface. Further, Asp 323, an important interface residue was mutated to His to discern its effect on PH-kinase allosteric interface. The results show that the mutation led to substantial displacement of ATP from the ATP binding pocket in Akt and led to kinase domain adopting a more open conformation. Additionally, the RMSD and RMSF profiles depict that D323H leads to an increase in conformational changes, and we deduce that although the mutation is approximately 21Å away from ATP binding site, perhaps there is an allosteric communication between these two functional sites in Akt. The modeled structures of full-length autoinhibited Akt state are best representations that would guide pharmaceutical chemists to develop Akt allosteric inhibitors, which require an intact PH-kinase interface, and ATP-competitive inhibitors that do not require such intact PH-kinase interface but might rely on intact kinase domain N- and C- lobes interface for their cellular activity. The development of allosteric and ATP-competitive inhibitors is crucial for targeting Akt since it is frequently activated in tumor cells, necessitating its regulation. The dissertation results have functional implications in developing inhibitors that would target CaM-PH domain complex and allosteric and ATP-competitive inhibitors that bind to the PH-kinase domain interface and ATP binding pocket in Akt, respectively. Finally, these results add to the already existing incredible wealth of information on the Akt kinase activation mechanism, which all seem to result from loosening the PH-kinase domain autoinhibition.

ÖZETÇE

Protein kinaz B (PKB, aynı zamanda Akt olarak da adlandırılır), hücre proliferasyonu, hayatta kalma, metabolizma, anjiyogenez ve apoptozda tartışmasız çok önemli bir oyuncudur. Akt, Ras-PI3K-Akt-mTOR sinyal yolunda önemli bir rol oynar. Plazma zarına Akt alımı, sinyal membran lipidi, PIP3 veya PIP2 ile etkileşime giren Pleckstrin homoloji (PH) alanı tarafından sağlanır. PH alanı ve PIP3 arasındaki etkileşim, sırasıyla PDK1 ve mTORC2 kompleksi tarafından kinaz alanındaki Thr308'in ve C-terminal düzenleyici alanındaki Ser473'ün fosforilasyonunu kolaylaştıran konformasyonel değişikliklerle sonuçlanır. Muazzam Akt aktivasyon mekanizmaları, çeşitli çalışmalar tarafından önerilmiştir; bunların tümü, Akt'nin plazma zarına yer değiştirmesinde PH alanına özgü bir rol ile sonuçlanmış gibi görünmektedir ve önceki NMR çalışmaları tarafından belirlendiği gibi, meme kanserinde PH alanı ile Calmodulin'in (CaM) moleküller arası etkileşime girdiğini ima etmektedir. Bununla birlikte, CaM'nin atomik düzeyde PH alanı ile nasıl etkileşime girdiğinin kesin mekanizması belirsizliğini koruyor. Ayrıca, Akt oto-inhibisyon durumunda veya bir "PH-in" konformerinde, PH alanı, kinaz alanındaki bir fonksiyonel kalıntının fosforilasyonunu önlemek için kinaz alanı ile intramoleküler olarak etkileşime girer. PH-kinaz allosterik arayüzündeki birkaç amino asit, PH-kinaz bölgesi oto-inhibisyonunu korur ve PH-kinaz bölgesi arayüzündeki kritik amino asitlerin mutasyonları, arayüzü bozma eğilimine sahiptir ve bu da bir “PH-out” konformer durumu ile sonuçlanır. PH alanının, Akt aktivasyonu için kritik bir olay olan membran lipidleri ile etkileşime girmesi için Akt'nin bir "PH-out" konformeri gereklidir. Ayrıca, PH-kinaz bağlayıcısında Arg 144 ile elektrostatik etkileşim oluşturan C-terminal kuyruğunda Ser 473'ün fosforilasyonu, Akt'yi aktive eden PH alanında konformasyonel yeniden düzenlemelere yol açar. Bununla birlikte, tam uzunluktaki Akt oto-inhibisyon durumunun yapısı, PH ve kinaz domain oto-inhibisyonunu anlamak için henüz kristalleştirilmemiştir. Burada, bu tezin amacı iki yönlüdür: Akt'yi plazma zarına almak için CaM'nin PH alanı ile nasıl etkileşime girdiğini ve PH alanının atomdaki kinaz alanı ile intramoleküler olarak nasıl etkileşime girdiğini PH-kinaz alanı oto-inhibisyonunda çok önemli bir rol oynayan arayüzey kalıntılarına vurgu yaparak anlamak için modelleme ve moleküler dinamik (MD) simülasyonlarını kullanmak. Tezin ilk bölümünde, CaM-PH alan kompleksleri modellenmiş ve tüm atomların MD simülasyonlarına tabi tutulmuştur. Simülasyon sonuçları, CaM-PH alan etkileşimlerinin termodinamik olarak kararlı olduğunu ve bir **α**-sarmal etkileşimi yerine bir **β**-sarmalını içerdiğini, her ikisinin de NMR verileriyle uyumlu olduğunu ve elektrostatik ve hidrofobik etkileşimlerin CaM-PH kompleksini sürdürmek için kritik olduğunu göstermektedir. PH alanı, CaM lobları ile etkileşime girer; bununla birlikte, çoklu modlar mümkündür ve IP4'ün dahil edilmesi, PIP3'ün kutup başı etkileşimini, plazma membranında salıverme mekanizmasını işaret ederek CaM-PH alan etkileşimini azaltır. Tezin ikinci bölümünde, PH ve kinaz alanları arasındaki molekül içi etkileşimi araştırmak ve PH-kinaz bozulmamış arayüzünü koruyan önemli arayüzey tortularını belirlemek için aktif olmayan durumda tam

uzunluktaki Akt'yi (480 tortu) modelledik. Ayrıca, Asp 323, önemli bir arayüz tortusu, PH-kinaz allosterik arayüzü üzerindeki etkisini ayırt etmek için His'e mutasyona uğradı. Sonuçlar, mutasyonun, ATP'nin Akt'deki ATP bağlama cebinden önemli ölçüde yer değiştirmesine yol açtığını ve kinaz alanının daha açık bir konformasyon benimsemesine yol açtığını göstermektedir. Ek olarak, RMSD ve RMSF profilleri, D323H'nin konformasyonel değişikliklerde bir artışa yol açtığını gösterir ve mutasyonun ATP bağlanma bölgesinden yaklaşık 21Â uzaklıkta olmasına rağmen, Akt'taki bu iki fonksiyonel bölge arasında belki de bir allosterik iletişim olduğu sonucuna varabiliriz. Tam uzunlukta oto-inhibe edilmiş Akt durumunun modellenmiş yapıları, farmasötik kimyagerlere, bozulmamış bir PH-kinaz arayüzü gerektiren Akt allosterik inhibitörleri ve bu tür bozulmamış PH-kinaz arayüzü gerektirmeyen ancak hücresel aktiviteleri için bozulmamış kinaz alanı N- ve C-lobları arayüzü gerektirebilecek ATP-rekabetçi inhibitörleri geliştirmeleri için rehberlik edecek en iyi temsillerdir. Allosterik ve ATP-rekabetçi inhibitörlerin geliştirilmesi, tümör hücrelerinde sıklıkla aktive edildiğinden ve düzenlenmesini gerektirdiğinden Akt'yi hedeflemek için çok önemlidir. Tez sonuçlarının, CaM-PH alan kompleksini ve sırasıyla Akt'ta PH-kinaz alanı arayüzüne ve ATP bağlama cebine bağlanan allosterik ve ATP-rekabetçi inhibitörleri hedefleyecek inhibitörlerin geliştirilmesinde işlevsel etkileri vardır. Son olarak, bu sonuçlar, tümü PH-kinaz alanı oto-inhibisyonunun gevşemesinden kaynaklanmış gibi görünen Akt kinaz aktivasyon mekanizması hakkında halihazırda var olan bilgi zenginliğine katkıda bulunur.

ACKNOWLEDGMENTS

I am thrilled and thankful to my supervisors: Prof. Dr. Z. Özlem Keskin Özkaya and Prof. Dr. Attila Gürsoy, for their guidance, support, and incredible contributions during my dissertation project and graduate studies. It was a special privilege to work with them as a research assistant. Also, I remain grateful to our outstanding collaborators: Dr. Ruth Nussinov, Dr. Hyunbum Jang, Mrs. Tammy Eyler, and Dr. Nussinov's group from the National Institute of Health/National Cancer Institute (NIH/NCI) for their enormous support and technical guidance.

I appreciate my dissertation committee members: Prof. Dr. E Demet A. Akdoğan and Prof. Dr. Halil Kavakli, for offering their feedback, advice, and comments, all of which have been great to make this dissertation a success. Also, I am thankful to my other jury members Dr. Ruth Nussinov, Assoc. Prof. Mehmet Sayer, and Prof. Dr. Attila Gürsoy, for their valuable time.

I want to thank my dear Cosbians: Damla Övek, Kayra Kösoğlu, Emine Sıla Özdemir, Serena Muratcıoğlu, Ayşe Derya Cavga, Ali Tuğrul, Asma Hakouz, Meltem Eda Ömür, Farideh Halakou, Zeynep Abalı, Sukejna Valjevac, Simge Şenyüz, Yunus Emre Köroğlu, Emre Küçük, Ece Tezsezen, Meryem Eren, Erxiati Paerhati, Melisa Ece Zeylan, Fatma Cankara, and Esra Başaran for their unwavering love, words of encouragement, and being by my side during these four challenging years in both social and academic life.

Again, I am grateful to my parents, mentors, friends, and relatives for their never-ending, guidance, patience, financial, and moral supports throughout this worthwhile journey.

I acknowledge the Scientific and Technological Research Council of Turkey (TÜBITAK) for supporting my doctoral program through the 2235–Graduate Scholarship for Least Developed Countries (BIDEB2235).

TABLE OF CONTENTS

LIST OF TABLES

LIST OF FIGURES

ABBREVIATIONS

Å	Ångström
ADP	Adenosine diphosphate
Akt/PKB	Protein Kinase B
A-loop	Activation loop
ATP	Adenosine triphosphate
CaM	Calmodulin
D or Asp	Aspartic acid
FOXO	Forkhead box
GSK3	Glycogen synthase kinase 3
HIF	Hypoxia-inducible factor
IP4	inositol 1,3,4,5-tetrakisphosphate
K or Lys	Lysine
K_d	Dissociation constant
KD	Kinase domain
MD	Molecular Dynamics
Mg^{2+}	Magnesium (ii) ion
mTORC2	Mammalian target of rapamycin complex 2
NMR	Nuclear Magnetic Resonance
PCA	Principal Component Analysis
PDB	Protein Data Bank
PDk1	3-phosphoinositide-dependent kinase 1
PHD	Pleckstrin Homology Domain
PHLPP	PH domain Leucine-rich repeat-containing Protein Phosphatase
PI3K	Phosphatidylinositol-3 kinase
PIP_2	Phosphatidylinositol-4,5-bisphosphate
PIP_3	Phosphatidylinositol-3,4,5-trisphosphate
PM	Plasma membrane
PM	Plasma membrane

PP2A	Phosphoprotein phosphatase 2A

PP2A	Phosphoprotein phosphate 2A
PTM	Post-translational modification
RTK	Receptor tyrosine kinase
Ser or S	Serine
Thr or T	Threonine
VL	Variable loop
WT	Wild type
ϒ	gamma
α	Alpha
β	Beta

Chapter 1

INTRODUCTION

The protein kinase B, PKB (also designated as Akt), is a Ser/Thr protein kinase that unarguably regulates a myriad of cellular processes such as cell survival, proliferation, apoptosis, metabolic regulation, and oncogenes[1]. Akt plays a crucial role in the PI3K-Akt-mTOR pathway, and it belongs to the AGC subfamily of protein kinases. The AGC family of kinases (designated after protein kinase A, protein kinase G, and protein kinase C) contains about sixty enzymes grouped into sixteen subfamilies[2]. Akt subfamily consists of three conserved mammalian isoforms, Akt1, Akt2, and Akt3 (traditionally known as PKBα, PKBβ, and PKBΥ respectively). Interestingly, these Akt's isoforms are transcribed from distinct genes and possess a conserved structural architecture, which includes an amino-terminal Pleckstrin homology (PH) domain, a centrally positioned kinase domain, PH domain-Kinase domain linker, and C-terminal regulatory domain[3, 4]. Akt1 (focused on herein and hereafter referred to as Akt) remains the most studied of these isoforms[1]. Structurally, the lipid binding PH domain of Akt consists of a C-terminal helix, seven antiparallel beta-sheet, and three distinct loops, and a binding site for PIP_3 or PIP_2. In the context of a function, the PH domain performs two essential functions: binding phospholipids and other proteins that drive Akt recruitment to the membrane (Akt membrane localization), and intramolecularly binding to the kinase domain that triggers Akt inactivation[5]. The later function of the PH domain creates an intricate balance in Akt enzymatic regulation; that is, the PH domain locks the kinase domain in an inactive conformation, whereas the Kinase domain disrupts the lipid-binding site of the PH domain[6, 7].

On the other hand, the kinase domain comprises a smaller C-terminal lobe, a larger C-terminal lobe, and a deep cleft that lies between these two lobes. The deep cleft between the N-and C-lobes of the kinase domain, which is located beneath the highly conserved G-loop (glycine-rich nucleotide positioning motif), accommodates adenosine triphosphate, ATP. Furthermore, the C-terminal regulatory domain of Akt contains a hydrophobic motif (HM) phosphorylation site [FxxF(S/T) Y], where x is any amino

acid[8].

Akt is activated indirectly by insulin and other growth factors stimulation of PI3K that directly converts phosphatidylinositol-4,5-diphosphate (PIP_2), a membrane-embedded substrate to phosphatidylinositol 3,4,5-triphosphate (PIP_3)[9, 10]. PIP_3 production at the plasma membrane drives Akt activation; PIP_3 interacts with the PH domain to recruit Akt to the plasma membrane[11, 12]. In the context of Akt activation, the intramolecular interaction between the lipid-binding PH domain and kinase domain, a "PH-in" conformer, hinders Thr308 phosphorylation in the action loop. When the PH domain interacts with the produced PIP_3, it drives a conformational change in Akt, "PH-out" conformer, which releases the domain-domain autoinhibition[13]. At the plasma membrane, Akt "PH-out" conformational state enables Thr308 phosphorylation by 3-phosphoinositide-dependent protein kinase 1 (PDK1)[6]. Thr308 phosphorylation by PDK1 along with phosphorylation of Ser473 in the carboxy-terminus regulatory domain by mammalian target of rapamycin complex 2 (mTORC2) fully activates Akt [14, 15]. The subsequent dephosphorylations of these residues, Thr308 and Ser473, are carried out by Protein Phosphatase 2A (PP2A) and PH domain Leucine-rich repeat-containing Protein Phosphatase (PHLPP), respectively[4].

A quantum leap of studies on Akt1 has revealed an incredible tapestry of Akt activation mechanisms, all of which seem to emphasize on the loosening of PH-kinase domains autoinhibition and the versatility of the PH domain. For instance, phosphatidylserine (PS) has been implicated in regulating Akt recruitment to the plasma membrane by interacting with key residues in the PH and regulatory domains. PS cooperativity with PIP_3 drives Akt interdomain-conformational changes that lead to phosphorylation of Thr308 in the A-loop of the kinase domain and Ser473 in the hydrophobic motif[16]. Also, mutational studies on key residues in the PH domain that weaken the interplay between the PH and kinase domains lead to constitutive activation of Akt that results in human diseases[17]. As stated early on, the lipid-binding PH domain is versatile and tends to participate in protein-protein interaction. For example, a recent study showed that calmodulin (CaM) interacts with the PH domain to facilitate Akt translocation to the plasma membrane, enabling Akt membrane anchoring, phosphorylation, and

activation[18, 19]. Along a similar line, we recently established via computation that the interaction between CaM and PH domain is thermodynamically stable and is attenuated by the interference of IP4, the polar head of PIP3[20].

Furthermore, the physical association of PDK1 with Akt was proposed to be necessary and sufficient for Akt phosphorylation at Thr308 independent of plasma membrane localization and PI3-kinase[21]. Expressed protein ligation (EPL) studies have shown that Akt activation is driven by C-terminal phosphorylation of Ser 473 in the HM motif[14]. Like other kinases, Akt utilizes ATP to phosphorylate its substrates by transferring the ϒ-phosphate group of ATPs. Recent studies have uncovered that ATP occupancy in the ATP-binding cavity of Akt prevents pThr308 dephosphorylation by PP2A, while ADP occupancy in the ATP-binding cleft does not protect the pThr308 level. pThr308 level protection by ATP suggests a unique allosteric communication between pThr308 in the catalytic cleft of the kinase domain and ATP since ATP is not close to pThr308 in three-dimensional space[8]. Another striking mechanism has revealed that Akt can be activated by ubiquitination[22]. A previous study has revealed that E3 ubiquitin ligase can ubiquitinate Akt kinase. Although in some situations, ubiquitination of Akt may signal its degradation, it has been shown that certain ubiquitination promotes Akt activation. As was reported by Yang et al.[22], Akt ubiquitination by E3 ligase TRAF6 on the PH domain drives Akt recruitment to the plasma membrane. It leads to subsequent phosphorylation of residues Thr308 in the kinase domain and Ser 473 in the HM domain, thus activating Akt. If true, this mechanism simply suggests that such ubiquitination has the propensity to loosen the PH-kinase domains interface or disrupt PH-kinase intramolecular interaction to relieve the autoinhibition. The PH-kinase linker in Akt has been mapped to several post-translational modifications (PTMs) such as Cys oxidation in Akt2 isoform[23], Lys methylation[24, 25], and Pro hydroxylation[26], which dephosphorylates Akt1. Collectively, these studies suggest that synergies between membrane lipids and PH domain, the intramolecular interplay between the PH domain and the Kinase domain; intermolecular association between CaM and the PH domain, physical association of PDK1 with Akt, and ubiquitination on PH domain by E3 ligase are perhaps required for Akt recruitment, phosphorylation, and activation, respectively. Taken in total, these

previous studies have proposed several different mechanisms of Akt translocation, phosphorylation, and activation. However, from the embers of proposed mechanisms, a common feature is that all allude to disrupting the "PH-in" conformer or loosening the PH-kinase domain allosteric interface to relieve the autoinhibition. Therefore, while the actual mechanism of Akt translocation, phosphorylation, activation remains obscure or a matter of debate, it comes unsurprisingly that the role of the PH domain in Akt activation is incredibly profound.

Previously, the association between the PH domain and the dumbbell shape molecule, CaM, has been established by Nuclear Magnetic Resonance (NMR) studies[18, 27]. However, the exact mechanism of the interplay between CaM and Akt PH domain at atomic level has not been established. In this dissertation, we predicted CaM-PH domain complexes using available crystal structures (1CCL and 1H10) with Interactive Rosetta[28] and investigated the underlying mechanism of how CaM interacts with the PH domain at atomic level. These findings established via computation then suggested how the mechanism can help to elucidate the crucial question of how CaM interacts with the PH domain at the atomic level and how the interference of IP_4, the polar head of PIP_3 can attenuate CaM-PH domain complex. Elsewhere, molecular modeling studies based on homology modeling using the crystal structure of Akt2 have attempted to uncover the nature of the domain-domain intramolecular interaction of Akt1[6, 7]. Still, these molecular modeling studies have some caveats, such as simulation time, six nanoseconds, and homology modeling based on Akt2 crystal structure. Although the validity of these studies cannot be questioned, but the result should be handled meticulously. Additionally, using only the kinase domain of Akt, the role of ATP protection of pThr308 was established in the absence of the PH domain[8, 29]. Of note, these computational studies have utilized crystal structure of only Akt kinase domain or PH domain, but not full-length Akt that comprise the kinase domain, PH domain, the PH-kinase linker, and the regulatory domain probably because of the unavailability of the full-length crystals structure at the time the studies were undertaken. Also, recently, crystal structures of full-length Akt have been deposited in the PDB. Still, these structures lack the linker between the PH domain and the kinase domain, and the C-terminal regulatory domain. However, these findings imply that implying the exact

mechanism of PH-kinase domain autoinhibition in full-length Akt has not been fully established at the atomic level. Here, for the first time we modeled full-length Akt using the existing crystal structures (PDB ID: 4EJN)[30] and (PDB ID: 6S9W)[31] with I-TASSER program[32, 33] and performed molecular dynamics (MD) simulation to elucidate the conformational changes of the domain-domain interaction that relieve the PH-kinase domain autoinhibition. The apostate, nucleotide-bound states (ATP-bound, ADP-bound,) and the mutant structures of full-length Akt were generated and subjected to MD simulations to uncover the domain-domain interactions at the atomic level.

Chapter 2 of the dissertation provides a descriptive, analytical, and comprehensive review of Akt kinase and the protein kinase A, protein kinase G, and protein kinase C (collectively known as the AGC protein kinases). Chapter 3 gives detailed information on the methodology – material, and methods used in this dissertation to achieve the intended objectives. In chapter 4, computational results of the interplay between CaM and the PH domain and the effect of the presence of IP_4 are presented and discussed in detail. Chapter 5 encapsulates the full-length Akt autoinhibition and conformational dynamics and further explains the autoinhibitory interplay between the lipid-binding PH domain and the kinase domain, identifies critical interface residues, role of the PH-kinase linker, and the C-terminal tail, and mutational effect on residues in PH-kinase allosteric interface. Finally, chapter 6 provides the conclusion and future direction, such as therapeutics development of Akt allosteric and ATP-competitive inhibitors to regulate frequent Akt activation in tumor cells.

Chapter 2

Literature Review

2.1 Historicity and background biology of the AGC protein kinases

The uncovering of the Ser/Thr protein kinase B (Akt subfamily of protein kinases) points to earlier experimental studies over decades ago, which involves the discovery of v-akt, an oncogene of the AKT8 transforming retrovirus[34]. Akt is well-conserved from primitive metazoans to humans, and it belongs to the AGC subfamily of protein kinases. The AGC subfamily of protein kinases named after protein kinase A, protein kinase G, and protein kinase C comprises over 518 members in humans[35]. The AGC family of kinases contains about sixty enzymes that are grouped into sixteen subfamilies[36]. The protein kinase A, also designated as the cyclic AMP-dependent protein kinase, is the most extensively studied of these AGC kinases. It serves as the paradigm to understanding the AGC kinases. Most AGC kinases members such as protein kinase A, protein kinase C, Akt1, Akt2, Akt3, PDK1, GRK, SGK, LAST1/2 are major hallmarks in cell signaling, permitting cells to respond to extracellular stimuli[36]. Of not with emphasis, the dysregulation of the AGC protein kinases is linked to several clinical conditions or abnormalities such as inflammation, neurologic diseases, cardiovascular disease, and cancer [37]. There are ongoing efforts to develop inhibitors to target these enzymes[38].

2.2 PI3K/Akt/mTOR signaling pathway.

The PI3K/Akt/mTOR signaling pathway is one of the most studied pathways in cancer biology. The protein kinase B (Akt) was propelled into this signal transduction pathway after it was found that Akt activation eventuates downstream of phosphoinositide 3-kinase (PI3K) – a lipid kinase associated with insulin response and cellular transformation[39]. At the plasma membrane, extracellular signals mediate physiological effects through G-protein-coupled receptors (GPCR) or receptors tyrosine kinase (RTK) to activate PI3K, which converts PIP_2 to PIP_3[40, 41]. In the absence of ligands mediated signals at the plasma membrane, Akt is localized primarily in the nucleus and cytosol. The production of PIP_3, a plasma membrane lipid, triggers Akt translocation to the plasma membrane by

interacting with the PH domain of Akt [42]. The PI3K/Akt/mTOR is tightly maintained by the phosphatase and tensin homolog (PTEN)[43] – a tumor suppressor phosphatase that opposes the action of PI3K. PTEN dephosphorylates PIP_3 to PIP_2, thereby acting as a negative modulator of PI3K[44, 45]. In cancerous cells, a mutation or the loss of PTEN expression is not uncommon – frequently observed events[46]. The dysregulation of the PI3K/Akt/mTOR signaling pathway plays a critical role in disease progression –especially so in cancers with poor prognoses[47, 48]. Of principal importance, cancers cells acquire mutations that often lead to constitutive activation of PI3K/Akt/mTOR pathway [49]. In this pathway, Akt is a central node with a pleiotropic effect on enormous cellular processes, playing a cardinal role in tumorigenesis when hyperactivated [48, 50]. Over one hundred Akt substrates have been identified, three of which are direct downstream substrates: glycogen synthase kinase (GSK), Forkhead box protein O1 (FoXO1), and the TSC1/TSC2 (hamartin-tuberin) complex are responsible for cell survival and death[51-53], growth and proliferation[54, 55], angiogenesis[56, 57], and glucose and glycogen metabolism[58-60].

Cell proliferation and survival – in the context of signaling, FoXO family of transcription factor proteins can efficiently respond to insulin or insulin-like growth factor (IGF) signaling within the cell[61]. When Akt is activated via insulin-like growth factor (IGF) signaling, it phosphorylates key-conserved residues on FoxO1: Thr 24, Ser256, and Ser319 at the amino-terminus, the nuclear localization sequence, and near the nuclear export sequence, respectively[62]. These phosphorylation events of FoxO1 are vital because they create motifs that can be recognized by 14-3-3 proteins, which help export FoxO1 from the nucleus to cytosol[63]. Additionally, the inhibition of FoxO1 results in the repression of transcriptional activity, leading to apoptosis, catabolism, autophagy, and cell cycle arrest[1, 64, 65].

Angiogenesis – Akt plays a role in upregulating the translation of hypoxia-inducible factor (HIF) in response to high level of glucose and oxygen in solid tumors[56]. Radiotherapy of tumors leads to the formation of free radicals, that is, HIF1 cumulates in the nucleus, which can be activated in response to reactive oxygen species (ROS)[66]. Structurally, HIF1 is a heterodimer protein that contains α and β-subunit. While the HIF1β-subunit can be activated constitutively and often insensitive to alteration in oxygenation, on the other

hand, the hydroxylation of Pro402 and Pro564 on the HIF1α subunit is said to be oxygen dependent[67]. Also, at normoxic conditions within the cell, it has been established that prolyl hydroxylases can tag HIF1α for ubiquitination and proteolysis[68]. However, in hypoxic conditions, especially so in the cancer cells, HIF1α escapes degradation, and accumulates to dimerize with HIF1β in the nucleus, which activates vascular endothelial growth factor (VEGF) – initiating angiogenesis and inhibiting apoptosis[68, 69].

Lipid synthesis – tumor cells can exhibit high de novo lipids production rates, which are building blocks for biological activities[70]. It has been shown that Akt affects lipids synthesis and degradation that are involved signaling for cell growth and survival, hence aberrant alterations to lipid metabolism leading to oncogenesis[70]. The mechanism of Akt-mediated activation of mammalian target of rapamycin complex 1 (mTORC1) is achieved via disruption of TSC1/TSC2 complex, a tumor suppressor protein. Upon insulin stimulation at the plasma membrane, Akt phosphorylates Ser939 and Thr1462 on TSC2, which triggers its disassociation from TSC1 and degradation to activate mTORC1[71]. Oppositely, mTORC1 also inhibits PI3K – through negative feedback mechanisms[71]. Akt-mediated degradation of TSC2 results in mTORC1 activation[1], and the nuclear transcription factor sterol regulation element-binding protein (SREBP1) activity depends on mTORC1 signaling[72]. In the process, both SREBP1 and ATP citrate lyase are activated, which leads to the induction of cholesterol synthesis, fatty acid synthase, and low-density lipoprotein (LDL)-receptor[73, 74].

Protein synthesis – the eIF4E-binding protein 1 (4EBP1) phosphorylation through the PI3k/Akt signaling pathway depends on activation by mTORC1[75]. Also, the mitogen-activated protein kinase (MAPK), which is supplementary to the PI3K/Akt pathway, regulates eukaryotic translation initiation factor 4E eIF4E), and mTORC1 phosphorylates 4EBP1 relieving its inhibitory binding of eIF4E[76]; eIF4E together with eIF4A and eIF4G forms a subunit of a huge complex, eIF4F. This complex binds to the 5’ cap of mRNA to recruit 40S ribosomal subunit, which initiates mRNA translation or protein synthesis[76-78]. On another high note, phosphorylation of eIf4E at residue, Ser 209, which was previously thought to be at Ser 53, is important for oncogenesis. Malignant transformation due to overexpression of eIF4E was first noticed in NIH/3T3 mouse fibroblast cells in vitro experiments[77] and was later observed in mouse models in vivo[78]. Additionally,

overexpression of eF4E has also been discovered in human tumor cells[76].

Glucose and glycogen metabolism by Akt – over 100 substrates of Akt have been discovered over the decades of study of this congenic protein. The first downstream and well-established substrate of Akt is GSK3[79]. There are two isoforms of GSK3: GSK3**α** and GSK3**β**, which are directly phosphorylated on Ser21 and Ser9 respectively, via insulin mediated Akt activation[60, 80]. Intriguingly, GSK3, in turn, modulates Akt activity by either regulating the PTEN expression[81] or translocating Akt in proximity to phosphatase PP2A[82]. Also, the inhibition of GSK3 has been implicated in regulating glucose uptake and glucose transporter (GLUT) protein expression[83], glycogen, and protein synthesis[79]. In the absence of Akt, GSK3 is implicated in the Wnt- **β**-catenin pathway that modulates gene transcription[84]. AXIN1 and AXIN2, adenomatous polyposis coli, and GSK3 are capable of forming a destructible complex that triggers **β**-catenin destabilization[85]. When Akt is constitutively active in the cell, it has the propensity to increase the rate of glucose metabolism and aerobic glycolysis[86] by activating a hexokinase– a metabolic enzyme. The hexokinase is phosphorylated by Akt, hence simulating phosphofructokinase activity to enhance ATP production[87, 88]. Strikingly, the inactive form of Akt inhibits insulin from transcribing GLUT mRNA, which implies that Akt's role in glucose metabolism is essential[87]. Figure 2.1 shows a simplified Akt signaling pathway.

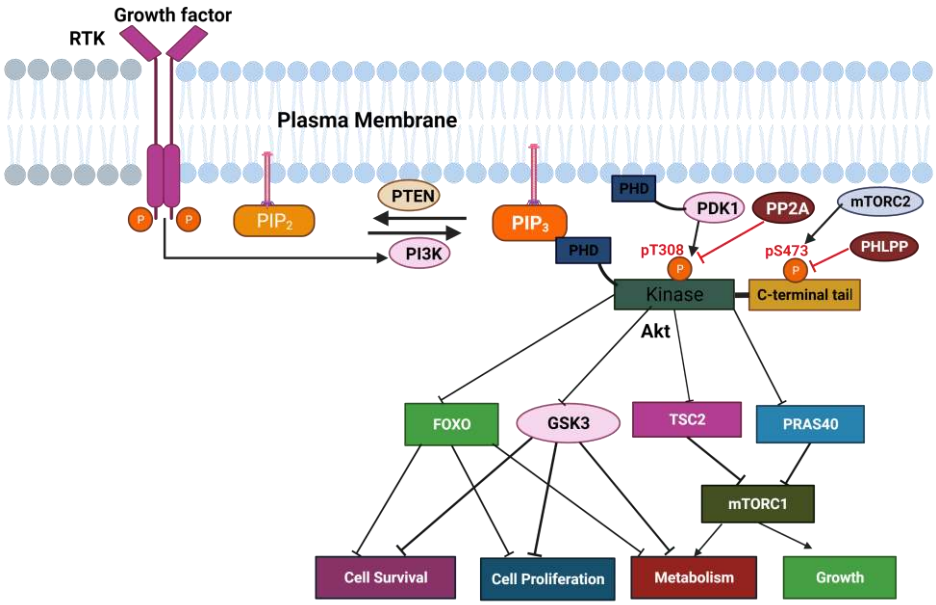

Figure 2.1 The Akt signaling pathway.

2.3 Akt/protein kinase B

Staal and co-workers identified Akt protein or protein kinase B in 1977 as transforming retrovirus isolated from AKR with T-cell lymphoma and called it Akt-8[89]. Subsequently, Staal established that Akt is an oncogene in humans[34], and activation of this kinase drives the switch to aerobic glycolysis because cancerous cells need a continuous supply of glucose, which makes them dependable on aerobic glycolysis for survival and proliferation[86].

2.3.1 The Isoforms of Akt

There are three isoforms of Akt protein with over 85% sequence similarity (Figure 2.2), which are expressed by all mammalian cells. These isoforms are Akt1, Akt2, and Akt3, also called PKB**α**, KPB**β**, and PKBϒ, respectively[90]. Akt1 serves as a paradigm for understanding the Akt isoforms. Akt1 is ubiquitously expressed in all tissues and is related to proliferation and antiapoptotic behavior[91]. Akt2 isoform is expressed in metabolically active tissues, for example, adipose tissue, liver, and muscle tissues. Akt2 deletion has been implicated in hyperglycemia – a type 2 diabetic phenotype and is also responsible for impairment of glucose uptake[92]. Akt3 is mainly expressed in the testes and brain [93, 94], and the absence of Akt3 leads to neuronal malformation and altered fatty acid metabolism [95]. Recent findings using lockdown studies have uncovered opposite roles of Akt1 and Akt2 in various tumor types. In an aggressive breast cancer context, the Akt2 isoform seems responsible for metastasis and invasiveness in advanced stages, indicating that selective inhibition of Akt2 would be the best therapeutic strategy[96]. On the other hand, a different behavior was observed for lung cancer, in which Akt functions as tumor initiator, whereas Akt2 had suppression behavior, suggesting an Akt1 selective strategy[97]. Of note with emphasis, all these results on isoform-specific functions within this intricate signaling pathway were based on knock-down studies[31]; therefore, a thorough investigation with chemical tools would aid in further clarifying this complex network and interplay through minimally invasive perturbation studies[98].

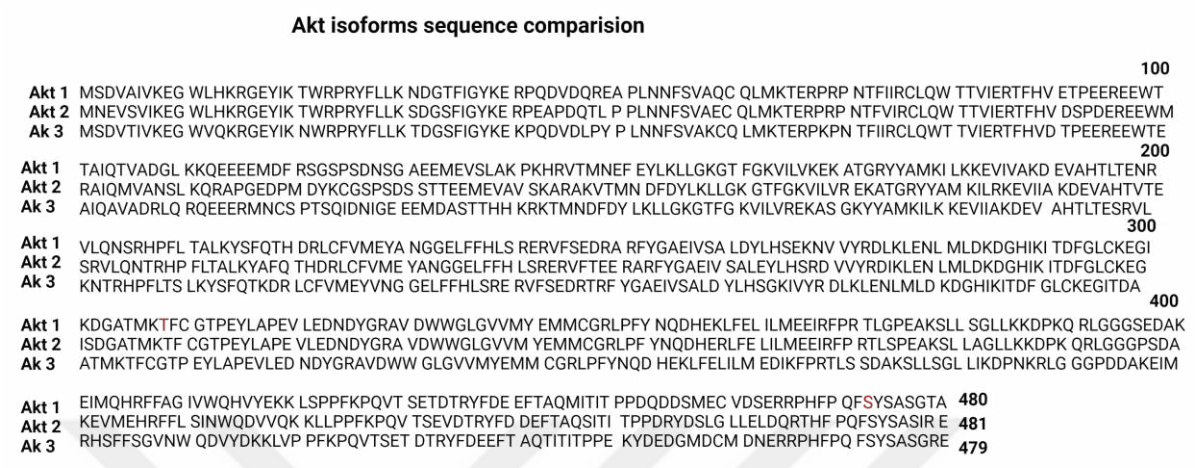

Figure 2.2 The sequence of Akt three isoforms with phosphorylation site residues (Thr308 and S473) in Akt1 colored red

Within the context of structure, the three isoforms of Akt have similar structural architecture. In a more perspective, Akt comprises an amino terminus pleckstrin homology domain (PH domain), followed by a linker region, connected to a centrally positioned kinase domain, and the C-terminus regulatory domain, which contains a hydrophobic motif, figure 2.3 [99]. Akt1 kinase domain shares about 85 percent sequence identity with the rest of the isoforms, Akt2 and Akt3, while Akt1 PH domain shares about 60 percent sequence identity with Akt2 and Akt3 [100]. Here, this dissertation focuses on Akt1, which serves as a paradigm for understanding all the Akt isoforms and is frequently hyperactivated in tumor cells

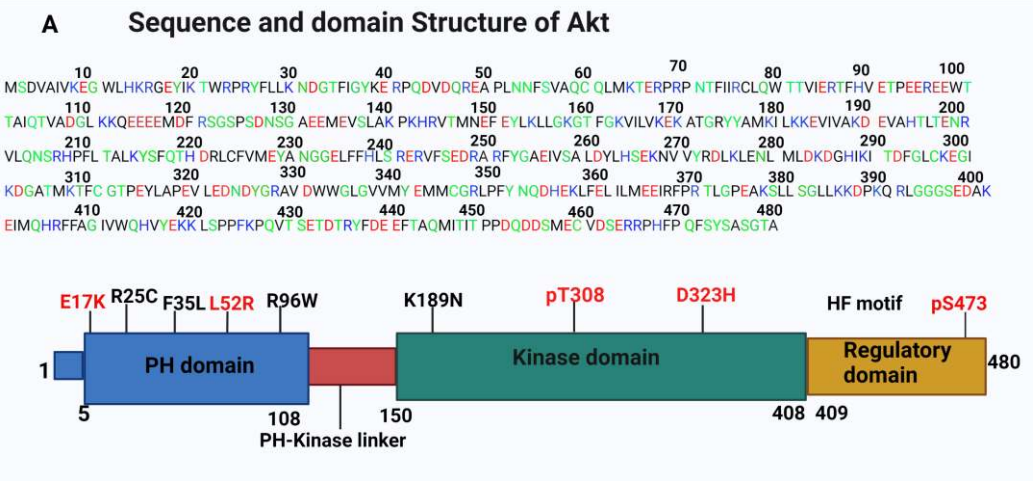

Figure 2.3 the sequence and domain structure of Akt; the PH domain is colored blue, the PH-kinase linker (red), the centrally kinase domain (cyan), and the C-terminal regulatory domain (orange)

The PH domain of Akt

The PH domain is a versatile domain, which often participates in protein-protein interaction (PPI) [101]. The PH domain was discovered decades ago, and it was found to have approximately 100 to 123 amino acid residues[102]. The Akt kinase contains a PH domain, which is located at its amino terminus. Structurally, the PH domain is a bend seven-stranded antiparallel **β**-sheet [103, 104] with three variable loops: V1, V2 and V3 and closed on one end by a C-terminal **α**-helix[105]. These structural architectures are recognized as general features for the PH domains in hundreds of proteins in bacteria and mammals. In the context of function, there are two principal functions of the PH domain of Akt: the binding to PIP_3 or PIP_2, which leads to translocation of Akt to the plasma membrane [5], and intramolecularly interacting with the kinase domain, which result in

PH-kinase domain autoinhibition or Akt inactivation[6, 7]. The recruitment of Akt to the plasma membrane via the PH domain facilitates Akt proximity to PDK1 and mTORC2, which leads to Akt phosphorylations in the activation loop and C-terminus, respectively[1]. The figure 2.4 depicts structure and sequence of the lipid-binding PH domain of Akt.

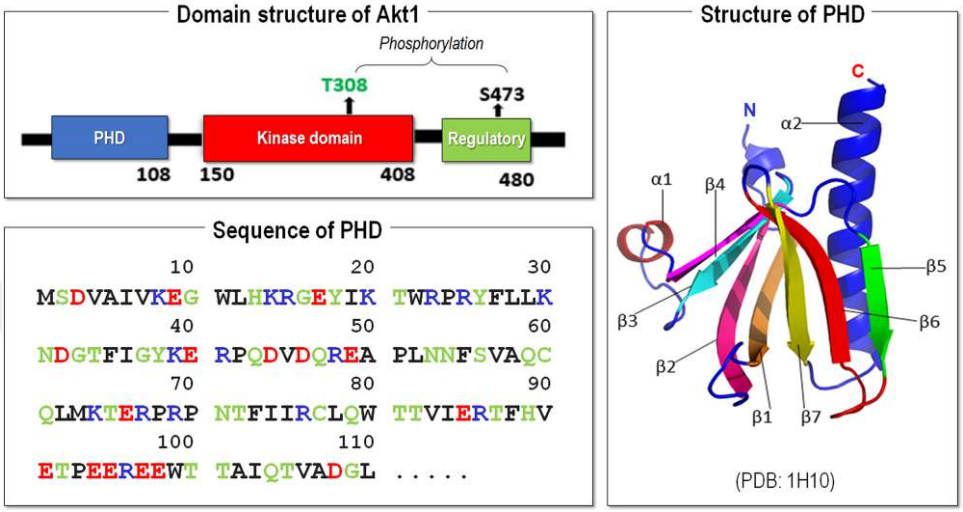

Figure 2.4. Sequence and domain structure of Akt PH domain

The kinase domain of Akt

All Akt isoforms contain a centrally positioned kinase domain. The kinase domain consists of the activation loop containing a functional site or phosphorylation site. Structural-wise, the kinase domain comprises two lobes: a smaller amino-terminal lobe and the larger C-terminal lobe[8]. Located between these two lobes is a deep cleft or cavity beneath a highly conserved glycine-rich nucleotide positioning motif, also referred to as the Glycine-loop (G-loop)[8]. The deep cleft between these lobes accommodates ATP; in other words, ATP is bound in the deep cleft between the N-and C-lobes in the kinase domain. In Akt1, the isoform under discussion in this dissertation (Akt), the binding cavity of ATP is about 20Å away from phosphorylated Thr308 (pThr308) in the activation loop of the bilobal kinase core domain[8]. Three amino acid residues encapsulate ATP in the catalytic cleft. These residues include HIS194, Arg273, and Lys297 – all of which are positively charged residues. The phosphorylation of Akt at Thr308 in the kinase domain acts as a switch on, enabling Akt to phosphorylate its downstream substrates[8]. Researchers have established that the binding of ATP in the binding cleft protects the phosphorylated Thr308 level[29, 106]. On the other hand, the occupancy of ADP in the binding cleft between the N-and C-

lobes of Akt apostate cannot maintain Thr308 phosphorylation level. To put this in more perceptive, ATP-loaded phosphorylated Thr308 of Akt can resist dephosphorylation by the phosphatase, PP2A, whereas Akt kinase ADP-loaded phosphorylated Thr308 cannot resist dephosphorylation by PP2A. In general, the function of ATP in kinases is to provide its ϒ-phosphate group, which kinases can utilize to phosphorylate their downstream substrates, hence the "on-off" switch mechanism through ATP binding to Akt is essential for the kinase activity[8].

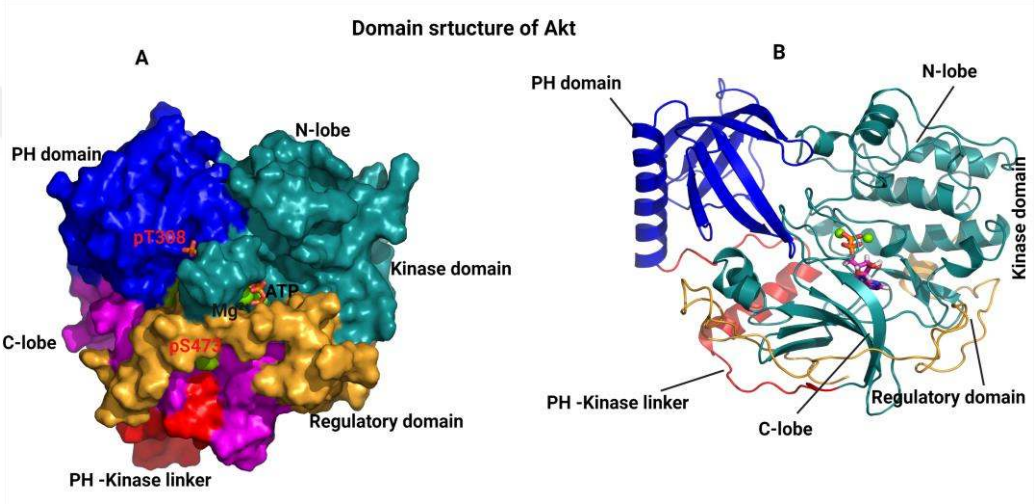

Figure 2.5: Domain structure of Akt with kinase domain; A (surface representation) and B (ribbon representation. The phosphorylation sites are marked with the various regions such as PH domain, the PH-kinase domain linker, kinase domain and C-terminal tail are colored differently. The APT binding pocket and the magnesium ion (ii) are also indicated

2.4 Akt activation and dissociation mechanisms

A study has established that Akt can be allosterically activated by membrane lipid, PIP_3, or PIP_2 at the plasma membrane. The interaction of PIP_3 or PIP_2 with Akt PH domain relieves the autoinhibitory intramolecular interaction, "PH-in" conformer between the PH domain and the kinase domain[107]. When the positively charged PH domain binds to the negative charge PIP_3 at the membrane, Akt undergoes a conformational change leading to its activation. This conformational rearrangement disrupts the interaction between the lipid-binding PH domain and the kinase domain, which exposes Akt phosphorylations sites and access for substrate binding, but not the binding of nucleotides such as ATP or ADP. The "PH-out" conformer enables Thr308 phosphorylation in the activation loop in the kinase domain by PDK1[7]. Thr308 phosphorylation by PDK1 along with phosphorylation of Ser473 in the carboxy-terminus regulatory domain by mammalian target of rapamycin complex 2 (mTORC2) fully activates Akt. Of note, Akt activity is restricted to membranes sites comprising membrane lipids, PIP_3 or PIP_2 [108]. Akt is unarguably a significant component of phospholipid signaling pathway, which involves phosphatidylinositol 3,4,5-triphosphate (PIP_3). PIP_3 levels in this pathway are usually controlled by two opposing actions of phosphatidylinositol 3-kinase (PI3K) and phosphatase and tensin homolog (PTEN)[43]. The activation of Akt is instigated upon growth factor stimulation of PI3K, which creates PIP_3, from phosphatidylinositol 3,4-bisphosphate (PIP_2) at the plasma membrane[10, 40, 41, 109, 110]. These phospholipids, PIP_3 and PIP_2, are localized in the plasma membrane and serve as docking sites of Akt, which gets translocated to the plasma membrane via its NH_3-terminal PH domain[18, 40, 42, 110, 111]. Contrary to most AGC kinases that lack PH domains, Akt contains a PH domain, which has a high binding affinity for PIP_3[1, 112]. The interplay between PH domain and PIP_3 is essential and has been considered a "hallmark" in the Akt pathways and is required for phosphorylation and downstream activations of effector proteins[18, 109]. Akt translocation to the plasma membrane containing PIP_3 is needed for its phosphorylations and subsequent activation, and Akt dissociation from the membrane leads to rapid dephosphorylations and inactivation[108]. The intramolecular interaction between the PH domain and the kinase domain of Akt, a "PH-in" conformer, hinders Thr308 phosphorylation in the activation loop by phosphoinositide-dependent kinase 1 (PDK1)[6]. When the PH domain interacts with PIP_3[13], it leads to a conformational change, "PH-out" conformer, releasing the domain-domain autoinhibition.

The "PH-out" conformer enables Thr308 phosphorylation in the activation loop of the kinase domain by PDK1[6]. Thr308 phosphorylation by PDK1 along with phosphorylation of Ser473 in the carboxy-terminus regulatory domain by mammalian target of rapamycin complex 2 (mTORC2) activates Akt fully within the cells [14, 15].The dephosphorylations of these residues, Thr 308 and Ser 473, are carried out by Protein Phosphatase 2A (PP2A) and PH domain Leucine-rich repeat-containing Protein Phosphatase (PHLPP), respectively[4]. Akt translocation to the plasma membrane was proposed to be regulated by phosphatidylserine (PS), where PS interacts with key residues in the PH and regulatory domains. The interaction promotes the binding of Akt to PIP_3. The association between PS and PIP_3 can trigger Akt interdomain conformational rearrangements that lead to the phosphorylation of Ser473 and Thr308 [16, 27]. Mutations in the PH domain that weaken the interaction between the PH domain and the kinase domain result in constitutive activation of Akt [17]. The PH domain of Akt has tends to bind to other proteins. For example, in breast cancer cells, Calmodulin (CaM) binds to the PH domain of Akt[18]. That is, upon epidermal growth factor (EGF) stimulation, CaM co-localizes with the PH domain at the plasma membrane to enable Akt membrane anchoring and activation [19], as depicted in Figure 3 (or 2.6). The interaction between CaM and PH domain by CaM's antagonist inhibited CaM-Akt translocation to the cellular membrane, resulting in apoptosis in tumorigenic mammalian carcinoma cells [19, 113]. Additionally, protein ligation studies have unearthed that pSer473-Akt activation is driven by an intramolecular interaction between the PH domain and kinase domain linker that relieves PH domain-mediated Akt autoinhibition. Phosphorylation of Ser477/Thr479 activated Akt via an allosteric mechanism requiring loop interaction, reducing PH domain autoinhibition, and lowering PIP_3 affinity [15], as illustrated in Figure 2.6. Furthermore, the physical association of PDK1 with Akt has been proposed to be sufficient for Akt activation/phosphorylation at Thr308 independent of plasma membrane localization and PI3k [21]. Also, elsewhere, molecular modeling based on homology modeling using the crystal structure of Akt2 has attempted to uncover the nature of the domain-domain intramolecular interaction of Akt [6, 7]. Everything considered, these findings suggest that synergies between membrane lipids, and the PH domain, the intermolecular interplay between the PH domain and the kinase domain linker, interaction between CaM and the PH domain, and physical association of PDK1 and Akt are perhaps required for Akt translocation, phosphorylation, and activation, respectively. Taken altogether, these pioneering studies have proposed several different

mechanisms of Akt translocation, phosphorylation, and activation. Resultingly, the actual mechanism of Akt translocation, phosphorylation, and activation remains obscure or a matter of debate. Also, how CaM interacts with the PH domain at the atomic level and the PH-kinase autoinhibition in full-length Akt have not been fully established and require additional studies, which this dissertation strives to uncover the underlying mechanisms of CaM-PH interplay and PH-kinase domain autoinhibition as in Figure 2.7

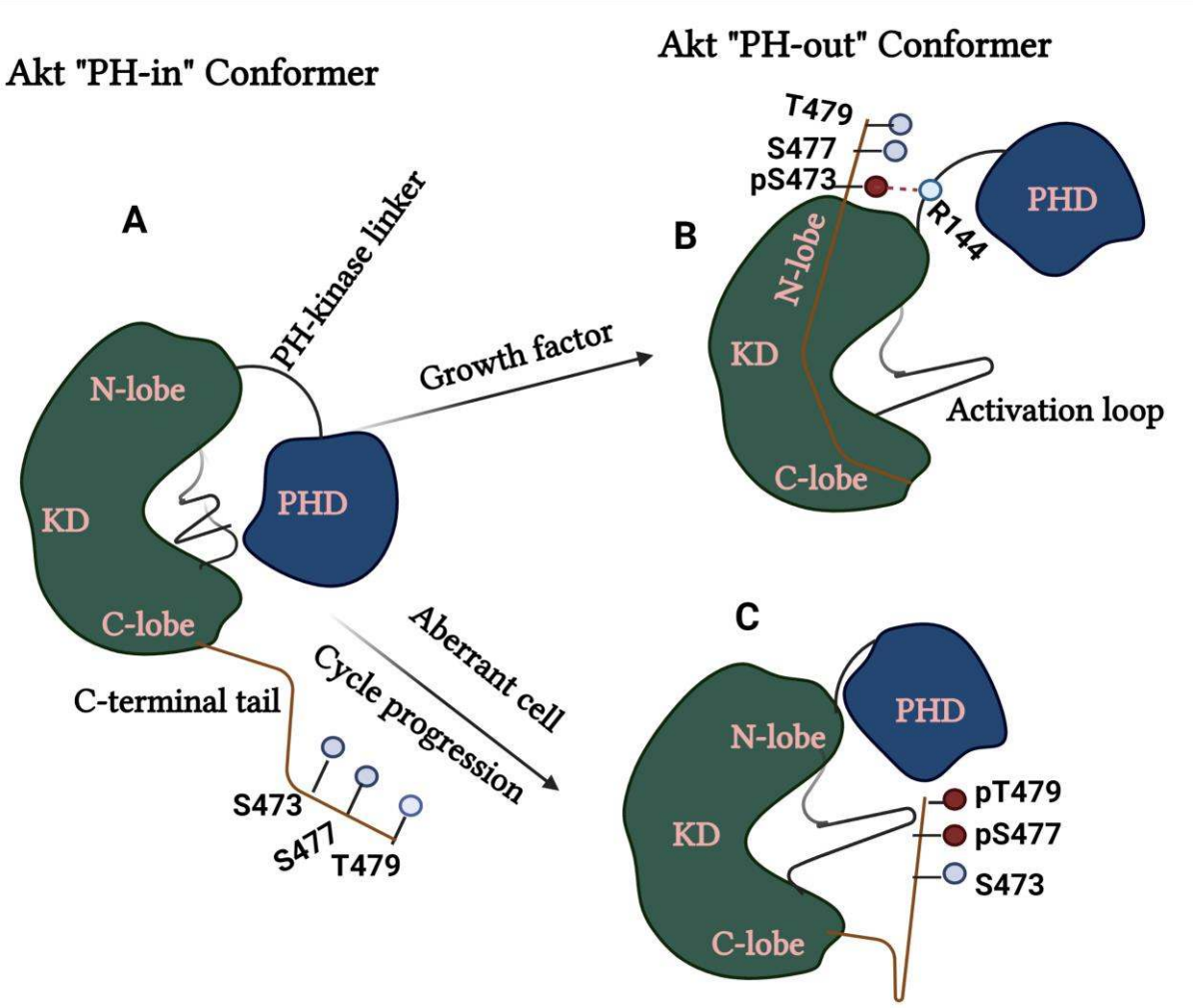

Figure 2.6 Akt activation mechanisms by Ser473 interaction with Arg144 in the PH-kinase domain linker and dual phosphorylation at S477/T479 releasing the "PH-in" conformer of Akt [14].

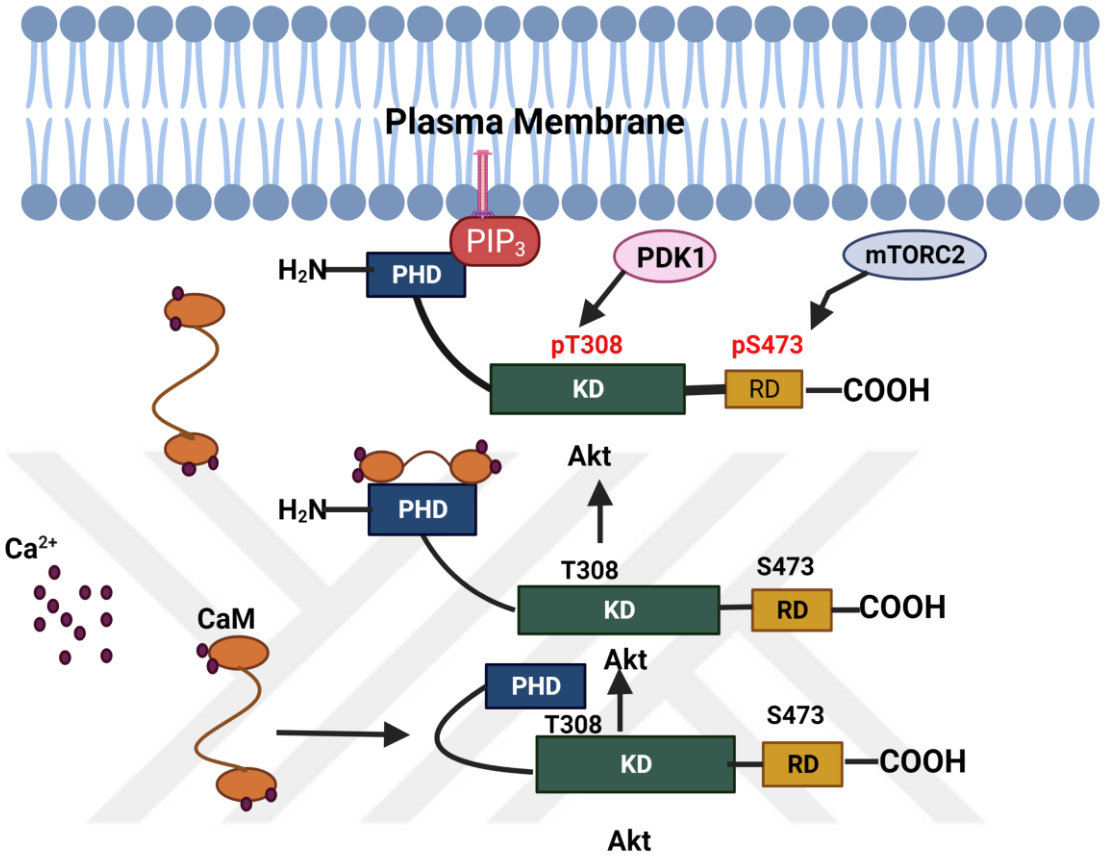

Figure 2.7 the proposed model of CaM-PH domain interaction that enabled the translocation of Akt to the plasma membrane resulting in conformational rearrangements that facilitate phosphorylation of Thr308 and Ser473 by PDK1 and mTORC2, respectively

When Akt dissociates from PIP_3 at the plasma membrane, it phosphorylates its downstream nucleotide and cytoplasmic proteins. It has been reported that the half-life of cytosolic active Akt is about 3 to 5 minutes before dephosphorylation by phosphatases[6]. A proposed mechanism of how Akt dissociate from the plasma membrane is the phosphorylation at residue, Thr34, which depends on the recruitment of PKCζ[114] or PDK1 – concurrent phosphorylation of Thr308[115], at the plasma membrane, which leads to a conformational change and inducing the detachment from the plasma membrane. There have been various outcomes of Akt protein-membrane dissociation depending on the required mutation at Thr34. For instance, the conversion of threonine to alanine, Thr34Ala mutant (T34A), has the potential to bind PIP_3 even when PKCζ is present[114], although conflicting observations of the Thr34Asp (T34D) mutant has been reported elsewhere. The Thr34Asp mutant was either reported to imitate phosphorylation, impairing Akt kinase translocation to plasma membrane

[114]. In reverse, it was observed to localize Akt protein prominently at the plasma membrane [116]. The reformation of the interplay between the PH domain and kinase domain enhances membrane dissociation and Akt subsequent dephosphorylation [107]. The dephosphorylations of Thr308 and Ser473 are carryout by the protein phosphates 2A (PP2A) and PH domain Leucine-rich repat-containing protein phosphate (PHLPP), respectively[4].

2.5 Proposed models of Akt activation in cells

There are several *in vitro* insights of Akt regulatory mechanisms, and it is important to consider the relevance of these proposed mechanisms in a cellular environment. In cellular environments, upstream and downstream lipids and protein kinases and phosphatases play a crucial role in the kinetics and activation mechanism of Akt. There are three popular proposed models of Akt regulation inside the cells: diffusive model, ATP on/off switch model, and allosteric lipid switch model[117].

The diffusive model – in the absence of growth factor and other stimuli, inactive Akt localizes in cell nucleus and cytosol. However, upon growth factor stimulation at the membrane that triggers the production of PIP_3 and PIP_2 results in PH domain-dependent accumulation of Akt at the respective plasma membranes. The PH domain-dependent accumulation of Akt at the plasma membrane is transient, usually peaking around 2 to 5 minutes after stimulation, but phosphorylation of Thr 308 in the kinase domain and Ser 473 in Akt C-terminal extension is sustained for at least 2 to 3 hours post-stimulation[6, 107]. These observations provide the basis for the classical or diffusive model of how Akt is activated inside the sides. According to this proposed model, following the transient PIP_3 – PH domain engagement and phosphorylation of Thr 308 and Ser 473 by membrane-associated PDK1 and mTORC2 respectively, activated Akt detaches from the plasma membrane and diffuses through the cell interior phosphorylating its enormous substrates in the cell nucleus and cytosol before it's inactivated by dephosphorylation by PP2A and PHLPP[117].

The ATP on/off switch model is an elegant extension of the classical or diffusive model, which is based on the observation that ATP-competitive inhibitors have the propensity to paradoxically induce hyperphosphorylation of Akt inside the cells. According to this model, when ATP is bound in the active site between the N-and C-lobes of the kinase domain, it protects Akt from dephosphorylation as it diffuses through the cell to phosphorylate its numerous substrates. Phosphorylations of substrates and the conversion of ATP to ADP concomitantly alter conformational changes in Akt rendering it a suitable substrate for cellular phosphatases and therefore rapidly inactivated upon dephosphorylation

[29]. It is worth emphasizing that the ATP on/off switch model limits kinase activity to a single round of catalysis, linking this model to empirical data demonstrating that Akt activity is closely coupled to membrane lipids – PIP_3 and PIP_2 dynamics. In contrast, in the diffusive model, there is no restriction of Akt activity or explicitly linking nucleotide exchange to Akt phosphorylation state. A finding challenged the ATP on/off switch model that Akt kinase-inactive mutant retaining ATP binding potential was dephosphorylated by phosphatases with the same kinetics as wild-type Akt[107]. While the diffusive and ATP on/off switch models have accounted for existing empirical data, a subsequent phosphoproteomic analysis[118, 119] uncovered that the substrates of Akt display different kinetics of phosphorylation, which is not compatible with the distributive kinetics implied by freely diffusing Akt in the cells. Additionally, a free diffusion at approximately 12 μm^2 would enable Akt to reach any of its substrates in cells within 3 seconds. Yet, FRET results have indicated much slower kinetics ($t_{1/2}$ 3 /5 minutes) of Akt activation in nucleus and cytosol, which suggest that Akt is not freely diffusing in the cells[6, 120]. The third model of Akt activation mechanism, the allosteric lipid switch model, states that in addition to phosphorylation of Akt that occurs at Thr 308 and Ser 473 in its kinase domain and C-terminal extension, respectively, Akt activity requires binding to membrane lipids, PIP3 or PIP2, a phenomenon that limits Akt kinase activity to a subset of subcellular membrane compartments[117]. This finding has important implications for regulating Akt activity and substrate phosphorylation in cells, indicating that active Akt is associated with the plasma membranes. This model ensures that Akt activity remains proportional to upstream regulators such as PI3K and PTEN and enables fine-tuning its activity in the cellular environment as per the identity and lifetime of its lipid ligands.

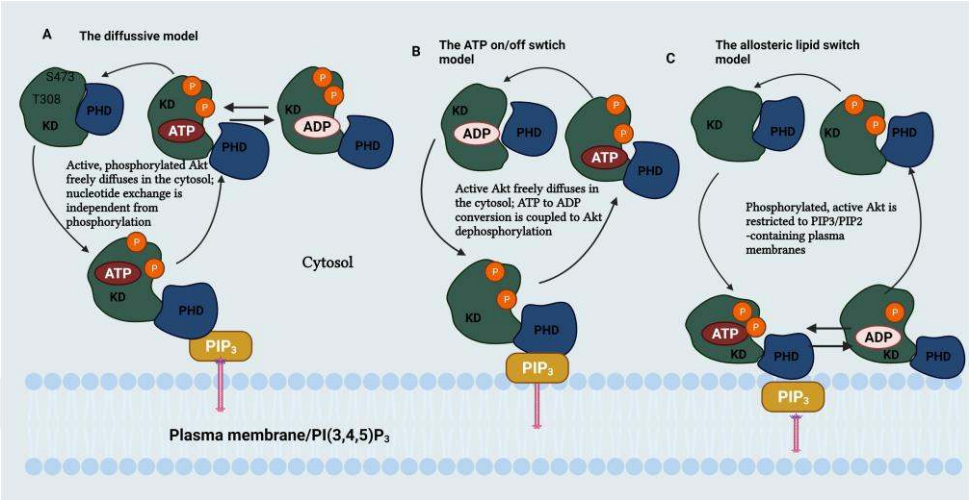

Figure 2.8 Proposed models of Akt activation in cell. (A) Active, phosphorylated Akt freely diffuses in the cytosol, and the nucleotide exchange is independent from phosphorylation. (B) Active Akt kinase freely diffuses in the cytosol and the ATP to ADP conversion is couple to Akt dephosphorylation. (C). Phosphorylated, active Akt is restricted to PIP3/PIP2-contianing plasma membranes. [117]

2.6 Akt post-translational modification

Like other nascent polypeptides, Akt undergoes several post-translational modifications such as phosphorylation, methylation, lysine modifications, ubiquitination, SUMOylation, and glycosylation. Phosphorylation – is a significant post-translational modification that most nascent polypeptides undergo and Akt kinase is not an exception. Akt phosphorylation and dephosphorylation are the most common post-translational modification of this enigmatic protein kinase. It is the primary mechanism by which Akt is activated to perform its cellular duties[93]. The receptors such as GPCR, RTK, and GLUT are stimulated by extracellular ligands, which include hormones, chemokines, epidermal (EGF), fibroblast, insulin-like (IGF) growth factors that activate intracellular PI3K at the plasma membrane. Upon PI3K activation, it converts PIP_2 to PIP_3, a process that PTEN deregulates; that is, PTEN converts PIP_3 back to PIP_2, regulating PI3K activity[45]. The inactive form of Akt also called the autoinhibited state, resides in the cytosol until it gets translocated to the plasma membrane. The binding of the PH domain to PIP_3[121], a docking site phospholipid, initiates the allosteric activation of Akt[13]. This conformational change results in phosphorylations of Thr308 and Ser47 in the kinase domain and regulatory domain, respectively[121, 122]. The residue, Thr308 phosphorylation by PDK1, is essential for Akt activation; it orders the activation loop and provides substrate-binding access, while Ser473 phosphorylation is needed for maximal activity and positioning of the catalytic residues[48]. Akt required minimal consensus sequence for phosphorylation is Arg-X-Arg-X-X-Ser/Thr-h, where X presents any amino acid residue and lower letter h is a bulky hydrophobic residue[99]. Additionally, a constitutively active phosphorylation site, Thr450, within the C-terminal regulatory domain, is important for the folding and stability of Akt[5]. Activated Akt dissociates from the plasma membrane upon phosphorylations into the cytosol, where it phosphorylates its downstream substrates or target proteins. Subsequently, cytosolic Akt get dephosphorylated rapidly by phosphatases, PP2A at Thr308 and PHLPP2 at Ser473[4]. Methylation – DNA methylation that usually occurs in the promoter CPG islands is an epigenetic modification, which maintains gene silencing[123]. It has been observed that Akt promoter region was significantly hypomethylated in tumor cells or patients with breast cancer[124]. Lysine modification or acetylation – Akt membrane-binding activity is often hindered by the reversible acetylation of lysine (Lys) residues. The acetylation of the Lys residues is carried by histone acetyltransferase and deacetylases. The residues, Lys14 and Lys20 acetylation inhibit the PH domain's binding to membrane lipid, PIP_3, thereby regulating

Akt activity[125]. The mutations of Lys14 to Arg, or Gln, and Lys20 to Gln have shown to be analogous to constitutive acetylation of Akt, resulting in Akt inactivation. Intriguingly, mutation Lys20 to Arg deacetylates Akt, which enables the PH domain to readily bind to PIP_3 –leading to subsequent phosphorylation of Akt[125]. Akt ubiquitination plays a pivotal role in its activation and stability. Akt in the "PH-out" conformer state is unable to be ubiquitinated. Proteins often undergo Lys48-associated ubiquitination that leads to the degradation and termination of their activity[126]. Intriguingly, Akt Lys63-associated ubiquitination at residues: Lys8 and Lys 14 does not induce degradation of the kinase but instead mediates plasma membrane binding and increases Akt phosphorylation[22]. SUMOylation – the covalent conjugation of a small ubiquitin-related modifier (SUMO) to an internal lysine residue in the protein kinase B is considered as a reversible post-translational modification that affects cell proliferation and apoptosis. A study has shown that SUMOylated Akt usually resides in the nucleus[127]. Also, several different reports implicated SUMO-modification sites to be considered as major receptors, for instance, Lys64 in the amino terminus PH domain, Lys182, Lys189[128], Lys276[129, 130], and Lys301[127] in the centrally positioned kinase domain of Akt. Mutations of these Lys residues in Akt kinase significantly reduce SUMOylation, thus perturbing Akt activity[128]. Akt SUMOylation *in vivo* has been detected under heat-shock stress conditions – indicating that Akt is not constitutively modified by SUMO[128]. Glycosylation – the modifications of threonine and serine residues in Akt kinase by O-linked N-acetylglucosamine are reversible post-translational modifications process that often inhibits phosphorylation of Akt protein [131]. The competitive association between Akt phosphorylation and glycosylation sites has been involved in cancer cell progression[132].

2.7 Akt mutation in Human cancers

Akt is a ubiquitously expressed protein kinase, and it has been implicated in various cancer types. For example, over 50% of the human cancers in the Catalogue of Somatic Mutations in Cancer (COSMIC) database have shown aberrant Akt expression. Mutations in Akt occur in about 3-5% of human cancers and are relatively conserved throughout Akt other isoforms, Akt2 and Akt3[133]. Akt function greatly depends on its lipid-binding PH domain; as a result, a disruption of the PH domain interaction is often implicated in tumor cells progression[134]. For example, somatic mutations of residues in the PH domain have frequently disrupted Akt

membrane binding and dissociation. These amino acid residues are often located close to the phospholipids binding pocket on Akt; hence aberrant structural alterations are direct attributes to these mutations. The most frequently observed somatic missense mutation in the PH domain is the Glu17 to Lys (E17K), which is located close to the phospholipids binding pocket. The Glu17 to Lys mutation accounts for about 36% of all Akt mutations (cBioPortal for Cancer Genomics)[133, 135, 136]. In breast cancer, the E17K mutation has been observed[134, 137, 138], and also in endometrial carcinoma[139], prostate[140], bladder[141], non-small cell lung cancer[142], melanoma[143] and acute leukemias [144]. This E17k mutation in the lipid-binding PH domain has the propensity to perturbs the interplay between the PH domain and the kinase domain to induce the hyperactivation of Akt either with or without insulin stimulation[22]. Additionally, other missense activating mutations in PH domain are Leu52 to Arg (L52R) and Gln79 to Lys (Q79K). These two mutations account for 1.2% of all Akt mutations [135, 136] in colorectal and breast cancers[137, 138]. Also, in the PH domain of Akt, Cys77 mutation has been detected in cancer patients (COSMIC). The Cys 77 to Phe (C77F) missense mutation in breast luminal carcinoma[138, 145], Cys77_Lys78ins10 (insertion of ten residues, in breast ductal carcinoma)[146], and the Cys77_Lys78ins12 (insertion of 12 residues, in frame) in ovarian granulosa cell tumor[147].

Additionally, on the PH domain of Akt, there are other inactivating mutations. The mutation of Arg15 to Ala (R15A) and mutation of Lys20 to Ala (K20A) have been shown to inhibit the translocation of Akt to the plasma membrane, despite the presence of signaling hormone insulin[16, 148]. From the COSMIC database, R15Q has been observed in cervical cancer. In the PH-in conformer of Akt, the PH domain interacts with the C-lobe of the kinase domain close to the residues, Asp323 and Asp325, and the unphosphorylated activation loop, where the phosphorylation site, Thr308, is located[108]. In a recent report, the double mutants, Asp323 to Ala and Asp 325 to Ala (D323A &D325A), disrupt the PH domain-mediated inactivation by permanently exposing the phosphorylation site in the kinase domain and rendering substrate access, thus leading to Akt constitutive activation[108]. Table 2.1 depicts mutation in Akt isoforms, and the spectrum of recurrent mutations in Akt1 are relatively conserved in Akt2 and Akt3 isoforms. This dissertation focuses on the D323H mutation in the Akt1 isoform, which occurs in the PH-kinase domain interface.

Table 2.1, various mutations that occur in Akt isoforms

Domain of Akt	Akt1	Akt2	Akt3
PH domain	E17K D32N/Y D46E P51L/S L52F/H/R, Q79K/R W80R	E17K D32H/N D46N W80C/L	E17K D32N D46H P50L/S L51L/R Q78K
PH-kinase linker	R121W		
Kinase domain	D221N S266N/S D323G/H/N/Y R367C R370C/H	D324G/H/N R368C/H/N R371C/H/L	D219N S264F D320H R367Q

Table 2.1 Taken from Yi, K.H & Lauring 2015 and the Catalogue of Somatic Mutations in Cancer (COSMIC)

2.8 Inhibitors of Akt in clinical studies

Akt protein kinase has long been an attractive target for cancer therapy due to its involvement in cancer initiation and progression. Akt targeting small molecules is limited by their lack of moderate potency, specificity, and poor solubility. Current Akt inhibitors in clinical studies have not been successful due to their toxicity properties or development of resistance[149]. Akt inhibitors can be categorized into three: ATP-competitive inhibitors, allosteric inhibitors, and PIP_3-analogues. A fairly common practice to inhibit protein kinases is targeting the binding activity with ATP-competitive inhibitors. However, for Akt there is a unique allosteric binding pocket with several advantages regarding the selectivity of developed small molecule inhibitors. For instance, active binders often target the conserved ATP-binding pocket[150], stabilizing the active conformation, "PH-out" conformer of Akt kinase. In contrast, allosteric inhibitors target the interdomain region between the kinase domain and the PH domain, stabilizing the inactive conformation, the "PH-in" conformer of Akt.

As their name suggests, ATP-competitive inhibitors act as small molecules that occupy the ATP binding pocket in the kinase[106]. The ATP binding pocket is conserved for all Akt isozymes[150]. A major drawback to ATP-competitive inhibitors is their lack of efficacy and specificity against the Akt isoforms and other AGC kinase members in pre-clinical and clinical

trials[149] – unexpectedly inducing hyperphosphorylation[151]. Due to the high sequence homology of Akt isoforms, there have been numerous challenges in developing Akt isoforms-specific inhibitors that could progress in clinical studies [152]. Additionally, the known Akt allosteric inhibitors target the PH domain to prevent Akt plasma membrane localization and activation[7, 149, 153]. The effectiveness of the allosteric inhibitors dramatically relies on the PH-kinase domain intact interface because as soon as the allosteric interface is comprised, drug sensitivity is lost, which drives Akt activation[17]. Furthermore, the PIP_3 or PIP_2 binding pocket on Akt is not an ideal target for allosteric inhibitors because of its shallow and highly charged nature[154].

Another competitive approach to target Akt involves the use of PIP_3-analogues. The PIP_3-analogues usually bind to the PIP_3 cavity with the amino-terminal PH domain and disable the kinase activation mechanism. However, the PIP3-analogues have several drawbacks, such as lack of selectivity because there are over 300 structurally related PH domains and poor drug-like properties. On a high note, even though enormous inhibitors have shown to be promising in inhibiting Akt kinase both *in vivo and in vitro*, only a handful of these inhibitors have entered clinical trials. For example, two ATP-competitive Akt inhibitors: Capivasertib (AZD5363) and ipatasertib (GDC-0068), are in phase I and Phase II clinical studies for mono- or combination therapy with diverse indications. However, the selectivity of these inhibitors in inhibiting Akt has been hindered due to the highly conserved ATP-binging pocket among the protein kinase family. Resultingly, dose-limiting side effects of these drug molecules during treatment and the lack of efficacy resulting from the inevitable dose reduction have occurred[155]. Due to these drawbacks, medicinal chemists have applied efforts to identify Akt specific and isoforms-selective inhibitors, which led to the discovery and development of bioactive allosteric inhibitors. As a result of this alternative approach, inhibitors such as MK-2206 and miransertib (ARQ092) have been identified with greater specificity, lower toxicity, and reduced side effects than the aforementioned target approach. For instance, MK-2206 – an orally active, highly potent, and selective allosteric pan-Akt inhibitor has been investigated in clinical trials to treat breast cancer[156]. Still, the expected clinical outcome is yet to be achieved. On the other hand, Miransertib and its next-generation small molecule Arq751, orally available highly selective pan-Akt inhibitors, undergo clinical evaluations. In the case of Miransertib, promising results have been observed in cells harboring the biomarker Akt E17K, and both inhibitors are undergoing investigations as a potential therapy for Proteus

Syndrome[157]. It is worth emphasizing that, although there are numerous clinical trials for targeting cancer; however, none of the targeted Akt inhibitors have reached phase III clinical studies, which highlights the enormous complexity of Akt-signal dependent malfunctions. For example, in diseases such as Proteus Syndrome, where the Akt E17K mutation has been a critical biomarker, promising response rates in monotherapy have been achieved[158, 159]. The drawbacks in clinical trials to ATP-competitive and allosteric inhibitors of Akt emphasize the need for innovative strategies to establish Akt's role in disease[160]. One of the innovative approaches is the development of covalent-allosteric Akt inhibits, hereinafter called CAAIs. As described by Wiesner and colleagues, this approach combines the selectivity of small allosteric molecules with irreversible covalent modification of two noncatalytic cysteine residues in the activation loop of Akt kinase domain. As a result, the CAAIS demonstrates prolonged residence time, which is somehow limited by the turnover of the kinases in the cell. For instance, the borussertib, the lead compound, has shown enhanced inhibitory efficacy than relevant Akt inhibitors. Moreover, borussertib shows strong antiproliferative effects and exhibits target engagement in cancer cell lines harboring changes in the PI3K/Akt signaling pathway. Furthermore, the efficacy of borussertib *in vivo* was proven in treatment combination studies with MEK-inhibitor, trametinib in Kras mutant patient-derived xenograft (PDx) models resulting in a partial response[161]. It is worth emphasizing that borussertib has shown promising results in preclinic studies despite its pharmacokinetic properties limitations, which underlines the potential of CAAIs for targeting Akt in relevant diseases. On the other hand, borussertib pharmacokinetics properties must be refined by structure-based design before peroral applications can be achieved[162]. Recently, structural insights into the allosteric site of the different Akt isoforms guided the discovery and development of specific CAAIs, enabling future investigations of isoform-specific functions through the use of selective probes[31]. Thus, CAAIs presents a powerful approach to scrutinize relevant questions about Akt's impact and regulation in various disease[160].

Here, intrigued by these findings, this dissertation intends to probe how CaM binds to the PH domain of Akt, the nature of the intramolecular interaction between the PH domain and the kinase domain or the role of the interface residues of the domain-domain interaction, and conformational changes that facilitate Akt translocation, phosphorylation, and activation at atomic level. In this dissertation, computational methods such as molecular modeling and MD simulations with CHARMM and NAMD were employed to explore the interplay between

CaM and PH domain, PH-kinase domain autoinhibition, and the role of interfacial residues or disruption of "PH-in" conformer, which releases Akt autoinhibition leading to Akt membrane anchoring and activation.

Methodology (Materials and Methods)

3.1 Molecular Modelling and Molecular Dynamics Simulation

3.1.1 Generating initial configurations of CaM-PH domain Complexes.

The crystal structures of calmodulin (CaM) with the extended and collapsed linkers (PDB ID: 1CLL; 1CDL respectively) and the PH domain of Akt (PDB: 1H10) were extracted from the protein data bank[163]. The crystal structure of CaM was bound to four calcium molecules, while the PH domain of Akt was bound to 1,3,4,5-tetrakisphosphate (IP_4), which is the polar head of PIP_3. Using InteractiveROSETTA[28], the structures were docked to obtain the initial complex structures of the CaM-PH domain that were subjected to molecular dynamic (MD) simulations. Residues 1- 4 in CaM were missing in the crystal structure but were inserted using Discovery Studio [164] before molecular docking. Further, multiple decoys of CaM-PH domain complexes were collected after a series of docking with InteractiveROSETTA [28]. The chemical shift perturbations (CSPs) from previous NMR studies[18, 27] were traced, and the highly perturbed residues (>0.1ppm) were mapped onto the crystal structures of both CaM and PH domain, which were utilized to guide the interface residues of the dimeric complexes. The predicted CaM-PH domain complex decoys were ranked based on the Rosetta energy scoring function. The CaM-PH domain complexes were carefully selected based on these energy scores, conformations, and interface residues that agreed with the available NMR data. It is worth emphasizing that for every CaM conformation, initial configurations of CaM-PH domain complex were selected: five configurations (Configs. 1-5) for extended CaM and three configurations (configs. 6-8) for collapsed CaM. Utilizing the NACCESS software [165], all configuration (Configs. 1-8) accessible surfaces (ASA) were computed as displayed in Table 3.1. Intriguingly, the molecular docking results of InteractiveROSETTA[28] uncovered that the N-lobe of extended CaM alone is unable to bind the PH domain, but the C-lobe alone is able to form a stable complex with the PH domain. Using another prediction tool, Protein Interactions by Structural Matching (PRISM) [166], similar binding modes between CaM and the PH domain of Akt were obtained. But what remains peculiar about the C-lobe in

forming a stable complex with the lipid-binding PH domain is yet to be established. Of note, during the docking process, IP_4, which lacks the acyl chains, and the glycerol group was excluded or removed for the lipid-binding PH domain to obtain the CaM-PH domain dimeric complexes. However, to observe the influence of IP_4 on the CaM-PH domain association, initial configurations of CaM-PH domain complex comprising IP_4 by adding IP_4 to the ***β***-sandwich pocket of the PH domain using the same Configs 1-8 were generated by PyMOL molecular graphic system [167]. Eight additional configurations with the small molecule, IP_4 were obtained: five configurations (Configs. 9-13) with extended CaM and three configurations (Configs. 14-16) with collapsed CaM (Table 3.2). All simulation inputs were built using the CHARMM all-atom additive force field (version c42) [163, 164]. For the simulations with IP_3/IP_4, the coordinates of 4IP (IP_4 in this dissertation) were extracted from the crystal structure of the PH domain (PDB 1H10). Additionally, the standard CHARMM program [168] provides the topologies and parameters for the phosphatidylinositol lipids, PIP_2 and PIP_3. The inositol head groups of the lipids were extracted and modified to IP_3 and IP_4. The same topologies and parameters adopted from the phosphatidylinositol lipids were applied to these small molecules.

Table 3.1. Accessible surface area (ASA) for Configs. 1-8 for initial docked structures. The ASA for each predicted configuration was calculated using Naccess standalone version. Here, to calculate the accessible area buried between CaM and Akt-PHD, we ran three separate calculations. Once for CaM (chain A), once for PHD (chain B), and a third time for the CaM–PHD (AB) complex. We then subtracted the AB surface from the (A+B) surfaces to obtain the buried surface in the CaM–PHD complex.

CaM–PHD complex	**Accessible surface area (Å^2)**				
	CaM (chain A)	**PHD (chain B)**	**CaM–PH (A+B)**	**CaM–PH (AB)**	**(A+B) - AB**
Configs. 1	11129.8	8231.8	19361.6	18039.5	1322.1
Configs. 2	10821.9	8283.0	19104.9	16877.0	2227.9
Configs. 3	10866.1	8385.2	19251.3	17386.8	1864.5
Configs. 4	10845.2	8348.1	19193.3	17578.0	1615.3
Configs. 5	10870.2	8361.3	19231.5	17948.2	1283.3
Configs. 6	10372.9	8459.0	18831.9	17664.2	1167.7
Configs. 7	10447.6	8321.2	18768.8	17686.9	1081.9
Configs. 8	10316.4	8414.1	18730.5	17421.1	1309.4

Table 3.2. Initial configuration of CaM-PH domain complexes

CaM–PHD complex	CaM conformation (PDB)	IP_4 binding to PHD
Configs. 1-5	Extended (1CLL)	Yes
Configs. 6-8	Collapsed (1CDL)	
Configs. 9-13	Extended (1CLL)	No
Configs. 14-16	Collapsed (1CDL)	

3.1.2 Atomistic molecular dynamics simulation procedure for CaM-PH domain complexes

Following the molecular docking, atomistic MD simulations for all sixteen configurations with and without IP_4 were performed in an aqueous solution. The MD simulation protocols described herein closely mirror those of the previous publications [169-179]. At the initial stages of the simulation, several rigid body minimization steps (10, 000 steps), followed by a dynamic cycle of 50,000 steps, were implemented for all the systems. The TIP3P water model was employed to obtain the isometric unit cell box containing the CaM-PH domain dimeric complex. The unit cell box dimensions were $100 \times 100 \times 100$ Å^3 consisting of 265 amino acid residues in total: 148 amino acid residues in CaM and 117 amino acid residues belonging to the PH domain. Subsequently, to maintain the system's neutrality, the systems were neutralized with counterions to satisfy the ion concentration close to 100mM: 68 Na^+ and 50 Cl^- (for non- IP_4 complexes) and 72 Na^+ and 46 Cl^- (for complexes with IP_4). Further still, in the pre-equilibration stages of the MD simulations, harmonic restraints were applied to every heavy atom ($k = 5$ kcal/mol/Å^2/atom) and eventually relaxed to $k = 0$ with a full particle mesh Ewald (PME) calculation for long-range electrostatic interactions. Additionally, a 12Å cutoff local interaction distance for electrostatic and van der Waals (VdW) calculations was considered along with a scaling

factor of 1-4 short-range electrostatic and VdW interactions. Subsequently, the Langevin temperature control was deployed for maintaining a constant absolute temperature at 310K, while the Nosé-Hoover Langevin piston pressure control was employed to sustain the pressure at 1 atm. The NAMD parallel-computing code [180] was utilized on the Biowulf cluster at the National Institute of Health (NIH) located in Bethesda, Maryland, USA for the production runs of 1 μs (1000 ns) at 2 fs/step. To guarantee that equilibrium was achieved for every system, the so-called root-mean-square deviation (RMSD), and the energy trajectories were calculated as a function of time. Ultimately, the CHARMM program [168] was employed to analyze the simulation trajectories, and the average were after 300ns to discard initial transient trajectories. The average interaction energy was computed over the last half of the 1,000ns trajectory to ensure that the systems reached to equilibration after 500ns. The total interaction energy presented here, which was computed by the CHARMM program [168], is simply the sum of electrostatic and vdW interactions between the CaM-PH domain dimeric complex.

3.1.3 Binding free energy calculation for CaM-PH domain complexes (MM-GBSA Calculations)

To determine the binding free energy of CaM-PH domain interplay or interaction, the molecular mechanics energies combined with the generalized Born surface area continuum solvation (commonly termed MM-GBSA) was employed. Equation 1 depicts the average binding free energy, which is obtained from the Gibbs free energy, constitutes three components: the gas phase contribution, the solvation contribution, and the entropic contribution.

$$\langle \Delta \boldsymbol{G_b} \rangle = \langle \Delta \boldsymbol{G_{sol}} \rangle + \langle \Delta \boldsymbol{G_{gas}} \rangle - \boldsymbol{T\Delta S}, \qquad \textit{(1)}$$

As depicted in equation 1 above, the $\boldsymbol{G_b}$ notation denotes the binding free energy, $\boldsymbol{G_{sol}}$ is the solvation energy contribution, $\boldsymbol{G_{gas}}$ is the gas phase contribution, and $\boldsymbol{T\Delta S}$ is the entropy contribution. Of note, the angle brackets in equation 1 indicate the average taken along the simulation trajectories. The solvation free energy constitutes the electrostatic contribution and the non-polar contribution, $\boldsymbol{\Delta G_{sol}} = \Delta \boldsymbol{G_{sol}^{elec}} + \Delta \boldsymbol{G_{sol}^{non-polar}}$, and was computed by GB using the GBSW module of the CHARMM program [168]. The electrostatic contribution to the solvation free energy, $\Delta \boldsymbol{G_{sol}^{elec}}$ was calculated by solving the Generalized

Born equation within the CHARMM program [168]. The non-polar contribution of the solvation free energy was calculated using the $\Delta G_{sol}^{non-polar} = \Upsilon\, SASA + \beta$, where *SASA* denotes the solvent accessible surface area with the set of surface tension parameters. The total entropy term, $T\Delta S$ is further portioned into translational, rotational, and vibration contributions as depicted here. $T\Delta S = T\Delta S_{trans} + T\Delta S_{rot} + T\Delta S_{vib}$. The translational and rotational entropies were evaluated from the calculation of the principal moment of inertia and obtained the vibration entropy from the quasiharmonic mode calculation in the VIBRAN module of the CHARMM program[168]. Overall, the alteration in the binding free energy due to complex formation between CaM and the PH domain of Akt is computed as follows.

$$\Delta G_b = G_b^{Complex} - (G_b^{CaM} + G_b^{PHD}). \quad (2)$$

A detailed description of the calculation protocol can be found in the previous publications [170-179]. The change in the binding free energy triggered by the small molecule, IP_4 in CaM-PH domain interaction can be obtained by equation three.

$$\Delta\Delta G_b = \Delta G_b^{with} - \Delta G_b^{without}, \quad (3)$$

Where the 'with' and 'without' superscript in equation three denote the involvement and non-involvement of IP4 in the CaM-PH domain association, respectively.

3.2 Generating the full-length Akt1.

The full-length Akt has 480 amino acids, and its sequence was obtained from UniProt KB [181] (ID: P31749). The crystal structures of wild-type Akt inactive state (PDB: 6S9W [31] and 4EJN [30]) were used to model the full-length Akt protein kinase as in Figure 3.3. The missing coordinates in the PH domain, the PH-kinase linker, and the C-terminal regulatory domain (residues 1-2, 113-141, 30-303, and 445-446 in 6S9W, and residues 1-3, 43-49, 110-143, 188-200, 302-306, and 439-446 in 4EJN) were obtained by a hierarchal iterative template-based threading method employing the I-TASSER predictor [32]. For 6S9W, the best model obtained from the I-TASSER program [32] has an acceptable C-score of -0.32 and an estimated TM-score of 0.67 ± 0.13. For 4EJN, it has a C-score of 0.06 and an estimated TM score of 0.72 ± 0.11. Two modeled structures of full-length Akt derived from different crystal structures (Models 1 and 2) were utilized to obtain the nucleotide-bound, mutational, and phosphorylated forms of Akt.

Both modeled Akts exhibit nucleotide-free kinase domains (hereafter called apostate). To construct ATP-bound Akt, the kinase domain of Akt (PDB: 4EKK, initially crystalized with non-hydrolyzable ATP derivative, adenylyl imidodiphosphate AMP-PNP, Mn^{2+}, and GSk3β-derived peptide [29]) was superimposed with the apostate Akt. The GSk3β-derived peptide was removed before superimposition, and AMP-PNP and Mn^{2+} were replaced with ATP and Mg^{2+}, respectively, obtaining the coordinates of ATP and Mg^{2+}. The ADP-bound Akt was further obtained by replacing ATP with ADP. To observe the disruption of PH-kinase domain interaction, the kinase domain residue Asp323 at the PH-kinase interface was mutated to His. The kinase domain mutation D323H is predicted to perturb PH-kinase domain interaction. To obtain the initial configuration of active Akt, we modified two phosphorylated sites at Thr308 and Ser473 by using Using Discovery Studio software [164], generating the phosphothreonine (pThr308) and phosphoserine (pSer473) residues. For each model of Akt, six configurations (Configs. 1-6) with Model 1 and the other six configurations (Configs. 7-12) with Model 2 were generated. For Model 1, these are apostate, ADP-bound, ATP-bound, apostate D323H mutant, ATP-bound D323H mutant, and phosphorylated forms of Akt for Configs. 1-6, respectively. The same for Configs. 7-12, respectively, for Model 2. A total of twelve configurations of Akt were subjected to MD simulations, each with 1 μs, as described in Table S1(table 3.3)

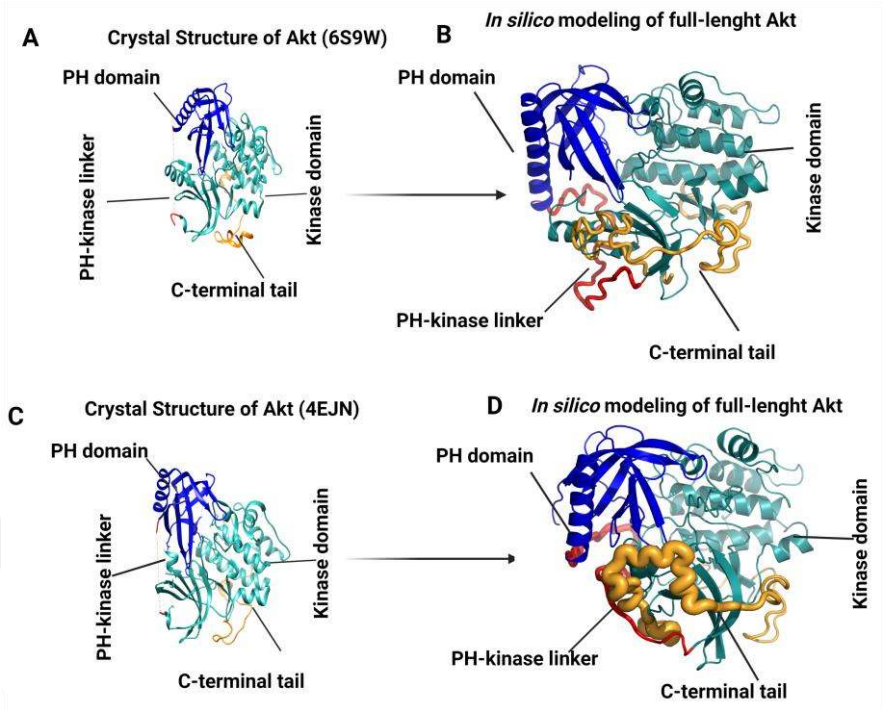

Figure 3.1 crystal and modeled structure of full-length AKT. The PH domain, PH-kinase domain, kinase domain, and the C-terminal tail are colored blue, red, cyan, and gold, respectively.

3.2.1 Atomistic molecular dynamics protocol of full-length Akt.

We employed the updated CHARMM [168] all-atom additive force field (version 36m)[182, 183]. Our simulations closely followed the same protocol as in our previous works [20]. TIP3 water model was used to solvate the systems, constituting the isometric unit cell box of 120 × 120 × 120 $Å^3$. The appropriate number of counterions (100 Na^+ and 95 Cl^-) were added to each system to maintain its neutrality. The solvents around the harmonically restrained protein were subjected to a series of minimization cycles of 10000 steps using the conjugate gradient method, followed by a dynamic cycle of 50000 steps. During the preequilibration stages, harmonic restraint (k = 5 kcal/mol/$Å^2$/atom) was applied to heavy atoms in the protein backbone and gradually relaxed to k = 0 with a full particle mesh Ewald (PME) calculation for long-range electrostatic interactions. In the production run, 2 fs/time step was selected, and the SHAKE algorithm was employed to constrain the length of bonds involving hydrogen atoms. The non-bonded cut-off interactions were set to 12.0 Å, and the PME algorithm was deployed to handle long-range electrostatic interactions. The Langevin temperature control was utilized to handle constant temperature at 310 K, and the Nosé-Hoover Langevin piston

pressure control maintains the pressure at 1 atm. The NAMD parallel-computing code [180] was employed for the production run of 1 μs for each system on a Biowulf cluster, National Institute of Health (NIH) in Bethesda, Maryland, USA. A total of 12 μs of simulations were performed. The root-mean-square deviation (RMSD) as a function of time and root-mean-square fluctuation (RMSF) of protein residues were computed to ensure that each system reached equilibrium. The trajectory files were analyzed with the CHARMM program [168]. All plots were generated with Python, and figures were generated with Pymol [167] and BioRender.

3.3 Clustering the ensembles of CaM-PH domain complexes

The ensemble Cluster in Chimera [184] can cluster members of a conformational ensemble of a protein containing the same atoms and present the clusters of protein conformations. To determine the most populated (favorable) state (conformation) of each CaM–PHD dimeric complex, we clustered all the simulation frames using Chimera [184] with a step size of 10 and selected the topmost clusters. The ensemble clustering in Chimera is based on pairwise best-fit RSMD values, which returns the clusters, their sizes, and their conformational representatives. In the clustering, 10,000 frames for each configuration from the simulations were employed in Ensemble Cluster using a tool in the MD/Ensemble Analysis categories. Bio-3D [185] was deployed to perform Principal Component Analysis (PCA) on the trajectories for each model to obtain a PCA conformer plot, a scree plot, and a collective motion defined by PC1.

Chapter 4

The interplay between Calmodulin and the PH domain of Akt

4.1 Calmodulin and the PH domain of Akt

In breast cancer cells, it has been reported that Cam binds to the PH domain of Akt upon epidermal growth factor stimulation. When Cam co-localizes with the PH domain, it recruits Akt to the plasma membrane to enable Akt membrane binding and activation. The disruption of the interplay between CaM and the PH domain by CaM antagonist inhibited CaM-PH domain complex translocation to the plasma membrane, resulting in cell death in tumorigenic mammary carcinoma cells. NMR experiments have established how CaM binds to the PH domain and showed the conformational rearrangements, which are involved that facilitate Akt translocation to the plasma membrane[18, 27]. In this section of the dissertation, atomistic MD simulations were carried out on the 16 configurations of CaM–PH domain complexes. Configs. 1-8 are without IP_4 (Figure B.2A) and Configs. 9-16 with IP_4 (Figure B.2B). During the simulations, the interaction between CaM and Akt-PH domain appears to be thermodynamically stable, favorable especially for configurations with extended CaM as depicted in the final conformations of the CaM–PH domain complex (Figure 4.1A). However, when IP_4 is loaded onto the PH domain (Figure. 4.1B), the CaM–PH domain interaction appears weaker, causing the N-lobe of CaM to dissociate from the complex rapidly. In the collapsed form of CaM, some configurations show stronger binding in the presence of IP_4, especially when IP_4 is far away from the CaM–PH domain interface. The root mean square deviation (RMSD) profiles (Figure B.3) of the configurations show that the PH domain is more stable compared to CaM, whose fluctuation increases when IP_4 was involved in the dimeric interface.

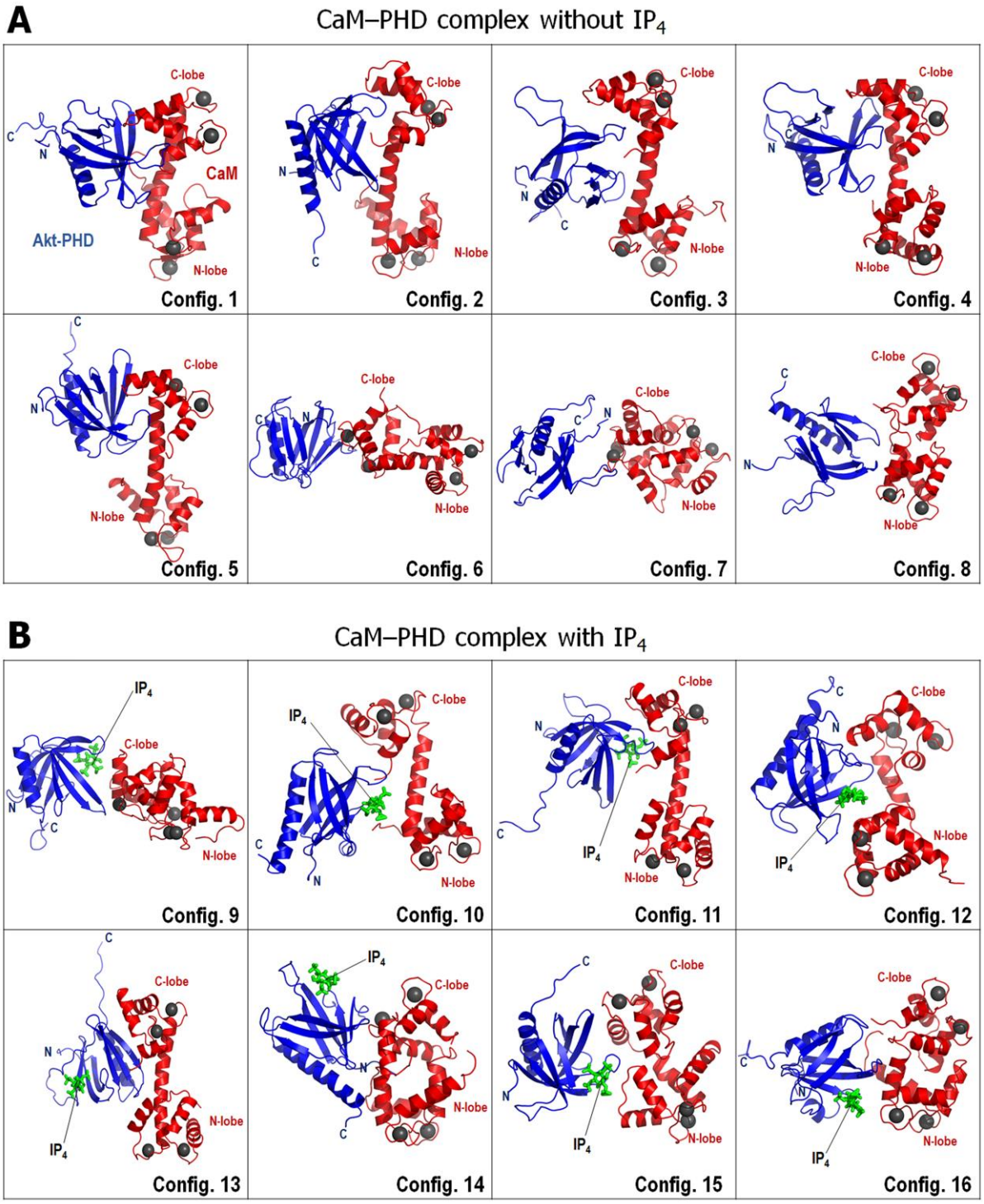

Figure 4.1 Final structures of the CaM–PHD complex. Cartoon representatives of the CaM–PHD complex for (A) Configs. 1-8 without IP_4 and (B) Configs. 9 -16 with IP_4. CaM is colored red and PHD is colored blue. The N-lobe and C-lobe of CaM are marked. The marked "N" and "C" denote the N- and C-terminus of PHD, respectively. A small molecule, IP_4, in the pocket of PHD is marked.

4.2 Selection of best models for CaM-PH domain dimeric complex.

Following the simulations of selected models, statistical and conformational analyses were performed to select the best would-be models of CaM–PH domain dimeric complexes. First, we computed the total interaction energy (contributions from electrostatic and vdW interactions) for the complex with and without IP_4. For Configs. 1-8 without IP_4 (Figure B. 4A), the averaged total interaction energy showed that the extended CaM (Configs. 1-5) appears to have a more robust interaction with Akt-PH domain than the collapsed CaM (Configs. 6-8), suggesting a favorable CaM conformation in the interaction with the PH domain. It is expected that in the presence of IP_4, the interaction of CaM with Akt-PH domain can decrease due to competition with IP_4. This prompts us to delineate probable models of the CaM–PH domain interaction. For CaM with the extended linker, Configs. 9, 11, and 13 decrease the CaM–PH domain interaction when IP_4 is loaded to the PH domain compared to the corresponding Configs. 1, 3, and 5 without IP_4, respectively (Figure B.4 B). This is consistent with experimental findings[18, 27] when CaM cannot extract Akt-PH domain from the plasma membrane. The experimental results showed that Akt-PH domain has a greater affinity to PIP_3-containing membranes, and CaM is displaced and unable to bind concomitantly [18, 27]. However, Configs. 10 and 12 with IP_4 increase the CaM–PH domain interaction compared to the corresponding Configs. 2 and 4 without IP_4, respectively, indicating a less favorable CaM–PH domain interaction model. For CaM with the collapsed linker, we also observed that Configs. 14-16 with IP_4 increase the CaM–PH domain interaction compared to Configs. 6-8 without IP_4, respectively. This suggests that the collapsed CaM may not be a populated conformation in interacting with the lipid-binding PH domain.

Next, we determined the Gibbs free energy from MM-GBSA calculations (Figure 4.2). The details of the decomposition of each term of the Gibbs free energy are summarized in Table S3. The MM-GBSA results were broadly consistent with the interaction energy. Configs.1, 2, 5, 3, and 4 are arranged in the order of decreasing binding free energy, all of which agreed with the NMR data[18, 27] except Config. 4. That is, Config. 12 with IP_4 has a more favorable binding free energy than Config. 4, which contradicts the experimental findings[18, 27]. Also, the MM-GBSA results indicate that the CaM with collapsed linker is not consistent with NMR experiments. For instance, Configs. 6 and 7 without IP_4 yielded positive binding free energy values, whereas Configs. 14 and 15 with IP_4 yielded negative

values of the binding free energy. Config. 8 without IP_4 produced negative binding free energy, but Config. 16 with IP_4 shows a better binding. Finally, we computed the change in binding free energy, $\Delta\Delta G_b$, due to the presence of IP_4 for all systems (Table 4.1). $\Delta\Delta G_b$ is increased for Configs. 1, 2, 3, and 5, indicating that IP_4 possibly disrupts or weakens the interaction between CaM–PH domain, consistent with the experiments. For the remaining configurations, we observed what was contrary to the NMR experiments [18, 27]. In short, Configs. 1, 2, 3, and 5 of CaM–PH domain complexes were selected as the best models based on the criteria, which are supported by the NMR data [18, 27]. The modeling suggests that the extended CaM may be the populated conformation in the interaction with the PH domain of Akt.

Table 4.1 The change in binding free energy, $\Delta\Delta G_b$, due to the presence of IP_4 in the CaM–PHD interaction calculated by equation (3).

CaM–PHD complex with IP_4		**CaM–PHD complex without IP_4**		**$\Delta\Delta G_b$ (kcal/mol)**
Config.	**ΔG_b (kcal/mol)**	**Config.**	**ΔG_b (kcal/mol)**	
9	13.66	1	-57.46	71.13
10	-8.73	2	-39.37	30.63
11	-6.19	3	-33.44	27.24
12	-47.46	4	-23.58	-23.88
13	- 4.38	5	-37.14	32.76
14	-32.77	6	10.83	-43.61
15	-5.78	7	10.25	-16.04
16	-19.74	8	-16.53	-3.21

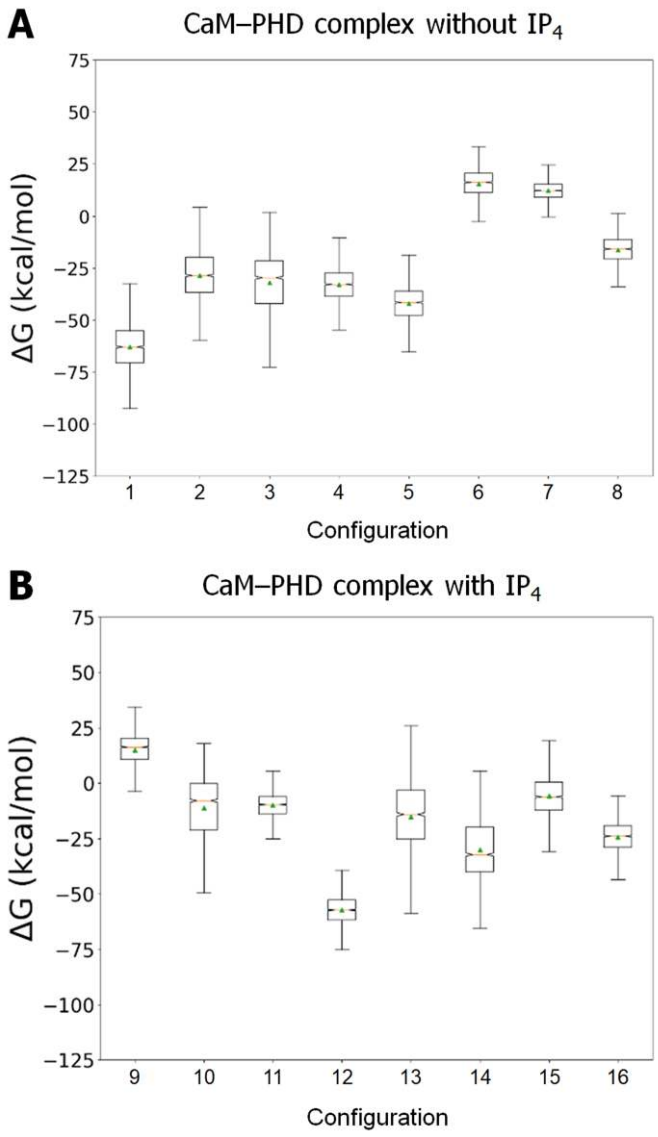

Figure 4.2 Energy profiles of CaM-PH domain complexes

The binding affinity of CaM–PHD. Using Matplotlib in Python, the binding free energy for the CaM interaction with the Akt-PHD during (A) Configs simulation. 1-8 without IP_4 and (B) Configs. 9 -16 with IP_4 have been plotted. In the box graphs, the triangle symbol and horizontal line indicate the mean and median values, respectively, whereas and the box plots and error bars represent the percentage and the standard deviation, respectively.

4.3 Interface residues of CaM-PH domain dimeric complexes.

The NMR and other biophysical and biochemical methods have unearthed CaM's binding to Akt-PH domain with a dissociation constant (K_d) of 100 nM in a 1:1 stoichiometry [18]. These

experiments have also revealed that CaM's N- and C-terminal lobes are essential for Akt-PHD binding and that electrostatic interactions significantly contribute to CaM–PH domain association. Moreover, favorable hydrophobic interactions appear to stabilize the CaM–PH domain dimeric complex [18]. Following the MD simulations, the types of intermolecular interactions (salt bridge, nonpolar, and H-bond) in CaM–PH domain complexes throughout the MD trajectories (Tables S4 and S5) were analyzed for all configurations. Here, the residue pairs are treated as interface residues and considered effective and counted if they have at least 50% occurrence. To corroborate the CaM–PH domain dimeric interface, essential residues involved in the dimeric complex were examined. For instance, in Config. 1, salt bridge formation between residues, R74-E85, D58-R67, E114-K14, E114-R25, E120-R25, E123-R23, K77-E85, D2-R76, E84-R76, and E120-R23 (where the former and latter residues respectively denote CaM and PH domain), retain the dimeric interface. Also, nonpolar interactions between residues, I9-M63, A73-M63, M124-I19, A128-I19, M144-I19, L112-I84, F92-I84, G113-F55, M71-P68, and L4-M63, contributed to the complex formation. Polar interactions between residues, T5-Q61, T70-T65, Q143-Y18, and Q3-Q61, and hydrogen-bond between A128-Y18, appear to contribute to the CaM–PH domain association strongly. Similar analyses were performed for the remaining complexes. In Config. 4, while both salt bridge and nonpolar interactions contribute to the binding, we observe no polar interactions and H-bond formations between CaM and PH domain of Akt, which may have led to a decrease in the overall binding strength. For the collapsed CaM without IP_4 (Configs. 6, 7, and 8), salt bridges, nonpolar and polar interactions contribute to the binding energy. H-bonds are observed in Configs. 6 and 8 but not Config. 7. It came as no surprise that in Config. 9 (IP_4 form of Config. 1) with fewer H-bonds, nonpolar and polar interactions salt bridges are lost suggesting that IP_4 weakened the interaction. Further still, in Configs. 10 and 11, salt bridges and nonpolar interactions occur. Polar interactions are observed in Config. 10 but are not in Config. 11, and both contain no H-bonds, also indicating that IP_4 disrupted the interaction. For Configs. 12 and 13, there is no loss of salt bridges, H-bonds, nonpolar and polar interactions; however, in Config. 12, while polar interactions and H-bonds occur, these interactions are lost in Config. 4. Finally, Configs. 14, 15, and 16 retain a more significant number of salt bridges, H-bonds, nonpolar and polar interactions than Configs. 6, 7, and 8, respectively, hence decreasing their binding free energies. This decrease in binding free energy between collapsed CaM and PH domain suggests that IP_4 plays an infinitesimal role in disrupting the interactions

but may contribute to the binding energy. This observation was also not surprising since the binding pocket of IP_4 in the PH domain is oriented differently from the binding region of the collapsed CaM. Taken together, it is hypothesized that IP_4 can weaken the interaction between the extended CaM–PH domain complex, whereas IP_4 is unlikely to disrupt the interaction between collapsed CaM–PH domain complex. Additionally, some common salt bridges were found in the following pairs of Configs: Config. 1 and Config. 2 (E114-R23), Config. 1 and Config. 3 (R74-E85, E123-R23, E120-R23), and Config. 1 and Config. 5 (E114-K14, E114-R25). Interestingly, no common salt bridges were found among the complexes, which may be attributed to different conformations of predicted docked structures. Additionally, comparing the complex without IP_4 and with IP_4 pairs (Tables S4 and S5), the following salt bridges were observed: for Config. 1, there are 10 salt bridges, all of which are lost in Config. 9; for Config. 2, there are 3 salt bridges, while in Config. 10 there are 2 salt bridges, and no common salt bridges were found between them. In Config. 3 and Config. 11 three common salt bridges are found (K115-E40, E114-R25, and E127-R69), and there are 9 salt bridges in Config. 3 compared to Config. 11 that has 4 salt bridges.

4.4 The interface residue of CaM-PH domain complexes corresponding to the NMR chemical shift data.

A significant number of residues that correlated with the experimental NMR data results were observed [18, 27]. For instance, upon titration of CaM's N-lobe into Akt-PHD, residues R16, I19, T21, V45, N53, T82, I103, T105, V106, D108, K111, T82, and W80 in the PH domain showed significant chemical shift changes. Titration of CaM's C-lobe into Akt-PHD led to noticeable chemical shift changes for residues including K14, R15, G16, I19, T21, W22, R23, V45, E49, and N53. To complement the NMR CSPs, we calculated the backbone amide CSPs for the PH domain residues using the SHIFTX2 program[186]. The program uses the protein coordinates as input to predict the backbone and sidechain 1H, 13C, and 15N chemical shifts for proteins. The best representative models of CaM–PH domain complex, Configs. 1, 2, 3, and 5 were subject to the CSP calculations. In the PH domain of Akt, many residues exhibit perturbations upon binding to CaM (Figure 4.3). Among the residues with >0.1 ppm, R15, G16, Y26, G37, D44, V45, Q59, and W80 significantly contribute to the interaction with CaM, consistent with the NMR CSPs. Also, in CaM, hydrophobic residues, or the methyl group (CH_3) of Met, M36, M51, M71, M72, M76, M109, M124, M144, and M145 located in the C-

terminal lobe within the hydrophobic patch contributed to Akt-PH domain binding. The NMR experiments also affirmed that Akt-PH domain engages both lobes of CaM, with CaM's N-lobe recognizing the loop connecting β6 and β7, while the C-lobe tends to bind to the loop connecting β1 and β2 [27]. Assessing the predicted complex for the occurrence of these residues in the interfaces, several residues were found within the interfaces that agreed with the NMR data [18, 27] (see Tables S4 and S5). For example, in Config. 1, salt bridge formation between the residues E114-K14, E114-R25, E84-R76, and nonpolar interactions between the following pair of residues, M124-I19, M144-I19, M71-P68, and H-bond between A128 and Y18 was observed. Similarly, for Config. 3, nonpolar interactions between the following pairs of residues, M109-I19, M144-I19, M145-I19, M72-W80, M76-W80, F92-I19, were also observed. Altogether, the occurrence of these residues in the interfaces of the predicted CaM-PH domain dimeric complexes confirms the predicted models in this dissertation. Correspondingly, I19 and Y18 in the Akt-PH domain were greatly involved in nonpolar and polar interactions, respectively. The involvements of I19 and Y18 in these atomic interactions were unsurprising since they are located within the loop connecting β1 and β2. The aromatic residue, W80 situated in the loop connecting β6 and β7, was significantly involved in nonpolar interactions with several CaM residues, M71, M51, and L69. An aromatic residue like Trp has a high tendency to anchor to hydrophobic regions of CaM. Taken together, these analyses showed that especially Configs 1, 2, 3, and 5 are good models for further studies to elucidate the association between CaM and the PH domain.

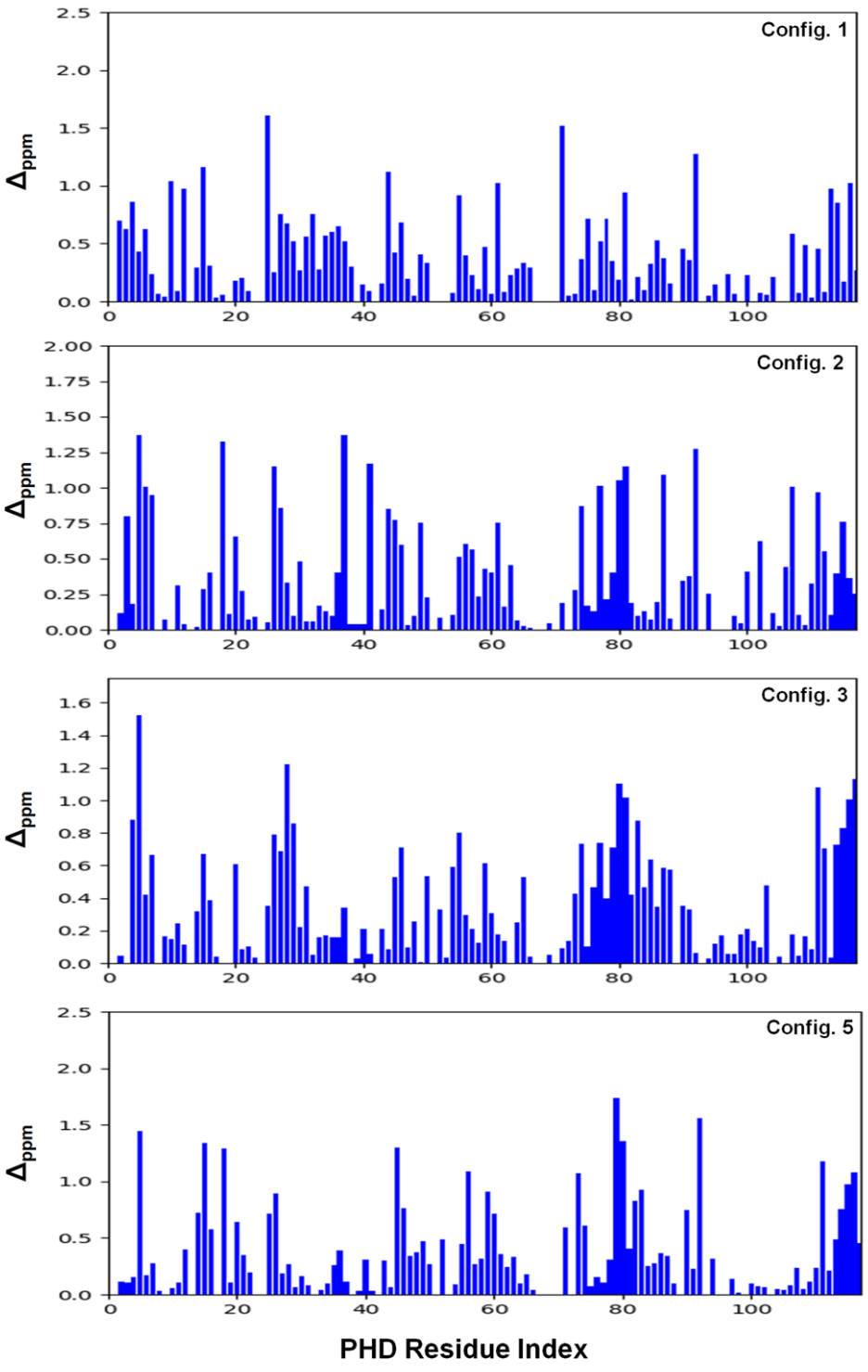

Figure 4.3 The calculated amide chemical shift perturbations (CSPs) for the PH domain residues in the CaM–PH domain configurations (Configs. 1, 2, 3, and 5). The ^{1}H, ^{13}C, and ^{15}N chemical shifts were computed by the SHIFTX2 program [186]. The combined CSPs for PH domain over the CaM–PH domain complex trajectory and the PH domain alone trajectory were computed during the MD simulations utilizing the equation, $\Delta_{ppm}= \sqrt{(\Delta\delta_{HN})^2 + (\Delta\delta_N\alpha_N)^2}$, where δ_{HN}, and δ_N indicate the ^{1}H, and ^{15}N chemical shift difference, in the order given between the CaM–PHD and the PHD trajectories. A scaling factor, $\alpha_N = 0.17$ was applied to the difference in ^{15}N chemical shift.

In a similar vein, we identified and mapped the interface residues of the best complex model using the best representative structures from the MD simulations. The goal was to evaluate the selected complex configurations and determine their agreements with the NMR data [18, 27]. Snapshots representing the conformations of the best configurations of CaM–PH domain dimeric complexes (Configs. 1, 2, 3, and 5) without IP_4 are illustrated in figure 4.4. The HotPoint server [187] was used to extract these interface residues. Consistent with the NMR data, for Config. 1, the occurrence of the residues, K14, R15, E17, Y18, I19, K20, R23, and R25 at the Akt-PHD interface, whereas, in CaM, M71, E114, M124, M144, M145, and A147 also occur at the interface (Table 2) were observed. The occurrence of CSP residues from the NMR experiments is observed in the remaining configurations. We observed that the β-sheets in the Akt-PHD, especially β1, β2, β6, and β7 and the loops that connect them are significantly involved in binding CaM, whereas the N-and C-terminal lobes and the central linker of CaM are required for Akt-PH domain binding. Taken together, the MD simulations indicate binding of CaM to Akt-PH domain is thermodynamically stable but differs from CaM's typical binding mode, which usually involves helical regions [188, 189].

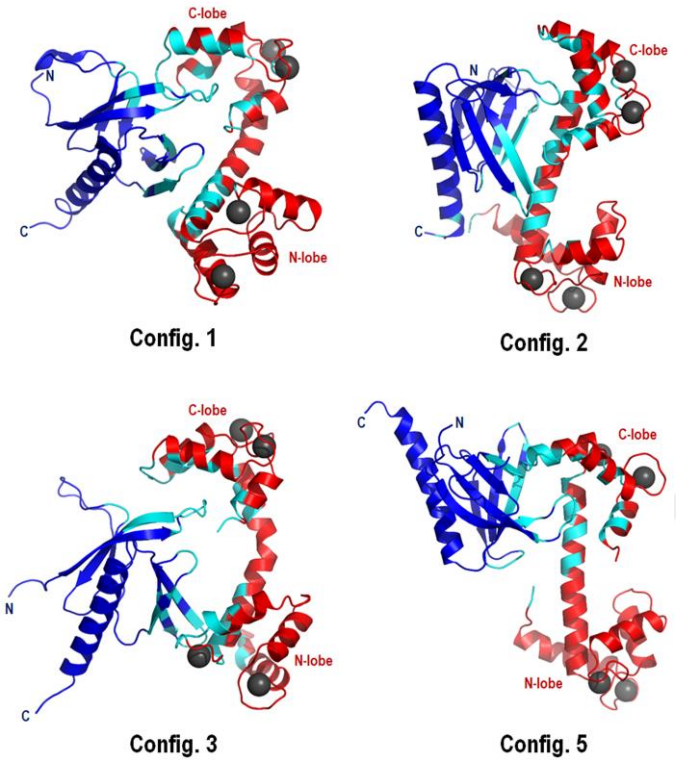

Figure 4.4 The best conformations of the CaM–PH domain complex. Snapshots representing the best conformations of the CaM–PH domain complex, Configs 1, 2, 3, and 5, without IP_4. In the solid ribbon presentation of the secondary structure, the PH domain and CaM are colored light blue and red, respectively. Ca^{2+} is colored grey depicted as a sphere. The interface residues between the CaM and PH domain are colored cyan and listed in Table 4.1.

TABLE 4.2 Interface residues of topmost cluster of the best models (Configs. 1, 2, 3, and 5). Of note these interface residues were obtained within 4 Å distance.

CaM–PHD complex	CaM	PHD
Config. 1	L4, T5, E6, Q8, I9, A57, E67, T70, M71, A73, M76, K77, L105, M109, L112, G113, E114, K115, L116, T117, E119, E120, E123, M124, E127, A128, V136, F141, M144, M145, A147, K148	K14, R15, G16, E17, Y18, I19, K20, T21, R23, R25, K39, P51, L52, N53, N54, Q61, M63, K64, T65, E66, R67, I74, R76, V83, I84, E85, R86, T87
Config. 2	A1, D2, M51, E54, V55, T70, M71, R74, K75, K77, D80, S81, E83, E84, E87, A88, V91, F192, I100, L105, V108, M109, L112, E114, L116, M124, I125, E127, A128, V136, F141, M144, M145, A147, K148	E17, Y18, I19, K20, T21, R23, T34, A50, P51, L52, N53, N54, F55, S56, A58, Q79, W80, T81, T82, V83, I84, E85, R86, Q113, E116,
Config. 3	E7, I9, D50, N53, E54, V55, D56, A57, D58, G59, D64, F65, P66, E67, L69, T70, R74, I85, E87, A88, V91, F92, L105, V108, M109, L112, G113, E114, K115, L116, E120, M124, M144, M145, A147, K148	R15, E17, Y18, I19, K20, T21, W22, R23, P24, R25, K39, E40, Q61, L62, M63, T65, R67, P68, R69, I74, R76, L78, W80, T81, T82, V83, E85
Config. 5	A1, D2, D80, S81, E84, I85, E87, A88, V91, F92, K94, I100, L105, V108, M109, T110, N111, L112, G113, E114, K115, L116, M124, I125, A128, V136, F141, M144, M145	K14, R15, E17, Y18, I19, K20, W22, P51, L52, N53, N54, F55, P68, R69, P70, W80, T82, I84, E85, R86, T87

4.4 Clustering CaM-PH domain dimeric complexes.

Using Chimera[184], the ensembles of the CaM–PH domain complex conformation were clustered. For Config. 1, the top cluster 1 contains 2,070 members, which corresponds to a probability, $p = 0.21$ (21%), 2,070 out of the total 10,000 frames. Also, for Configs. 2, 3, and 5 in cluster 1, there were 1,380, 2,050, and 980 members corresponding to 14%, 21%, and 10%, respectively. The structures for each configuration's best-approximated representative clusters for Configs. 1, 2, 3, and 5, which were selected as the best models based on the criteria, are presented in Figure 4.5. For comparison purposes, the structures for the other models, Configs. 4, 6, 7, and 8 in (Appendix, Figure B.6) were also collected. Based on the information obtained from the clustering coupled with conformational analyses, the favorable configurations for CaM binding to Akt-PHD were presented or proposed. It was deduced that both the N-lobe and C-lobe as well as the central linker of CaM, are vital for Akt-PHD binding. However, whilst the tightly bound C-lobe and the central linker of CaM may be enough for Akt-PH domain binding, the N-lobe alone is not sufficient enough, with the weak binding rapidly dissociating when IP_4 is loaded onto the PH domain of Akt. To observe the conformational changes for configurations with and without IP_4, the top two cluster representatives for selected models (Configs. 1, 2, 3, and 5) (Figure 4.5) were aligned or superimposed. The aligned results show Significant conformational rearrangements of CaM in the complex due to the presence of IP_4 in PH domain were observed.

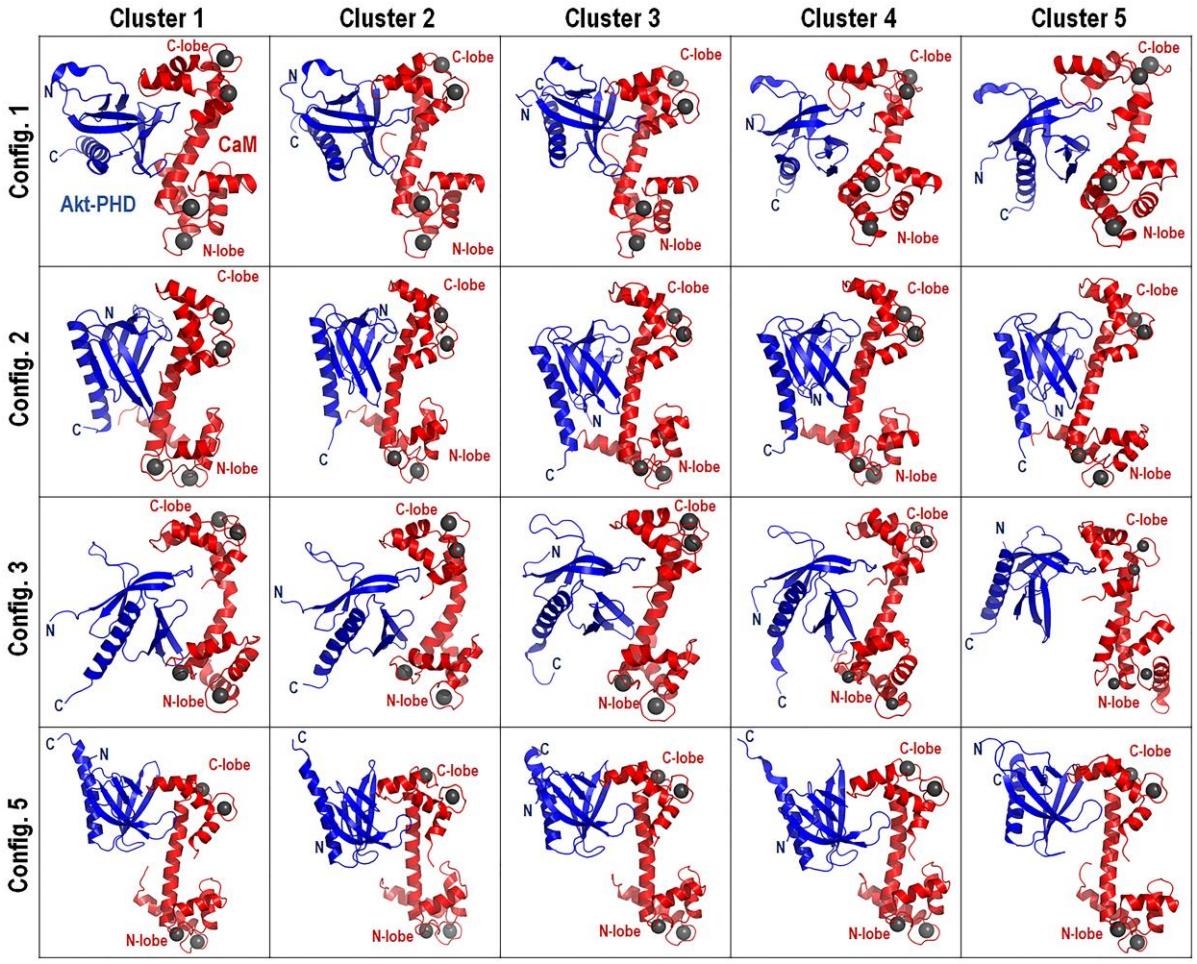

Figure 4.5 The best approximated representative clusters of the CaM–PH domain complex for Configs. 1, 2, 3, and 5. Conformation of the best approximated representative clusters of each model. The top five cluster representatives of best model for Config. 1 were defined with probabilities, p = 0.21, 0.18, 0.12, 0.10, and 0.08 for clusters 1-5, respectively. For Config. 2, p = 0.14, 0.10, 0.09, 0.07, and 0.06; for Config. 3, p = 0.21, 0.10, 0.09, 0.08, and 0.07; for Config. 5, p = 0.10, 0.09, 0.07, 0.61, and 0.06 for clusters 1-5, respectively. The ensemble clustering was based on pairwise best-fit RSMD values, which returns the clusters, their sizes, and their conformational representatives.

4.5 Principal component analysis of CaM-PH domain complexes.

Deploying the Bio-3D [185], an R package for comparative analysis of protein structures, the Principal Component Analysis (PCA) plots were obtained for all models using the simulation trajectories. The PCA is a widely established multivariate method utilized to reduce the number of dimensions required to describe protein dynamics via a decomposition process that filters observed dynamics from the largest to the minor spatial scales [190]. PCA extracts the essential elements in the data by using a covariance matrix or a correlation matrix (hereafter

called C-matrix) constructed from atomic coordinates that describe the protein's accessible degree of freedom, such as the Cartesian coordinates that define atomic displacements in each conformation in the trajectory [191]. Additionally, an eigenvalue decomposition of the C-matrix usually results in a complete set of orthogonal collective modes (eigenvectors), where each eigenvector constitutes a corresponding eigenvalue (variance), which characterizes a portion of the motion, where larger eigenvalues describe motions on larger spatial scales [192]. PCA transforms atomic coordinates into a few PCs (usually 2 or 3) that represent directions where the structure set displays the largest collective variances for protein structural analysis. Of principal importance, PCA generates a conformer plot that permits interpreting inter-conformers relationships. Also, a scree plot, which displays the eigenvalues arranged in descending order, can be utilized to determine significant PCs that capture domain collective variances in the structure set. PCA also outputs a representation of the collective structure motions captured by the top PCs, often related to the protein function [193]. The PCA examines the relationship between the various conformations sampled over a subset of the trajectory of 500-1000 ns (6,000 frames) using the Cα atoms of all models of CaM–PH domain complexes (265 Cα atoms) without IP_4 (Figure 4.6 and Figure B.7). Using hierarchical clustering in Bio-3D [185], the PC1 versus PC2 conformer plot, scree plot, and the collective motion defined by PC1 for all models without IP_4 to depict important variations or conformational changes in CaM–PH domain dimeric complex were generated. For the best models (Configs. 1, 2, 3, and 5), the PC1 versus PC2 conformer plot of Config. 1 account for over 46% of the variance; likewise, Configs. 2, 3, and 5 plots account for over 59%, 43%, and 45% of the variance, respectively (Figure 4. 6). Similarly, for the less favorable models, the PC1 versus PC2 plots of Configs. 4, 6, 7, and 8 account for over 57%, 62%, 79%, and 48%, respectively (Figure B. 7), with Config. 7 capturing most variation or essential dynamics. The scree plots showed the eigenvalues arranged in descending order for all models. For instance, the eigenvalues of the scree plot for Config. 1 dropped from 89.2 to 36.5. The collective motion defined by PC1 presented the CaM–PH domain complex structure colored by the *B*-factor, representing the similar ensembles of the conformations as observed in cluster 1 by Chimera. These conformer plots, scree plots, and collective motions defined by PC1 for all eight models that were sampled throughout the simulations succinctly uncovered important conformational variations or essential dynamics for CaM–PH domain dimer association. Figure 4.6 below depicts the plots.

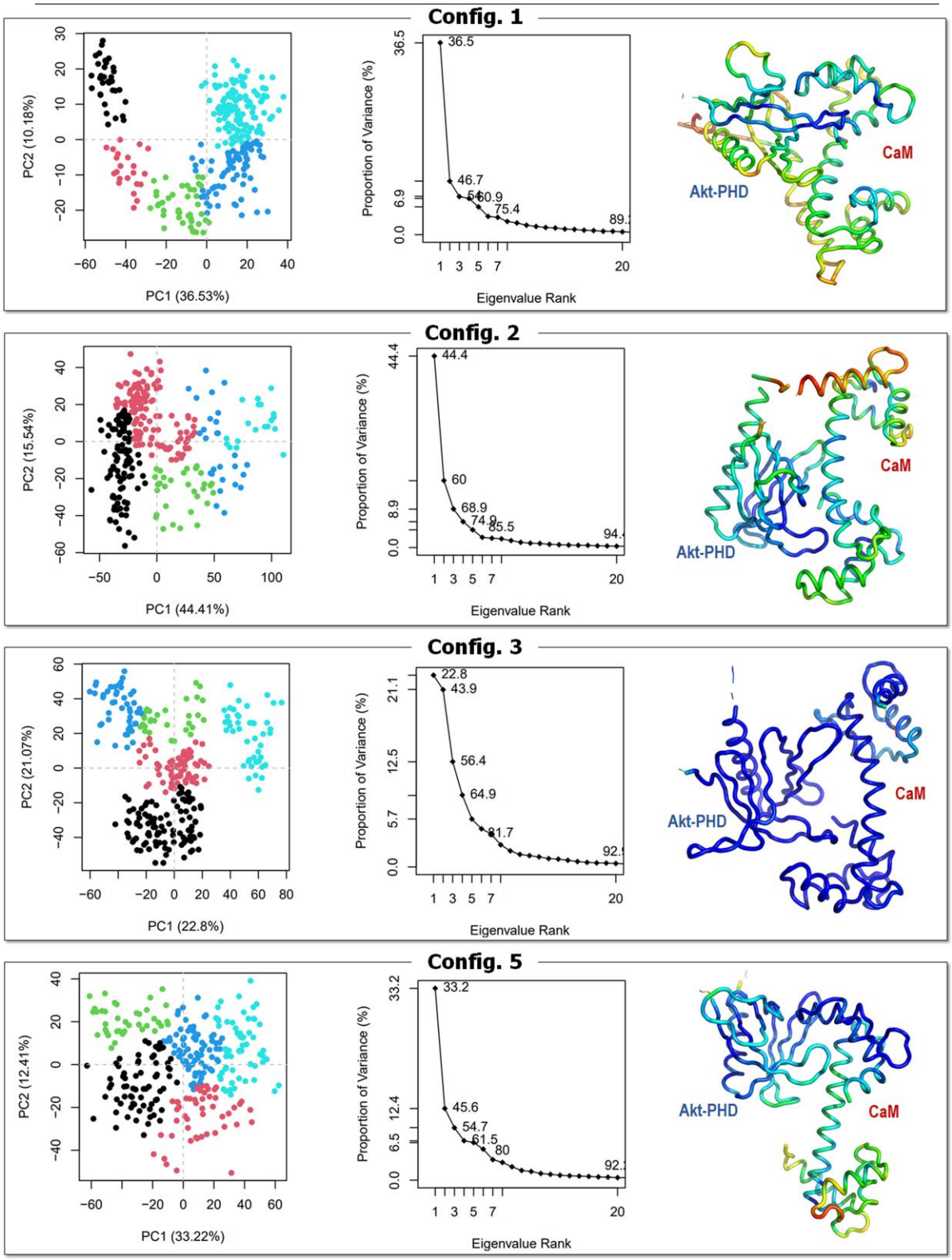

Figure 4.6, Principal component analysis (PCA) for the best models. PC1 versus PC2 conformer plot for Configs. 1, 2, 3, and 5 shows five distinct clusters obtained via hierarchical clustering (hc, $k = 5$, left panels), the eigenvalue scree plot (middle panels), and the collective motion for CaM–PHD complex defined by PC1 representing the structure colored by *B*-factor or temperature factor (right panels). In the *B*-factor structure, blue and red denote atoms with low and high-temperature values, respectively, while light blue, white, and pink denote intermediate temperature values.

4.6 Discussion.

Activation of Akt, the paradigmatic lipid-activated kinase, is crucial for modulating apoptosis, cell proliferation, and oncogenesis. Akt activation is a relatively common tumorigenic occurrence in many cancer types, such as breast cancer [1, 40, 42]. Like other AGC kinases, Akt possesses an N-terminal PH domain, which shares similar structural features with hundreds of analogs in mammals and bacteria [194-196]. The PH domain of Akt plays a critical role in recruiting Akt to the plasma membrane for activation. Akt-PH domain interacts with PIP_3, a signaling phospholipid localized on the inner leaflet of the plasma membrane [40, 42, 111]. Akt translocation to the plasma membrane - an event that triggers its subsequent phosphorylation and activation was proposed to be regulated by PS [16] to promote binding of Akt-PH domain to PIP_3. A study by Lucic *et al.* [108] suggested that Akt phosphorylation and activation by association with membrane lipids are mutually independent. The study further proposed that, in the absence of PIP_3, Akt is dephosphorylated – an event enhanced by the interaction between its kinase domain and PH domain, which leads to Akt autoinhibition [108]. Recent investigations have also suggested that pSer473-Akt activation may be driven by the interplay between the PH domain and kinase domain linker that relieves PH domain-mediated Akt autoinhibition. In that proposed mechanism, two-fold phosphorylation at Ser477/Thr479 activated Akt through allosteric mechanisms involving activation loop interaction, which relieves the autoinhibition by PH domain and weakens PIP_3 affinity [14]. Finally, another proposed mechanism posited that Akt activation in breast cancer involves interaction between its PH domain and the dumbbell-shaped CaM [19, 113]. Disruption of the CaM–PH domain association by an Akt's antagonist inhibited CaM–PH domain recruitment to the plasma membrane and resulted in cell death in mammary carcinoma [19]. Collectively, several mechanisms for Akt translocation to the plasma membrane and activation have been proposed. Here, via MD simulations, the detailed intermolecular interaction between CaM and Akt-PHD and the consequences of the IP_4 interaction, thereby clarifying the mechanism of recruitment to – and release at – the plasma membrane, was established.

Calcium-binding triggers conformational changes in CaM, which expose hydrophobic residues enabling binding to cytosolic target proteins, including partners that are implicated in controlling cell shape and migration [197] and different targets [198]. Computational

modeling supported by NMR established that CaM uses its lobes for binding to the hypervariable region (HVR) and the catalytic domain of K-Ras [199] and the cSH2 and nSH2 domains of p85α, the regulatory subunit of PI3Kα [200]. In the Ca^{2+} bound state, electrostatics alters CaM conformational distributions and dynamics [201], and ensemble analyses with ClustENM [202] showed that CaM's C-lobe has greater mobility compared to the N-lobe. Genetic analysis and protein co-precipitation indicated that the CaM binding segment on Akt is within the first 42 residues [203], which forms a three-stranded β-sheet. CaM binding to the β-sheet is rare because CaM binding fragments often populate α-helical regions [188, 189]. Usually, CaM binding segments on target proteins are about 15-20 residues, hydrophobic/non-polar with a basic character, and high tendency to form an α-helix [189, 204]. The NMR experiments [18, 27] and our MD simulations do not point to α-helical region. The NMR data [18, 27] and our simulations clearly showed that CaM interaction with Akt-PHD involves β-sheets and the loops that connect them. A similar binding mode has been observed for CaM and the Itk-PH domain. Itk (interleukin-2-inducible tyrosine kinase) belongs to the Tec kinase family [205]. Also, a more recent study that aimed to investigate the direct interaction between CaM and the growth receptor bond 7 (Grb7) protein showed that CaM interacts with the PH domain of Grb7 [206]. There, CaM's peculiar binding motif was mapped to β-sheet and not α-helical region [206]. The NMR chemical shift perturbation data for Akt-PHD indicated that it interacts with CaM via the β1/β2 and β6/β7 loops [27]. Itk-PH domain interacts with CaM via β3/β4 and β5/β6 loops [205]. Altogether, in Akt, Itk, and Grb7, the mode of PHDs binding to CaM deviates from that involving helical structures. Here, the modeling and simulations results indicate that the CaM–PH domain association is thermodynamically stable and is maintained by strong intermolecular H-bonds, salt-bridges, polar and non-polar interactions. CaM contains nine critical Met residues located in the N-lobe, the central α-helix, and the C-lobe. Met residues, M109, M124, M144, and M145 in the CaM C-lobe form a hydrophobic region essential for hydrophobic interaction with the hydrophobic residues, I19, W22, and W80 in the PH domain. We propose four models for dimeric representations of CaM–PH domain association based on the MD trajectories analyses. We observe that the C-lobe of CaM is critical for binding. The central helix region and the weak-binding N-lobe of CaM also play a role in binding, especially in the absence of IP_4. When IP_4 is loaded onto the PHD, the interactions between CaM–PHD become weaker; the N-lobe of CaM easily dissociates when IP_4 interferes with the interaction at the C-lobe of CaM, hence weakening the overall

interactions. We cluster the trajectories and present the most populated state for each proposed model and the key interactions that are essential for maintaining the dimeric complexes.

4.6 Concluding Statement on CaM-PH dimeric complex.

Akt activation mechanisms have been proposed. Here, we provide detailed conformational views into how CaM binds to Akt-PHD at the atomic level and the involvement of IP_4 in the CaM–PH domain complex, which weakens or partially displaces CaM. Akt is recruited to the plasma membrane by specific interactions between its PH domain and CaM and PIP_3, a phospholipid found in the plasma membrane that serves as the docking site of Akt [40, 111]. NMR experiments established the binding mode of CaM to the Akt-PH domain, and the observations by both the NMR and our simulations deviate from CaM typical binding mode, which usually involves α-helices [188, 189]. The results here suggest that CaM binds to the β-sheets in Akt-PHD, which is rare, but such binding has been reported by another NMR study as well, where CaM binds to Itk-PHD [205]. Mechanistically, CaM's N- and C-terminal lobes and the central linker simultaneously engage the Akt-PH domain. Akt-PHD binds to one end of CaM, especially the C-lobe, and induces conformational rearrangements engaging the central linker and the N-lobe. Further, the docking and simulation results enable us to select and propose four models (Configs. 1, 2, 3, and 5) of CaM–PH domain dimeric complexes, showing the β-sheets in Akt-PHD binding to CaM. A high percentage of the NMR chemical shift residues were observed in the interface, and most of these residues play an important role in maintaining the dimeric CaM–PH domain complex. The most populated state of each proposed model as well as critical intermolecular interactions that are cardinal to maintain the dimeric complex, CaM–PH domain, is presented. Also, the PC1 versus PC2 conformer plots, scree plots, and collective motions defined by PC1 for all eight models succinctly revealed essential conformational changes or essential dynamics that were sampled throughout the MD simulations. These models indicate how IP_4 acts by weakening, or partially displacing CaM, thereby revealing the detailed molecular basis of the Akt kinase translocation, phosphorylation, and activation. They may also serve as a guide for future research on CaM–PH domain association or serve as a basis for drug development to disrupt the CaM–PH domain complex.

Chapter 5

Mechanism of full-length Akt autoinhibition

5.1 Mechanism of full-length Akt autoinhibition

Molecular dynamics simulations at the atomic level were performed on full-length Akt for 1μs, and the equilibrium conditions were tested, checking the RMSF and RMSD profiles as a function of time. Akt autoinhibition is important for its biological regulations. In this inactive state, the PH domain interlocks the kinase domain to hinder the phosphorylations of Thr 308 in the kinase domain. Here, we performed MD simulations of full-length Akt at the atomic level for comparative analysis to identify the determinants of Akt autoinhibition in the apostate, nucleotide (ADP and ATP)-bound states. Following the molecular dynamics simulations of the full-length Akt systems, the root-mean-square deviation (RMSD), root-mean-square fluctuations (RMSF), and the distance profiles were computed with Pymol and the CHARMM program. As stated earlier, the simulation trajectories of the apostate were clustered using the MD/Ensemble Analysis categories in Chimera software to provide the best representative conformation of Akt autoinhibition. The top five most populated cluster representatives of the trajectories for the apostate were further analyzed.

On the other hand, the nucleotide-bound configurations were not clustered since they are in a transient state, indicating that the 1 μs is insufficient to observe releasing the lipid-binding PH domain from the bilobal kinase core domain. However, the intermolecular interaction of Akt with the nucleotide (ATP and ADP) and magnesium (Mg^{2+}) were analyzed with Discovery Studio (version 19.10) set on the default parameters (Table 1 supplemental material). Also, the PH-kinase allosteric interface residues were determined in Discovery studio and depicted in PyMOL.

5.2 Conformational analysis of full-length Akt apostate

Employing Chimera software[184], we clustered the ensembles of the apostate configurations to provide the best representative conformation of Akt autoinhibition state. The top five most populated cluster representatives from the trajectories for the apostate were further analyzed. The cluster members and their representative frames at which they occurred were considered. The structures for the autoinhibited Akt apostate configuration's best five approximated representative clusters are given in Figure 5.1. From the clustering results and the conformational analysis of Akt configurations, we propose and present the favorable configurations of full-length autoinhibited Akt, where the lipid-binding PH domain intramolecularly interacts with the kinase domain. Following the clustering of the apostate, to determine the interacting residues of the most populated states for each configuration, we selected the topmost cluster structure (cluster 1). We analyzed the interactions in the PH-kinase domain allosteric interface. Our goal was to determine essential interactions that retain the PH-kinase interface. These interactions were determined in Discovery Studio software (version 9) and were further depicted using the PyMOL molecular graphic interface. Several essential interactions were observed in the PH-kinase interface. For instance, in the apostate of model 1, the interface contains critical interactions in the PH-kinase domain allosteric interface, as in Figure 5.2. Table S1 contains the interaction types and details of the interacting residues of model 1. Additionally, in the apostate of model 2, the interface comprises important interactions in the PH-kinase domain interface shown in Figure 5.2.

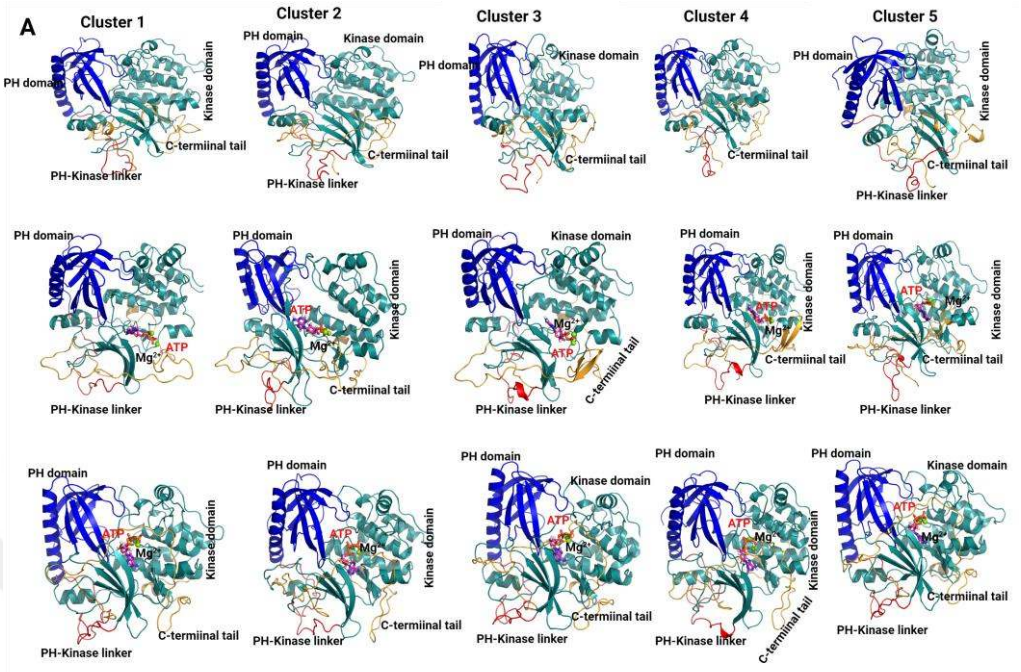

Figure 5.1 Cluster representative of the topmost 5 clusters of apostate Akt. The PH domain, PH-kinase domain, kinase domain and the C-terminal tail are colored blue, red, cyan, and gold respectively. The ATP and Mg 2+ are colored pinked and green respectively.

5.3 The PH-kinase interface residues that retain Akt autoinhibition

This section analyzed the PH-kinase domain interface of the most populated (apostate) of model1 and 2 to determine key residues that maintain the PH-kinase interface in autoinhibited AKT. Figure 5.2 depicts the PH-kinase interface residues shown as sticks, where the PH domain residues are colored blue and kinase domain residues colored cyan. The disease-associated mutations are colored red. In model 1, the following pairs of interacting residues in the PH-kinase interface were determined for cluster 1 using Discovery studio: K14-D323, K20-D302, R23-E322, R25-D325, E17-R273, Y18-K273, Y18-K297, Y18-L316, and Y18-V320, where the former and latter residues in each interaction represent residue in the PH and kinase domains, respectively. For model 2, the following pairs of interacting residues were also determined in the PH-kinase domain interface: K20 -D302, R23-D323, K39-E322, R76-D190, R86-D325, K112 -E198, K14-D325, E17-D323, Y18-D323, R23-D323, and R25-E322, where the former and latter residues in each represent residue in the PH and kinase domains, respectively.

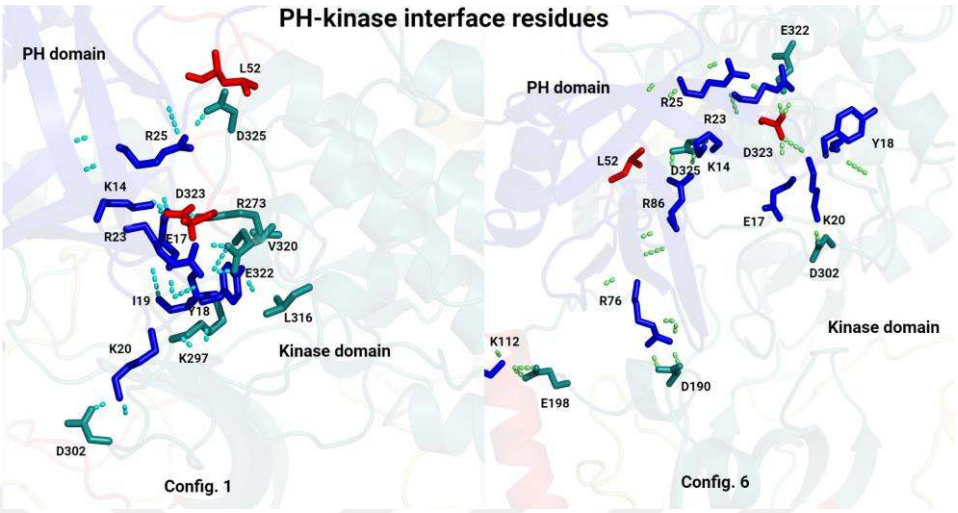

Figure 5.2 PH-kinase interface residues of AKT, residues from the PH domain are colored blue depicted as sticks, and residues from the kinase domain are colored cyan (deepteal)

5.4 Conformational analysis of Akt nucleotide-bound state

To determine the interactions of the nucleotides (ATP and ADP) and Mg^{2+} in the nucleotide-bound configurations, we clustered the nucleotide-bound and selected the most populated states for the nucleotide-bound configurations for analysis. The aim here was to determine vital intermolecular interactions of the nucleotides and Mg^{2+} in the ATP binding pocket of Akt kinase domain. These interactions were determined in Discovery Studio software (version 9) and were further depicted using the PyMOL molecular graphic interface. Several essential interactions were observed between the nucleotide and the residues in the ATP bind pocket. For instance, in the ATP and the ADP-bound states of model 1, we observed interactions that maintain these small molecules in the active site of Akt kinase domain.

On the other hand, most of these interactions were lost in the mutant system of the ATP-bound states of model1. Table S1 contains the interaction types and details of the interacting residues of model 1. Additionally, in the ATP-bound and the ADP-bound states of model 2, we observed critical interactions that retain the nucleotides in the binding site of AKT. However, most of these interactions were interrupted or lost due to the mutation in the ATP-bound state. Table S2 contains the interaction types and details of the interacting residues of model 2.

5.6 Close view of the nucleotide-bounding pocket of Akt

In the topmost cluster (cluster 1) of the ADP- bound state of model 1, the β-phosphate group makes ionic interactions and metal-acceptor with both Mg $^{2+}$ ions and an H-bond with Arg 436. Also, the **α**-phosphate group forms an H-bond with Asn 279 and ionic interactions with both Mg $^{2+}$ ions in the ATP binding pocket. Additionally, the ADP creates a conventional H-bond with Lys 158, a pi-alkyl interaction with Val 164, and van der Waals interactions with Lys 154, Leu 156, Phe 293, and Gly 294. Notably, no unfavorable interactions such as acceptor-acceptor interactions were observed in the ADP-bound configuration of model 1.

In the ATP-bound form of model 1, the gamma phosphate group forms attractive charge or ionic interactions with Lys 276, Lys 301, both Mg^{2+} ions, and H-bond bond with Lys 301; the β-phosphate group forms ionic interactions with Lys 297, and both Mg^{2+} ions, and H-bond with Lys 297 and Glu 298. The **α** phosphate group was involved ionic interactions with Lys 297, and both Mg^{2+} ions, and H-bond with Lys 297. The ATP also forms pi-alkyl interaction with Val 164, amide-pi stacked Phe 293, carbon H-bond with Cys 296, Leu 156, Gly 194; conventional H-bond with Leu 295, and van der Waals interaction with Gly 157, Gly 159, Thr 315, and Thr 448.

In the ADP-bound state of model 2, the β-phosphate group of ADP forms ionic interaction or salt bridge with Lys 276. Both Mg^{2+} ions and an unfavorable acceptor-acceptor interaction with a Mg^{2+} ion and unfavorable bump with Glu 278. The **α** phosphate group forms ionic interactions or salt bridge with Lys 907, an ionic interaction with both Mg^{2+} ions and an H-bond with Lys 907. On the other hand, the ADP forms pi-pi alkyl with Ala 177, Leu 156; pi-pi stacked with Phe 293, and pi-sigma with Val 164; H-bond with Lys 179 and van der Waals with the following residues: Met 227, Tyr 229, Glu 234, Thr 312, Ala 304, Cys 296, and Gly 159.

For the ATP-bound of model 2, the gamma phosphate group of ATP forms ionic interactions with Lys 276, Lys 301 and both Mg2+ ions, and metal-acceptor with one of the Mg^{2+} ions; the β-phosphate group was involved in ionic interactions with the Mg^{2+} ions, while the **α** phosphate group was engaged in ionic interactions and metal acceptor with Lys 276 and Mg^{2+} ions. The ATP in general forms pi- alkyl interaction with Val 164; pi-pip stacked with Phe 293; amide-pi stacked with Gly 157; pi-sulfur interaction with Cys 296; H-bond with Cys 296, Gly 294, Phe 293, and van der Waals interactions with Gly 159, Leu 295, Cys 310, Gly 311, Glu 278, Glu 314, and Leu 136.

5.7 D323 mutation in full-length Akt displaces ATP

In AKT inactive state, the PH domain locks the kinase domain, which leads to a "PH-in" conformer that prevents the phosphorylation of Thr 308 in the activation of the kinase domain. The PH domain and kinase domain form a robust interface with several significant intramolecular interactions in our predicted models. One of the key residues in the PH-kinase interface is Aspartic acid (D323) in the kinase domain. Our initial configuration of model 1, D323 forms an ionic interaction with Lysine (K14) in the PH domain. Here, we mutated D323 to Histidine (D323H) to observe its effect on the PH-kinase interface. On a high note, D323 mutation has been established experimentally to disrupt the interface. The D323H mutation, which occurs at the PH-kinase allosteric interface, leads to cellular transformation as identified in urinary carcinoma in previous studies[17, 133]. For the apostate and the ATP-bound systems of both model 1 and model 2, we mutated Asp 323 to His and subjected them to one microsecond MD simulations. These systems were treated similarly to their counterparts – unmutated systems of apostate and the ATP-bound. From the RMSD and the RMSF profiles of the systems, the mutation leads to higher fluctuations in both models – apostate and ATP-bound systems, with more significant fluctuations in model 1 than model 2. Strikingly, although the mutation is about 21Å away from the ATP binding pocket, we observed substantial displacement of ATP from the binding pocket during the simulation period for both models. Intrigued by this observation, we probe to determine the allosteric communication between the ATP binding pocket and the allosteric interface of the PH-kinase domain.

Also, the mutation resulted in repulsion between the K14 in the PH domain and HIS 323 in the kinase domain – both amino acid residues as basic, so the mutation replaces an ionic interaction to a basic repulsion, perhaps, one of the reasons for the movement of ATP in the binding pocket during the simulation. Also, substantial conformation rearrangements occur in the PH domain, PH-kinase interface, the PH-kinase linker, kinase domain, and the C-terminal tail.

5.7 Close view of the nucleotide-binding pocket of mutant Akt

In the ATP-bound D323H of model 1, the gamma phosphate group forms ionic interaction (attractive charge) with Lys 20, Arg 67, and Mg^{2+} ions; on the other hand, the β-phosphate group from ionic interaction with Arg 15, Lys 20, and both Mg^{2+} ions, and the **α**-phosphate

group form ionic interactions with Arg 15, and both Mg^{2+} ions and H-bond with Arg 15. The ATP was involved in the H-bond bond with His 13, Trp 22, Lys 20, Arg 69, and van der Waals interactions with Thr 21, Pro 68, and His 89. In comparing the wild type of ATP -bound and the mutant ATP, D323H, we observe that most of the interactions are lost in the mutant system, and the interacting residues of the ATP D323H are in the PH domain, which indicates the substantial displacement of the ATP during the simulation, whereas, in the wild type of ATP-bound the interacting residues are primarily in the kinase domain and a few residues from the C-terminal regulatory domain. Table S1 contains the interaction types and details of the interacting residues of model 1

In the ATP-bound D323H system of model 2, most of the interactions were lost immensely due to the mutation. For instance, the gamma phosphate group forms ionic interactions with Lys 276, metal-acceptor with Mg2+ ions, and an unfavorable acceptor-acceptor interaction with Glu 278. The α and β-phosphate groups only interact with the Mg^{2+} ions with no other interactions with any residues. The ATP also forms pi-cation or attractive charge interaction with Mg^{2+} ions; pi-sigma interaction with Gly 159, and van der Waals interactions with Glu 314, Thr 160, Phe 293, and Glu 441. Unlike the ATP-bound D323H of model 1, the residues involved in the intermolecular interactions between the ATP and Akt in model 2 are mainly in the kinase domain and C-terminal tail, not in the lipid-binding PH domain. Table S2 contains the interaction types and details of the interacting residues of model 2.

Altogether, these intermolecular interactions depict that in ATP-bound D323H systems, there was a substantial displacement of the ATP in model 1 compared to model 2. In both systems, key interactions were lost due to mutation, as depicted in Figure 5.3. Therefore, we deduce that, although the mutation occurs in the PH-kinase interface, it has the proclivity to disrupt the ATP binding in the ATP binding cleft of Akt. And perhaps there is an allosteric communication that exists between the PH-kinase interface and ATP binding pocket. Intrigued by this observation, we sought to determine the optimal allosteric path and identify residues that play a pivotal role in the allosteric communication between these functional sites in the Akt protein kinase. Another possible reason would be that ATP requires an intact N-C lobes interface of the kinase. Since the mutation resulted in Akt adopting an open conformation, the ATP can no longer bind effectively in the binding cleft between the N-lobe and the C-lobe of the kinase domain.

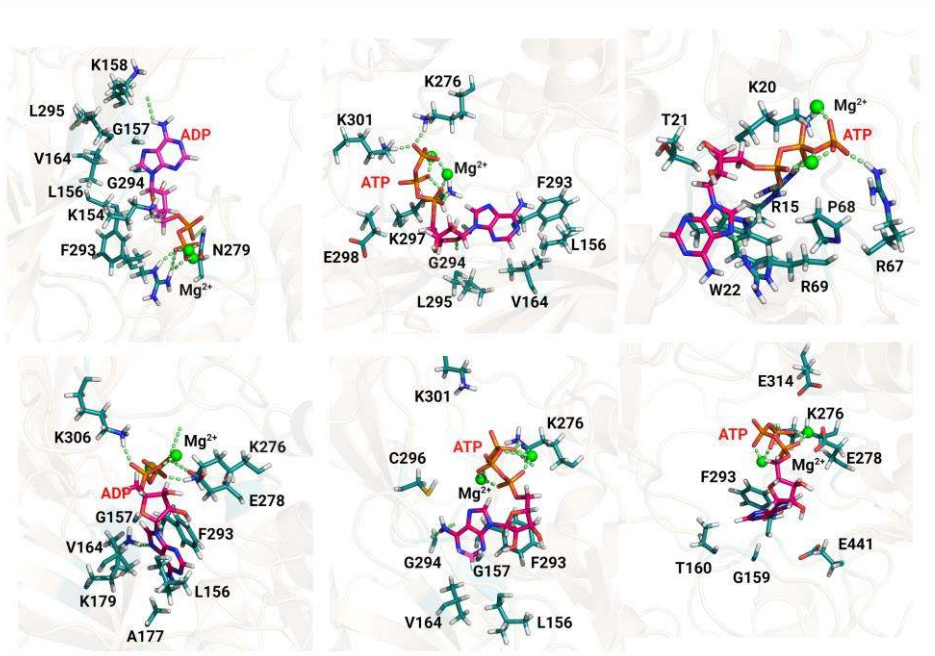

Figure 5.3 Close view of the ATP binding pocket. Close view of ATP binding pocket of AKT for model 1 and model 2. In row 1, the model 1 ADP-bound left, ATP-bound (middle), and the ATP D323H (right) And in row 2, model 2 ADP-bound (left), ATP-bound (middle) and ATP D323H (right).Atom types color the interacting residues: carbon (green), Nitrogen (blue), hydrogen (white), sulfur (yellow), the Mg2+ ions are colored green, and the ATP is color according to atom types, but the carbon is color pink, and the phosphate groups are colored orange.

5.8 Phosphorylation of full-length Akt

In the full-length Akt phosphorylated states, we analyzed and provided detailed intramolecular interactions of pThr308 and pSer473 in the activation loop and hydrophobic motif, respectively. We utilize cluster 1, the topmost populated cluster of each model, to determine the intramolecular interactions of pThr308 and pSer473, as depicted in Figure 5.4. In model 1, the pThr308 forms essential interactions with residues: R15, K20, G299, and M306; the polar interactions are colored lime-green, whereas pSer473 was involved in crucial interactions with residues: R200, L213, and Y215 – the dotted line, polar interactions are colored lime green. Also, in model 2, pThr308 forms critical interactions with residues: R15, K20, and C310, and the pSer473 make crucial interactions with residues: H143, R144, V145, and Q218. Comparing the pThr308 form of both models, we observed that both R15 and K20 interact with the phosphate group, whereas pSer473 in both models have no common interacting residues.

On high note, we measured the distance in Armstrong (Å) between ATP and Thr 308, ATP and Ser 473, and Thro 308 and Ser 473 in models 1 & 2 for the initial configuration and the topmost cluster representative of each model. For instance, in the initial configuration of mode1, the distance between the ATP and Thr 308 is approbatively 16.4Å, and the distance between ATP and Ser 473 is 23.0Å, whereas the distance between these two phosphorylated residues is about 34.3Å in three-dimensional space. In the topmost cluster of the models, the distance between the ATP and Thr 308 is approbatively 17.7Å, and the distance between ATP and Ser 473 is 22.1Å, whereas the distance between these two phosphorylated residues is about 32.4Å in three-dimensional space. Due to conformational changes, we observed slight differences in values between ATP and the phosphorylated residues and between the Thr 308 and Ser 473 residues. The exact distances for both models are depicted in Figure 5S1.

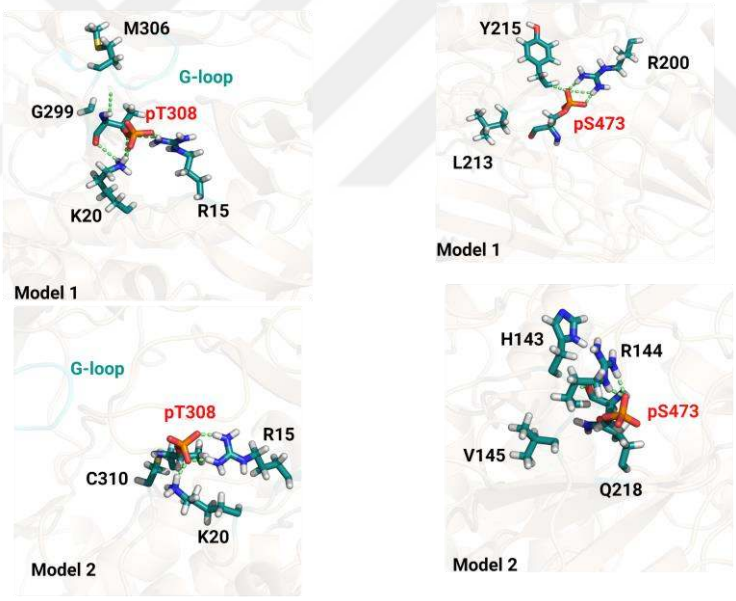

Figure 5.4 Close view of the pThr308 and pS473 interactions. The detail of pThr308 and pSer473 interactions; the interacting residues are colored by atom types, and the G-loop in the kinase domain is colored cyan.

5.9 Comparison of Akt apostate, nucleotide, and mutant states

To understand the system's dynamics and observe the effects of the mutations, we compared the RMSF and RMSD profiles of all the systems in both model 1 and model 2 (Figure 5.5A).

For the RMSD profile of model 1, the ATP-bound mutant (D323H) exhibited the highest deviation, approximately 8.3Å around 600ns, toward the end of the MD simulation. The APO D323H showed a slightly higher variation at the beginning of the simulation and around 400ns and 600 ns. It became stable toward the end of the simulation showing a similar trend to the other systems, except the ATP-bound D323H. The pThr & pSer system shows its highest deviation at the beginning of the simulation, approximately 5.0Å, and became stable toward the end of the simulation after 300 ns. Overall, except ATP-bound D323H, the rest of the systems show stability and deviate between 3Å and 5Å throughout the trajectories.

On the other hand, in model 2, we observe a difference in the RMSD profile of pThr & pSer – it shows the highest deviation (10.0 Å) between 300 ns to 800 ns and becomes stable toward the end of the simulation. After 400ns of the simulation, the apostate exhibits the second highest deviation between 7.0 Å to 9.0 Å, approximately from 400 ns toward the end of the simulation. The ATP D323H also shows the third-highest deviation, and the Apo 323H shows a higher deviation at the beginning of the simulation and becomes stable toward the end of the simulation. Comparing both models, the ATP-bound D323H of model 1shows a higher deviation than ATP D323H, whereas pThr & pSer of model 2 exhibit higher deviation and is less stable than pThr & pSer of model 1. Also, the apostate of model 2 shows a higher variation than the apostate of model 1. The ADP form of both models seems stable, showing similar RMSD profiles, and the apostate of D323H in both models shows a similar trend.

Taken together, both models somehow differ in their RMSD profiles, and which is relatively reasonable since both models have different initial configurations and were generated from two other PDB IDs with an RMSD value of 0.60Å. Also, in model 2, the linker region has a longer **α** helix inserted within the PH-kinase linker. However, both systems do not look completely different in their deviations; they are similar in behavioral patterns as discerned from their RMSD profiles in Figure 5.5A.

Similar to the RMSD profiles, we computed the RMSF profiles of all systems to discern the behavioral pattern of each system, as depicted in figure 5.5B. We compared the RMSF values as seen in the profiles for all systems. From the RMSF profile, it is glaring that both models exhibit similar fluctuations, with the highest fluctuations being observed in the PH-kinase linker region (residues 108 – 150) followed by the C-terminal regulatory domain (residues 409 – 480). The initial N-terminal of the PH domain 1-5 shows a high fluctuation similar to the linker region and C-terminal regulatory domain. Also, around residues 300 to 210, higher

fluctuations are observed, corresponding to loop regions in the kinase domain and the activation loop (A-loop).

With these profiles, in model 1, the ATP D323H shows the highest fluctuation compared to the rest of the systems, a trend similar to the RMSD profiles discussed above. In contrast, the pThr & pSer of model 2 shows the highest fluctuation compared to the remaining systems in model 2. In both models, the fluctuations are between 1.5Å and 14 Å, and 2 Å and 15 Å, respectively for models 1 and 2. The highest fluctuations in the PH-kinase linker depict the flexibility of the linker region. The linker region in model 1 is more flexible than model 2 because a closer look at the initial configurations of both systems shows that model 2 has a longer **α** helix within the PH-kinase linker. In contrast, in model 1, there is a short **α**-helical region.

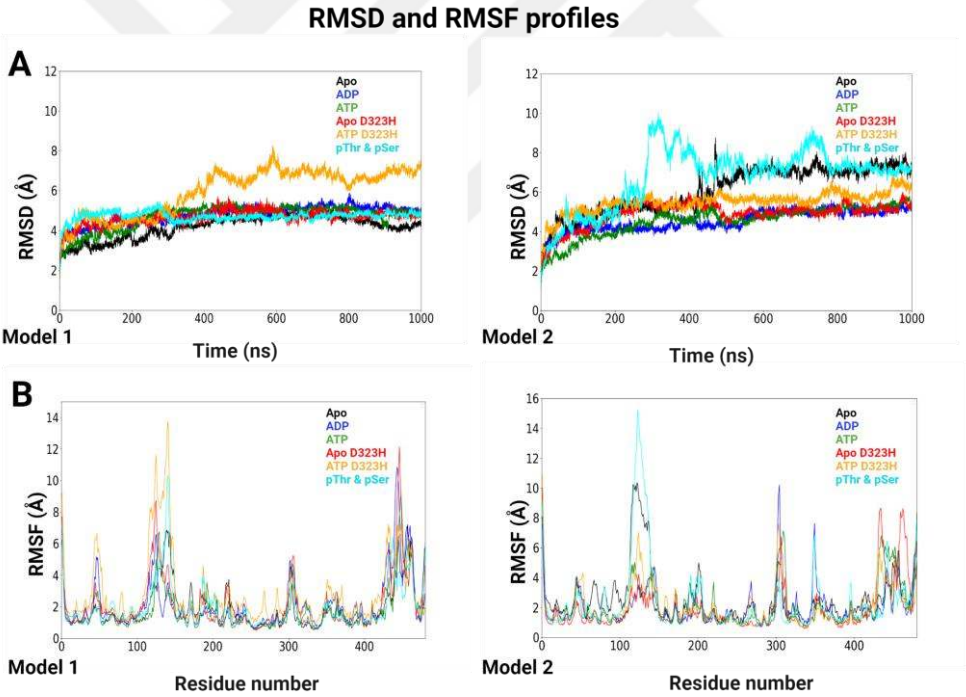

Figure 5.5A, the RMSD profiles of the systems upper panel, model 1 (left) and model 2 (right). The colorations are APO (black), ADP-bound (blue), ATP-bound (green), APO D323H (red), ATP D323H (orange), and pThr & pSer (cyan). **B,** the RMSF profiles of the systems lower panel, model 1 (left) and model 2 (right). The colorations are APO (black), ADP-bound (blue), ATP-bound (green), APO D323H (red), ATP D323H (orange), and pThr & pSer (cyan).

5.10 Discussion

AKT is a crucial player in the PI3K/Akt/mTOR pathway. In Akt, the lipid-binding PH domain interacts with the kinase domain to induce AKT inactive state, also called AKT autoinhibition. Autoinhibition is very common for protein kinases, such as PKA and PKG, where a protein segment covers its functional site. Autoinhibition is important in signaling because it guards against protein degradation and specious signaling, although imperfectly as a basal activity under unstimulated cellular environments depicts [207, 208]. AKT, for example, undergoes autoinhibition, where the PH domain covers a functional site in the kinase domain, preventing phosphorylation of Thr308 by PDK1. The autoinhibition is released when the PH domain interacts with PIP_3, PIP_2, or CaM, which results in AKT recruitment to the plasma membrane. Figure 5.6 shows a proposed activation mechanism of AKT, where cytoplasmic "PH-in" conformer interacts with CaM or PIP3 to recruit AKT to the plasma membrane for phosphorylation and complete activation. Protein kinases such as AKT use ATP as a source of phosphate groups to phosphorylate their specific substrates. Also, previous research has uncovered that ATP can act as an allosteric modulator, which triggers other studies to strive to understand the allosteric mechanism of ATP in AKT to provide insight into the pivotal role of ATP and its mechanism as an endogenous modulator in cell signaling and is an important class of enzymes [8]. Furthermore, the bilobal kinase domain of AKT has N- and C-lobes, which play a crucial role in Akt kinase activity. Like other protein kinases such as PKA and PKG, AKT catalytic activity is controlled via alignment of the conserved residues in the regulatory and catalytic hydrophobic spines (C-and R- spines) that linked the kinase domain N- and C-lobes[209]. When protein kinases are in an active conformation, a proper alignment of the C-and R- spines residues provide an optimal architecture of the active site to accommodate ATP binding and the subsequent transfer of phosphate onto the bound substrate molecule. On the flip side, the disassembly of either the C- or R- spine inactivates the protein kinases, a phenomenon that allows them to act molecular switches in cells[117]. For Akt kinase, in particular, the hydrophobic spines assembly and disassembly are controlled through post-translational modifications and allosterically, through conformational changes trigger by the interplay between the PH domain and membrane lipids, PIP_3 or PIP_2[117]. Also, phosphorylation of Thr 308 by PDK1 activates AKT by promoting ordering of A-loop and alignment of the C-and R- spines residues, which enable the binding of ATP and transferring of a phosphate group to the substrate[117]. For instance, AKT phosphorylated and

unphosphorylated crystal structures showed that phosphorylation leads to the flipping of Phe 293 in the DFG motif of the C-spine to accommodate the ATP adenine ring and restore the R-spine simultaneously. The resulting conformation rearrangement is accompanied by repositioning of Lys 179 and Asp 292 residues that coordinate the ATP phosphates, closure of the glycine-rich loop (β1/ β2), and ordering of the **α**C helix in the A-loop, thereby completing the kinase domain and preparing it for catalysis[150, 210].

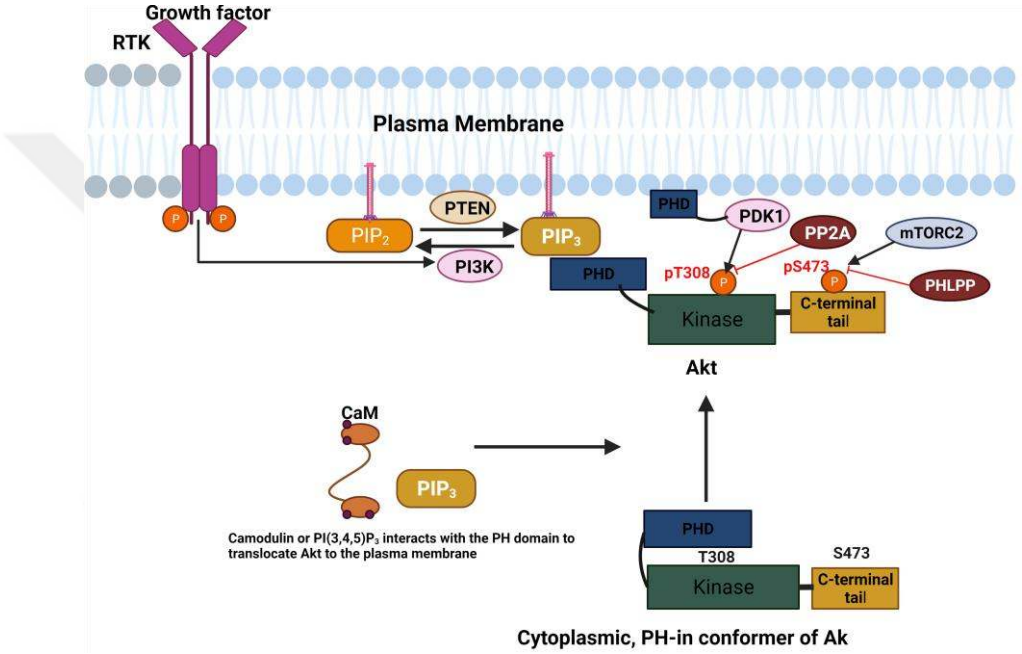

Figure 5.6 Cytoplasmic "PH-in" conformer of AKT interacts with either CaM or PIP3 to translocate AKT to the plasma membrane for phosphorylation of Thr 308 in the kinase domain and Ser 473 in the C-terminal tail. The dephosphorylation of these critical residues are carried out PP2A and PHLPP, respectively as AKT dissociates from the plasma membrane.

5.11 The "PH-in" conformer maintains Akt in its autoinhibited state

Under basal conditions, the PH domain intramolecularly interacts with the kinase domain to maintain Akt in an autoinhibited or closed conformation [6, 7]. In the "PH-in" conformer of AKT, the kinase domain covers the PIP_3 binding, whereas the PH domain covers the phosphorylation site in the kinase domain. The PH domain has a penchant for interlocking the centrally positioned kinase domain to form the "PH-in" conformer. The "PH-in" conformer of AKT has a two-fold function, preventing the phosphorylation of Thr308 in the kinase domain and preventing the intermolecular interface between the PH domain and membrane

lipids such as PIP_3 and PIP_2, which hinders the recruitment of the AKT to the plasma membrane for diphosphorylation and subsequent activation.

In the C-terminal regulatory domain, mTORC2 phosphorylates S473 (pS473), promoting its interaction with Arg 144 in the PH-kinase linker and the N-lobe of the kinase domain to relieve the PH-kinase domain autoinhibition. Also, the interaction between pS473 and Arg144 tends to arrange the HF motif (^{469}FPQF^{472}), allowing Thr308 in the kinase domain accessible for phosphorylation by PDK1 and activation of Akt through the open "PH-out" conformer state[17]. On another note, the insertions of Gly residues in the linker region indicate that the PH-kinase linker flexibility tends to stabilize the PH-kinase domains autoinhibited interaction. However, diphosphorylation at Ser477 and Thr497 activates Akt via an alternative allosteric mechanism. The dual phosphorylation enables the C-terminal regulatory region to interact with the activation loop – the connector between the smaller N- lobe and the larger C-lobe, and the PH domain, which partially displaced the PH domain from the kinase domain. This dual phosphorylation event partially relieves the autoinhibition of Akt via weakening the PIP_3 and PH-kinase domain binding rather than through the PIP3 site itself. Hence, rather than the PH domain -PIP_3 interplay directly relieving the autoinhibition, the PIP_3 acts to translocate Akt to the plasma membrane, followed by phosphorylation of Thr308 and Ser473 PDK1 and mTORC2, respectively [14]. The disruption of PH-kinase domain interface by mutation of interfacial residues, for instance, tends to render Akt insensitive to PIP_3 but enhances its association with PIP_3-containing liposomes and accumulation of Akt at the plasma membrane upon growth factor stimulation[107]. These phenomena indicate that the PIP_3-binding is site is close-up partially when Akt is autoinhibited. As observed from or predicted models, indeed, the PIP_3-binding site is occluded; however, as reported [108] autoinhibited Akt likely exists in open and closed conformers at equilibrium with a dissociation constant (k_d) 7μM corresponding to the fraction of the "PH -in" (closed) conformer equivalent to 98.8% at equilibrium, which would be further increased to 99.9% if one considers a more compacted PH-kinase domain linker[108]. In our predicted models, the interfacial residues that retain AKT inactive state were determined and found to agree with previous studies.

5.12 The PH-kinase interfacial residues play a crucial role in Akt autoinhibition

The autoinhibited state of Akt is maintained by intact-intramolecular interactions between residues in the PH and kinase domains. The interfacial residues are involved in various interactions supporting the PH-kinase interface and maintaining Akt in its autoinhibited state. The previous study has identified key residues in the PH-kinase interface responsible for maintaining the interface or the autoinhibited form of Akt. Also, mutation of some of these interface residues leads to disruption of the interface, which triggers a "PH-out" conformer state of Akt. The PH-out conformer state of Akt has the propensity to interact with membrane lipids such as PIP_2 and PIP_3, or CaM as in breast cancer, to recruit Akt to the plasma membrane for phosphorylations and subsequent activation. For example, a recent study by Truebestein et al.[211] determined a near-full length crystal of AKT and identified the following interface residues (Q79, W80, T81, F55, D323, L52, R23, N53, E17, D325, and L78) to be PH-kinase interface residues. The study also established that residues D323 to D325 in the centrally positioned kinase domain intramolecularly associate with K14, R23, R25, N53, and Q79 of the lipid-binding PH domain, and L316, V320, L321, F358, and L362 in the kinase domain interacts with Y18 and I19 of the PIP_3-binding PH domain[211]. Along a similar line, we identified the PH-kinase domains interface residues in both models 1 and 2. We found the following pairs of interacting residues, where the former denotes residues from the PH domain and the latter indicates residues from the kinase domain. K14-D323, K20-D302, R23-E322, R25-D325, E17-R273, Y18-K273, Y18-K297, Y18-L316, and Y18-V320 for model 1 and K20 -D302, R23-D323, K39-E322, R76-D190, R86-D325, K112 -E198, K14-D325, E17-D323, Y18-D323, R23-D323, and R25-E322 for model 2. These residues are shown in Figure 5.2 as sticks, and the interaction types determined from Discovery studio are in Table 1. To a very high extend, these interface residues in our study agreed with the previous studies. For example, K14, R23, R25, E17, Y18 in the PH domain and E322, D323, D325, E198 in the kinase are critical residues in the PH-kinase interface. For instance, E17K, a driver mutation, weakens the PH and kinase domain interaction and is linked earlier to alter lipid-binding specificity. In contrast, residues D323 and D325 mutations are associated with cellular transformation[17, 133]. Resultingly, we deduce that our models of full-length Akt are good representations of the autoinhibited state of Akt that would help to further decipher the dynamics of the "PH-in" conformer of Akt at the molecular level and would be handy in the development of allosteric inhibitors that bind in the PH-kinase interface or

require an intact PH-kinase domain interface.

5.13 Critical interactions of pThr308 and pSer473 in full-length Akt

When Akt kinase is phosphorylated at Thr 308 and Ser 473, it becomes fully activated, but Akt can adopt a "PH-in" conformer (inactive state) irrespective of the phosphorylation state. The PH domain can dissociate from the centrally positioned kinase domain when Akt is at the membrane, where the PH domain interacts with membrane lipids, PIP_3 or PIP_2. In the absence of PIP_3 binding, the PH domain falls back to interact with the kinase domain regardless of Akt phosphorylation state, and the "PH-in" conformer renders its accessibility to phosphatases to dephosphorylate the phosphorylated residues. The PH-kinase domain autoinhibitory interface is retained when Akt is constitutively phosphorylated[212] and even after stoichiometric phosphorylation, thereby restricting Akt maximum activity to PIP_3 or PIP_2-containing plasma membranes[211]. Prompted by these experimentally proven observations, we constructed autoinhibited phosphorylated forms of Akt by replacing Thr 308 and Ser 473 to pThr 308 and pSer 473, respectively. Though pThr 308 and pSer 473 of autoinhibited AKT not biologically relevant; however, the goals were to observe the interactions of these phosphate groups and how phosphorylation of the A-loop affects autoinhibited AKT.

Previously, it has been established that the phosphate moiety of pT308 in the A-loop of the kinase domain was surrounded by the catalytic cleft residues – His 194, Arg 273, and Lys 297. Also, the Thr 160 hydroxy group side chain formed a hydrogen bond with the gamma-phosphate moiety of ATP, but the study was conducted in the absence of the C-terminal regulatory domain. In other words, the study did not utilize a full-length AKT structure.

Here in model 1 topmost cluster (cluster 1, Figure 5.1), we observed that the pThr308 in the activation loop of the kinase domain forms significant interactions with residues: R15, K20, G299, and M306; whereas the pSer473 in the C-terminal tail makes key interactions with residues: R200, L213, and Y215. Also, in model 2, pThr308 forms critical interactions with residues: R15, K20, and C310, and the pSer473 make important interactions with residues: H143, R144, V145, and Q218 as in Figure 5.4. R144 has been reported previously to play a pivotal role in releasing Akt autoinhibition, and it has been established that Q218 forms H-bond to Ser 473 in Akt active conformation, an interaction that stabilizes the hydrophobic motif and the conformation of the **αC** helix in the kinase domain[210]The pT308 in the kinase

domain interacting residues in our study differ from those of the previous research. It is worth emphasizing that the previous study by Lu et al. [8]was conducted using only the Akt kinase domain, not full-length Akt as we have undertaken for the first time. Hence, it is no surprise that the interacting residues slightly differ from those of the previous due to conformational differences between the full-length Akt and the kinase Akt domain. Also, Ser 473, absent during the previous study, would be another reason for the different conformation or interaction of the pT308 in the kinase domain.

5.14 D323H mutant in PH-kinase allosteric interface destabilizes Akt autoinhibition

Akt kinase is frequently mutated in various types of cancer, which drives cell proliferation. In the Akt PH domain, a mutation of Glu 17 to Lys (E17K) results in constitutive activation of the central position kinase domain [134]. Also, a mutation of Arg 25 to Cys (R25C) in the PH domain leads to inefficacious membrane lipid, PIP_3 binding, subsequently preventing localization of Akt to the plasma membrane for phosphorylation and activation[10]. As a result of this mechanism, Akt structures without the PH domain suggest that the interplay between the C-terminal regulatory domain and the kinase domain N—lobe promotes Akt activation [150, 210]. On the flip side, AKT structures with the PH domain, but lacking the C-terminal region complex with allosteric inhibitors, lead to an autoinhibited state. The PH domain intramolecularly interacts with the kinase domain [152]. Mutations diminish the romantic interaction between the PH domain and kinase domain in the PH-kinase domain interface, which can lead to the PH domain disengaging from the kinase domain [17]. For instance, E17K, L52R, and D323H oncogenic mutations occur in the PH-kinase interface, and they have the proclivity to disrupt the interaction between the PH domain and the kinase domain. On another note, mutations such as F35L and R96W in the PH domain and K189N in the kinase domain do not reduce interaction signal, but L52R in the PH domain and D323H in the Kinase domain reduce interaction signal between the PH and kinase domains. Also, E17K, a driver mutation in the PH domain, modestly weakens the intramolecular interaction between the PH and kinase domain and is earlier linked to altering lipid-binding specificity [134, 213]. Notably, the D323 mutation has been experimentally established to disrupt the PH-kinase domain interface. The D323H mutation leads to cellular transformation as identified in urinary carcinoma in previous studies [17, 133]. Also, mutation of D323 and D325, interfacial residues in the kinase domain results in PIP_3 independent activity, increased PIP3 and protein

substrate affinity, and a disruption of the PH-kinase interface, which are consistent with the crucial roles of these interface residues to maintain Akt in the autoinhibited state[107, 212]. Here in our work, the RMSD and the RMSF profiles depict that the mutation (D323H) resulted in high fluctuations in both models: apostate and ATP-bound AKT systems with more significant fluctuations in model 1 than model 2.

Interestingly, even though D323H is about 21Å away, as depicted in figure 5.7 from the ATP binding site we observed substantial movement of the ATP from the binding pocket during the simulations. Intrigued by this observation, we aim to determine the allosteric communication between the ATP binding pocket and the allosteric interface of the PH-kinase domain. Additionally, D323H resulted in repulsion between the K14 in the PH domain and HIS 323 in the kinase domain. Both residues are basic, so the mutation replaces an ionic interaction with a basic repulsion, perhaps, one of the reasons for the movement of ATP in the binding pocket. Further, the D323H resulted in substantial conformation rearrangements in Akt, with the kinase domain adopting a more open conformation. The mutation also distorts the linker and the C-terminal tail.

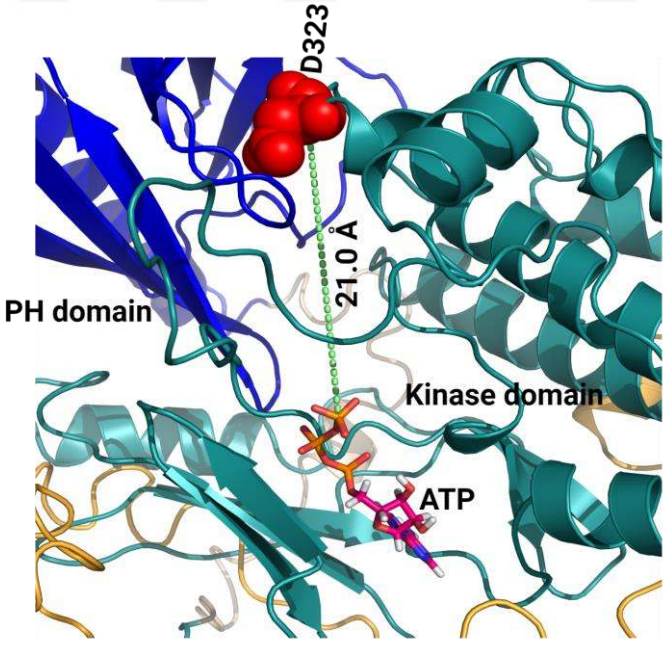

Figure 5.7 The distance of ATP from the mutation site (D323H), the mutant residues are shown as red sphere and ATP as sticks colored by element types. The mutation is approximately 21Å from the ATP binding pocket in AKT.

5.15 Allosteric inhibitors require intact PH-kinase domain interface

Akt crystal structure bound to allosteric inhibitor has identified critical interfacial residues that retain the PH-kinase domain interface. For instance, K14 and E17 in the lipid-binding PH domain form salt bridges with D323 and R273 in the C-lobe of the kinase domain, respectively[117]. A mutation of critical allosteric interface residues such as E17, W80, D323 and D325 can render Akt kinase insensitive to allosteric inhibitors, leading to Akt activation and cellular transformation[17]. For example, E17K, a charge-reversal mutation in the PH-kinase interface, increases Akt plasma membrane association and constitutive activity, driving cellular transformation as observed in patients with Proteus syndrome megalencephaly, colorectal, breast, and ovarian cancers[134, 213]. While being interesting phenomenologically, these correlated observations between mutations occurring at the PH-kinase interface and their cellular transformation potential highlight the significance of the autoinhibitory mechanism in restricting Akt cellular activity *in vivo[117]* Also, the allosteric interface in the crystal structure contains residues in the PH domain that directly bind to membrane lipids, PIP3 or PIP2, and observation that prompts one to suggest that Akt cannot be membrane-bound and autoinhibited simultaneously[117].

The effectiveness of Akt allosteric inhibitors depends on an intact PH-kinase domain interface [7, 152, 214] and mutations such as E17K, L52R, and D323H that tend to dislodge the PH-kinase domain interface diminish the response to allosteric inhibitors [17]. Hence, mutations occurring at the PH-kinase domain interface that results in constitutive activation of Akt perhaps may hinder the effectiveness of allosteric Akt inhibitors since they require an intact PH-kinase domain interface. Here, we introduced a mutation, D323H, in the PH-kinase domain intact interface to observe the disruptiveness of the interface or the conformational changes it induces in full-length Akt. On a high note, D323H is approximately 21 Å from the ATP binding pocket, and no directions exist between them, but the mutation resulted in a substantial displacement of the ATP from the ATP binding site in Akt. To unravel the mechanism of signal propagation between the PH-kinase domain interface and the ATP binding pocket of Akt, we aim to identify residues involved in the allosteric communication between the PH-kinase domain interface and the ATP binding cleft in the Akt kinase domain. Previously, in elsewhere [8], the optimal allosteric path from ATP to pThr 308 has been identified as follows: ATP – Thr 160 – Phe 161 – Glu 191 – H194 – pThr 308 using a method based on Markov propagation analysis[215]. In this optimal

allosteric path from ATP to pThr 308, four residues were involved in propagating the signal from ATP to pThr308, and these residues are in the Glycine rich loop (Thr 160 and Phe 161) a helix αC (Glu 191 and His 194)[8].

5.16 Phosphorylation of Ser473 in the Akt C-terminal tail induces PH domain releasement

Our modeled Akt structures contain the C-tail or C-terminal regulatory domain. The C-terminal consists of two phosphorylations sites, T450 in the turn motif and S473 in the hydrophobic motif. The Phosphorylation of T450 in the turn motif occurs co-translationally [216], and it's not affected by growth factor-induced signaling [217]. Also, T450 Phosphorylation tends to protect Akt from ubiquitin-mediated degradation [216, 217]. On the other hand, S473 phosphorylation promotes disorder to order transitions of the hydrophobic motif [210], which in synergy with T308 phosphorylation in the activation loop and ATP stabilizes a resistant conformation to phosphatases [8, 29, 106, 108, 150].

Additionally, a previous study established that Akt lacking phosphorylations of T450 and S473 is catalytically inactive[107]. Also, S473 phosphorylation by mTORC2 activates AKT via a formation of electrostatic interaction between the phosphate group and the Arg 144 in the PH-kinase linker, thereby relieving AKT PH domain-mediated autoinhibition. In a recent study, the phosphorylation of the S473 activation mechanism that induces PH domain displacement greatly depends on conformational changes in the PH domain [218], thereby activating Akt independent of its PH domain binding to membrane lipids, PIP_2 and PIP_3. Here, in model 2, we observed a formation of electrostatic interaction between the phosphate group of S473 and Arg 144 in the PH-kinase domain linker. This interaction may be observed in a different conformation of model 1 because we only visualized the most populated conformation of each model. Also, T450 in the turn motif was unphosphorylation in this study. Also, the configurations with pThr 308 and pSer 473 are in transient states, implying that 1 μs MD simulation is insufficient to monitor the PH domain releasement from the kinase domain in autoinhibited Akt. However, the results provide some intramolecular insights into how pSer 473 interact with critical residues in such as R144 and Q218 in the PH-kinase domain and the kinase domain, respectively. For instance, it has been reported that Q218 forms H-bond to Ser 473 in Akt active conformation. This intramolecular interaction stabilizes the hydrophobic motif and the conformation of the αC helix in the centrally positioned kinase domain[210].

5.17 The PH-kinase linker interaction with pS473 is critical for Akt activation

Crystal structure of Akt showed that Arg 144 in the PH-kinase domain linker is approximately 6Å away from the phosphate group of pSer 473, which led the authors to propose that pSer473 could interact with Lys142-His143-Arg144, conserved basic patch residues of the PH-kinase domain linker in full-length Akt[14]. Further experimental investigations by the authors led them to conclude, based on their results, that the proposed basic patch residues and Gln218 intramolecular interaction with pSer 473 are indeed critical for Akt activation[14]. Our modeled structures contain the PH-kinase linker (residues 108 -150), which includes the basic patch residues, and Arg 144, a basic patch residue, electrostatically interacts with pS473 in the hydrophobic motif. In model 1, the linker is a loop structure with a short **α** helical segment, whereas in model 2, the PH-kinase linker has longer **α** helical region, one of the key differences structural-wise between the two predicted models. Taken altogether, we have predicted Akt full-length structure that comprises the PH domain, PH-kinase domain linker, the centrally positioned kinase domain, and C-terminal regulatory domain and analyzed the structural conformation of the autoinhibited state of Akt and identified key residues that play a paramount role in maintaining the PH-kinase domain interface. Everything considered, the elucidation of the conformational plasticity of full-length Akt uncovered here for the first would be handy for further studies on the autoinhibition dynamic of Akt – a vital protein kinase in the Ras-Akt-mTORC2 pathway.

5.18 Conclusion on Akt autoinhibition state

In Akt autoinhibited state, the lipid-binding PH domain romantically interacts with the kinase domain, preventing Thr308 phosphorylation by PDK1 in the kinase domain, an important event for Akt activation. The binding of PIP_3 or PIP_2 to the PH domain promotes the release of the autoinhibition, and exposure of Thr308 and Ser473 in the activation loop and hydrophobic motif, respectively, for phosphorylation. Also, phosphorylated Ser 473 (pSer473) in the C-terminal regulatory domain can establish electrostatic interaction with Arg 144, a basic residue in the basic patch of the PH-kinase domain linker to release the PH domain and is critical for Akt activation[14]. Allosteric Akt inhibitors require an intact PH-kinase domain interface for their efficacious activity in cells, and mutation of critical residues in the interface can impair the PH-kinase domain contacts making allosteric inhibitors to be less

efficacious. On the other hand, ATP-competitive inhibitors do not require an intact PH-kinase domain interface and can effectively block the activity of wild-type and mutant (E17K, L52R, and D323H) Akt [17]. In this dissertation, D323H mutation led to the displacement of ATP in the binding site of the kinase. It enabled the kinase domain to adopt a more open conformation, which implies that ATP-competitive inhibitors might require intact N- and C-lobes interface of the kinase domain for their activity. Here, for the first time, we have modeled the structure of full-length Akt and present the best-autoinhibited states of full-length Akt. The structures would guide medicinal chemists in developing Akt allosteric inhibitors that require intact PH-kinase domain interface and ATP-competitive inhibitors that do not require such intact interface but might rely on intact kinase domain N- and C- lobes interface for their activity. The development of allosteric and ATP-competitive inhibitors is essential for targeting Akt since it is frequently activated in tumor cells, necessitating its regulation.

Chapter 6

Conclusion

Akt protein, a Ser/Thr protein kinase regulates enormous biological process including cell survival, proliferation, and apoptosis. The Akt activation mechanisms have been proposed by numerous studies and still remain controversial, but all centered around the profound role of the PH domain. The first part of this dissertation provides detailed conformational analysis of how CaM binds to Akt PH domain at the atomic level and how IP_4 involvement in CaM-PH domain complex weakens or partially displaces CaM from CaM-PH domain dimeric complex. Akt kinase is translocated to the PIP_3-containing plasma membrane by specific interactions between its PH domain and CaM or PIP_3, a phospholipid in the plasma membrane that serves as Akt docking site [40, 111]. NMR experiments established the binding mode of CaM to the PH domain of Akt, and the observations by both the NMR and the simulations deviate from a typical binding mode of CaM, which unusually involves **α**-helical regions [188, 189]. The simulation results suggest that CaM binds to the **β**-sheet in the PH domain, which is rare, but not unsurprising because such binding has been observed by another NMR experiment, where CaM binds to the PH domain of Itk [205]. From a mechanistic perspective, CaM's N-lobe, C-lobe, and the central linker simultaneously engage the PH domain. In other words, the PH domain binds to one end of CaM, especially the C-lobe, and induces conformational rearrangements engaging the central linker and N-lobe of CaM. Furthermore, the molecular modeling and simulation results in this dissertation empower us to select and propose four models of CaM-PH domain complexes, depicting the **β**-sheets in the PH domain binding to CaM. On another note, a high percentage of the NMR chemical shift residues were observed in the CaM-PH domain interface. Most of the interfacial residues play an essential role in retaining CaM-PH domain dimeric complex. We present the most populated state of each proposed model and crucial intermolecular interactions, which are cardinal in maintaining the CaM-PH domain dimeric complex. These handy models reveal how IP_4 acts by attenuating or

partially displacing CaM from the PH domain, thereby uncovering the detailed molecular basis of Akt translocation, phosphorylation, and activation. These results may also serve as basis for small molecules inhibitors or drug molecules development to disrupt the CaM-PH domain interaction. The details of CaM-PH domain release mechanism obtained here uncovered a potentially promising therapeutic strategy for breast cancer and other related cancer types.

Along a similar line, the dissertation also explored the autoinhibition state of Akt, where the PH domain romantically interacts with the centrally positioned kinase domain to prevent Thr308 phosphorylation in the kinase domain by PDK1, an essential event, which is necessary for Akt activation. In Akt autoinhibited state, the lipid-binding PH domain romantically interacts with the kinase domain, preventing Thr308 phosphorylation by PDK1 in the kinase domain, an important event for Akt activation. The binding of PIP_3 or PIP_2 to the PH domain promotes the release of the autoinhibition, and exposure of Thr308 and Ser473 in the activation loop and hydrophobic motif, respectively, for phosphorylation. Also, phosphorylated Ser473 (pSer473) in the C-terminal regulatory domain can establish electrostatic interaction with Arg 144, a basic residue in the basic patch of the PH-kinase domain linker to release the PH domain and is critical for Akt activation[14]. Allosteric Akt inhibitors require an intact PH-kinase domain interface for their efficacious activity in cells, and mutation of critical residues in the interface can impair the PH-kinase domain contacts making allosteric inhibitors to be less efficacious. On the other hand, ATP-competitive inhibitors do not require an intact PH-kinase domain interface and can effectively block the activity of wild-type and mutant (E17K, L52R, and D323H) AKT[17]. Here, the mutation of Asp323 to His led to the displacement of ATP in the binding site of the kinase domain. It enabled the kinase domain to adopt a more open conformation, which implies that ATP-competitive inhibitors might require intact N- and C-lobes interface of the kinase domain for their activity. Here, for the first time, we have modeled the structure of full-length Akt and present the best-autoinhibited states. The structures would guide medicinal chemists in developing Akt allosteric inhibitors that require intact PH-kinase domain interface and ATP-competitive inhibitors that do not require such intact interface but might rely on an intact kinase domain N- and C- lobes interface for their cellular activity. The development of allosteric and ATP-competitive inhibitors is essential for targeting Akt since it is frequently activated in cancerous cells, which necessitate the regulation of Akt. Taken together, the

results of the dissertation on CaM-PH domain interplay and the romantic interaction of PH and kinase domains of Akt add more insightful tips to the already existing rich tapestry of Akt autoinhibition, translocation, phosphorylation, and activation, which greatly depends on the peculiar role of the PH domain. In conclusive, the dissertation results have an important functional implication in developing inhibitors that would target CaM-PH domain dimeric complex and allosteric and ATP-competitive inhibitors, which bind to the PH-kinase domain interface and ATP binding pocket in Akt, respectively. Finally, the results add on to existing incredible tapestry of information on Akt kinase activation mechanism, which all seem to be the result of loosening the PH-kinase domain autoinhibition and highlighting the profound role of the PH domain.

BIBLIOGRAPHY

1. Manning BD, Toker A. AKT/PKB Signaling: Navigating the Network. Cell. 2017;169(3):381-405. Epub 2017/04/22. doi: 10.1016/j.cell.2017.04.001. PubMed PMID: 28431241; PubMed Central PMCID: PMCPMC5546324.
2. !!! INVALID CITATION !!! [2, 3].
3. Hanada M, Feng J, Hemmings BA. Structure, regulation and function of PKB/AKT--a major therapeutic target. Biochimica et biophysica acta. 2004;1697(1-2):3-16. Epub 2004/03/17. doi: 10.1016/j.bbapap.2003.11.009. PubMed PMID: 15023346.
4. Liao Y, Hung MC. Physiological regulation of Akt activity and stability. American journal of translational research. 2010;2(1):19-42. Epub 2010/02/26. PubMed PMID: 20182580; PubMed Central PMCID: PMCPMC2826820.
5. Bellacosa A, Chan TO, Ahmed NN, Datta K, Malstrom S, Stokoe D, et al. Akt activation by growth factors is a multiple-step process: the role of the PH domain. Oncogene. 1998;17(3):313-25. Epub 1998/08/05. doi: 10.1038/sj.onc.1201947. PubMed PMID: 9690513.
6. Calleja V, Alcor D, Laguerre M, Park J, Vojnovic B, Hemmings BA, et al. Intramolecular and intermolecular interactions of protein kinase B define its activation in vivo. PLoS biology. 2007;5(4):e95. Epub 2007/04/05. doi: 10.1371/journal.pbio.0050095. PubMed PMID: 17407381; PubMed Central PMCID: PMCPMC1845162.
7. Calleja V, Laguerre M, Parker PJ, Larijani B. Role of a novel PH-kinase domain interface in PKB/Akt regulation: structural mechanism for allosteric inhibition. PLoS biology. 2009;7(1):e17. Epub 2009/01/27. doi: 10.1371/journal.pbio.1000017. PubMed PMID: 19166270; PubMed Central PMCID: PMCPMC2628406.
8. Lu S, Deng R, Jiang H, Song H, Li S, Shen Q, et al. The Mechanism of ATP-Dependent Allosteric Protection of Akt Kinase Phosphorylation. Structure (London, England : 1993). 2015;23(9):1725-34. Epub 2015/08/11. doi: 10.1016/j.str.2015.06.027. PubMed PMID: 26256536; PubMed Central PMCID: PMCPMC7734571.
9. Burgering BM, Coffer PJ. Protein kinase B (c-Akt) in phosphatidylinositol-3-OH kinase signal transduction. Nature. 1995;376(6541):599-602. Epub 1995/08/17. doi: 10.1038/376599a0. PubMed PMID: 7637810.
10. Franke TF, Yang SI, Chan TO, Datta K, Kazlauskas A, Morrison DK, et al. The protein kinase encoded by the Akt proto-oncogene is a target of the PDGF-activated phosphatidylinositol 3-kinase. Cell. 1995;81(5):727-36. Epub 1995/06/02. doi: 10.1016/0092-8674(95)90534-0. PubMed PMID: 7774014.
11. Alessi DR, James SR, Downes CP, Holmes AB, Gaffney PR, Reese CB, et al. Characterization of a 3-phosphoinositide-dependent protein kinase which phosphorylates and activates protein kinase Balpha. Current biology : CB. 1997;7(4):261-9. Epub 1997/04/01. doi: 10.1016/s0960-9822(06)00122-9. PubMed PMID: 9094314.
12. Stokoe D, Stephens LR, Copeland T, Gaffney PR, Reese CB, Painter GF, et al. Dual role of phosphatidylinositol-3,4,5-trisphosphate in the activation of protein

kinase B. Science (New York, NY). 1997;277(5325):567-70. Epub 1997/07/25. doi: 10.1126/science.277.5325.567. PubMed PMID: 9228007.
13. James SR, Downes CP, Gigg R, Grove SJ, Holmes AB, Alessi DR. Specific binding of the Akt-1 protein kinase to phosphatidylinositol 3,4,5-trisphosphate without subsequent activation. The Biochemical journal. 1996;315 (Pt 3):709-13. Epub 1996/05/01. doi: 10.1042/bj3150709. PubMed PMID: 8645147; PubMed Central PMCID: PMCPMC1217264.
14. Chu N, Salguero AL, Liu AZ, Chen Z, Dempsey DR, Ficarro SB, et al. Akt Kinase Activation Mechanisms Revealed Using Protein Semisynthesis. Cell. 2018;174(4):897-907.e14. Epub 2018/08/07. doi: 10.1016/j.cell.2018.07.003. PubMed PMID: 30078705; PubMed Central PMCID: PMCPMC6139374.
15. Sarbassov DD, Guertin DA, Ali SM, Sabatini DM. Phosphorylation and regulation of Akt/PKB by the rictor-mTOR complex. Science (New York, NY). 2005;307(5712):1098-101. Epub 2005/02/19. doi: 10.1126/science.1106148. PubMed PMID: 15718470.
16. Huang BX, Akbar M, Kevala K, Kim HY. Phosphatidylserine is a critical modulator for Akt activation. The Journal of cell biology. 2011;192(6):979-92. Epub 2011/03/16. doi: 10.1083/jcb.201005100. PubMed PMID: 21402788; PubMed Central PMCID: PMCPMC3063130.
17. Parikh C, Janakiraman V, Wu WI, Foo CK, Kljavin NM, Chaudhuri S, et al. Disruption of PH-kinase domain interactions leads to oncogenic activation of AKT in human cancers. Proceedings of the National Academy of Sciences of the United States of America. 2012;109(47):19368-73. Epub 2012/11/09. doi: 10.1073/pnas.1204384109. PubMed PMID: 23134728; PubMed Central PMCID: PMCPMC3511101.
18. Agamasu C, Ghanam RH, Xu F, Sun Y, Chen Y, Saad JS. The Interplay between Calmodulin and Membrane Interactions with the Pleckstrin Homology Domain of Akt. The Journal of biological chemistry. 2017;292(1):251-63. Epub 2016/11/23. doi: 10.1074/jbc.M116.752816. PubMed PMID: 27872186; PubMed Central PMCID: PMCPMC5217684.
19. Coticchia CM, Revankar CM, Deb TB, Dickson RB, Johnson MD. Calmodulin modulates Akt activity in human breast cancer cell lines. Breast cancer research and treatment. 2009;115(3):545-60. Epub 2008/07/01. doi: 10.1007/s10549-008-0097-z. PubMed PMID: 18587642; PubMed Central PMCID: PMCPMC3736740.
20. Weako J, Jang H, Keskin O, Nussinov R, Gursoy A. The structural basis of Akt PH domain interaction with calmodulin. Biophysical journal. 2021. Epub 2021/03/30. doi: 10.1016/j.bpj.2021.03.018. PubMed PMID: 33775637.
21. Ding Z, Liang J, Li J, Lu Y, Ariyaratna V, Lu Z, et al. Physical association of PDK1 with AKT1 is sufficient for pathway activation independent of membrane localization and phosphatidylinositol 3 kinase. PloS one. 2010;5(3):e9910. Epub 2010/04/03. doi: 10.1371/journal.pone.0009910. PubMed PMID: 20361045; PubMed Central PMCID: PMCPMC2845649 Zhiyong Ding and Gordon B. Mills are inventors of a pending patent application, “Methods and compositions related to identifying protein-protein interactions”, International Patent Application No. PCT/US2005/024677. The declared competing interests do not alter the authors' adherence to all the PLoS ONE policies on sharing data and materials.
22. Yang WL, Wang J, Chan CH, Lee SW, Campos AD, Lamothe B, et al. The E3 ligase TRAF6 regulates Akt ubiquitination and activation. Science (New York, NY). 2009;325(5944):1134-8. Epub 2009/08/29. doi: 10.1126/science.1175065. PubMed PMID: 19713527; PubMed Central PMCID: PMCPMC3008763.
23. Wani R, Qian J, Yin L, Bechtold E, King SB, Poole LB, et al. Isoform-specific regulation of Akt by PDGF-induced reactive oxygen species. Proceedings of the

National Academy of Sciences of the United States of America. 2011;108(26):10550-5. Epub 2011/06/15. doi: 10.1073/pnas.1011665108. PubMed PMID: 21670275; PubMed Central PMCID: PMCPMC3127936.
24. Guo J, Dai X, Laurent B, Zheng N, Gan W, Zhang J, et al. AKT methylation by SETDB1 promotes AKT kinase activity and oncogenic functions. Nature cell biology. 2019;21(2):226-37. Epub 2019/01/30. doi: 10.1038/s41556-018-0261-6. PubMed PMID: 30692625; PubMed Central PMCID: PMCPMC6377565.
25. Wang G, Long J, Gao Y, Zhang W, Han F, Xu C, et al. SETDB1-mediated methylation of Akt promotes its K63-linked ubiquitination and activation leading to tumorigenesis. Nature cell biology. 2019;21(2):214-25. Epub 2019/01/30. doi: 10.1038/s41556-018-0266-1. PubMed PMID: 30692626; PubMed Central PMCID: PMCPMC6414065.
26. Guo J, Chakraborty AA, Liu P, Gan W, Zheng X, Inuzuka H, et al. pVHL suppresses kinase activity of Akt in a proline-hydroxylation-dependent manner. Science (New York, NY). 2016;353(6302):929-32. Epub 2016/08/27. doi: 10.1126/science.aad5755. PubMed PMID: 27563096; PubMed Central PMCID: PMCPMC5326551.
27. Agamasu C, Ghanam RH, Saad JS. Structural and Biophysical Characterization of the Interactions between Calmodulin and the Pleckstrin Homology Domain of Akt. The Journal of biological chemistry. 2015;290(45):27403-13. Epub 2015/09/24. doi: 10.1074/jbc.M115.673939. PubMed PMID: 26391397; PubMed Central PMCID: PMCPMC4646410.
28. Schenkelberg CD, Bystroff C. InteractiveROSETTA: a graphical user interface for the PyRosetta protein modeling suite. Bioinformatics (Oxford, England). 2015;31(24):4023-5. Epub 2015/09/01. doi: 10.1093/bioinformatics/btv492. PubMed PMID: 26315900; PubMed Central PMCID: PMCPMC5013933.
29. Lin K, Lin J, Wu WI, Ballard J, Lee BB, Gloor SL, et al. An ATP-site on-off switch that restricts phosphatase accessibility of Akt. Science signaling. 2012;5(223):ra37. Epub 2012/05/10. doi: 10.1126/scisignal.2002618. PubMed PMID: 22569334.
30. Ashwell MA, Lapierre JM, Brassard C, Bresciano K, Bull C, Cornell-Kennon S, et al. Discovery and optimization of a series of 3-(3-phenyl-3H-imidazo[4,5-b]pyridin-2-yl)pyridin-2-amines: orally bioavailable, selective, and potent ATP-independent Akt inhibitors. Journal of medicinal chemistry. 2012;55(11):5291-310. Epub 2012/04/27. doi: 10.1021/jm300276x. PubMed PMID: 22533986.
31. Quambusch L, Landel I, Depta L, Weisner J, Uhlenbrock N, Müller MP, et al. Covalent-Allosteric Inhibitors to Achieve Akt Isoform-Selectivity. Angewandte Chemie (International ed in English). 2019;58(52):18823-9. Epub 2019/10/05. doi: 10.1002/anie.201909857. PubMed PMID: 31584233; PubMed Central PMCID: PMCPMC6972997.
32. Roy A, Kucukural A, Zhang Y. I-TASSER: a unified platform for automated protein structure and function prediction. Nature protocols. 2010;5(4):725-38. Epub 2010/04/03. doi: 10.1038/nprot.2010.5. PubMed PMID: 20360767; PubMed Central PMCID: PMCPMC2849174.
33. Yang J, Zhang Y. Protein Structure and Function Prediction Using I-TASSER. Current protocols in bioinformatics. 2015;52:5.8.1-5.8.15. Epub 2015/12/19. doi: 10.1002/0471250953.bi0508s52. PubMed PMID: 26678386; PubMed Central PMCID: PMCPMC4871818.
34. Staal SP. Molecular cloning of the akt oncogene and its human homologues AKT1 and AKT2: amplification of AKT1 in a primary human gastric adenocarcinoma. Proceedings of the National Academy of Sciences of the United States of America. 1987;84(14):5034-7. Epub 1987/07/01. doi:

10.1073/pnas.84.14.5034. PubMed PMID: 3037531; PubMed Central PMCID: PMCPMC305241.
35. Manning G, Whyte DB, Martinez R, Hunter T, Sudarsanam S. The protein kinase complement of the human genome. Science (New York, NY). 2002;298(5600):1912-34. Epub 2002/12/10. doi: 10.1126/science.1075762. PubMed PMID: 12471243.
36. Pearce LR, Komander D, Alessi DR. The nuts and bolts of AGC protein kinases. Nat Rev Mol Cell Biol. 2010;11(1):9-22. Epub 2009/12/23. doi: 10.1038/nrm2822. PubMed PMID: 20027184.
37. Lahiry P, Torkamani A, Schork NJ, Hegele RA. Kinase mutations in human disease: interpreting genotype-phenotype relationships. Nature reviews Genetics. 2010;11(1):60-74. Epub 2009/12/19. doi: 10.1038/nrg2707. PubMed PMID: 20019687.
38. Ferguson FM, Gray NS. Kinase inhibitors: the road ahead. Nature reviews Drug discovery. 2018;17(5):353-77. Epub 2018/03/17. doi: 10.1038/nrd.2018.21. PubMed PMID: 29545548.
39. Cantley LC. The role of phosphoinositide 3-kinase in human disease. Harvey lectures. 2004;100:103-22. Epub 2006/09/15. PubMed PMID: 16970176.
40. Dillon RL, White DE, Muller WJ. The phosphatidyl inositol 3-kinase signaling network: implications for human breast cancer. Oncogene. 2007;26(9):1338-45. Epub 2007/02/27. doi: 10.1038/sj.onc.1210202. PubMed PMID: 17322919.
41. Miao B, Degterev A. Targeting phospshatidylinositol 3-kinase signaling with novel phosphatidylinositol 3,4,5-triphosphate antagonists. Autophagy. 2011;7(6):650-1. Epub 2011/04/05. doi: 10.4161/auto.7.6.15248. PubMed PMID: 21460619.
42. Altomare DA, Testa JR. Perturbations of the AKT signaling pathway in human cancer. Oncogene. 2005;24(50):7455-64. Epub 2005/11/17. doi: 10.1038/sj.onc.1209085. PubMed PMID: 16288292.
43. Fruman DA, Chiu H, Hopkins BD, Bagrodia S, Cantley LC, Abraham RT. The PI3K Pathway in Human Disease. Cell. 2017;170(4):605-35. Epub 2017/08/13. doi: 10.1016/j.cell.2017.07.029. PubMed PMID: 28802037; PubMed Central PMCID: PMCPMC5726441.
44. Carracedo A, Pandolfi PP. The PTEN-PI3K pathway: of feedbacks and cross-talks. Oncogene. 2008;27(41):5527-41. Epub 2008/09/17. doi: 10.1038/onc.2008.247. PubMed PMID: 18794886.
45. Chalhoub N, Baker SJ. PTEN and the PI3-kinase pathway in cancer. Annual review of pathology. 2009;4:127-50. Epub 2008/09/05. doi: 10.1146/annurev.pathol.4.110807.092311. PubMed PMID: 18767981; PubMed Central PMCID: PMCPMC2710138.
46. Leslie NR, Downes CP. PTEN function: how normal cells control it and tumour cells lose it. The Biochemical journal. 2004;382(Pt 1):1-11. Epub 2004/06/15. doi: 10.1042/bj20040825. PubMed PMID: 15193142; PubMed Central PMCID: PMCPMC1133909.
47. Bellacosa A, Kumar CC, Di Cristofano A, Testa JR. Activation of AKT kinases in cancer: implications for therapeutic targeting. Advances in cancer research. 2005;94:29-86. Epub 2005/08/13. doi: 10.1016/s0065-230x(05)94002-5. PubMed PMID: 16095999.
48. Testa JR, Bellacosa A. AKT plays a central role in tumorigenesis. Proceedings of the National Academy of Sciences of the United States of America. 2001;98(20):10983-5. Epub 2001/09/27. doi: 10.1073/pnas.211430998. PubMed PMID: 11572954; PubMed Central PMCID: PMCPMC58668.

49. DeBerardinis RJ, Lum JJ, Hatzivassiliou G, Thompson CB. The biology of cancer: metabolic reprogramming fuels cell growth and proliferation. Cell metabolism. 2008;7(1):11-20. Epub 2008/01/08. doi: 10.1016/j.cmet.2007.10.002. PubMed PMID: 18177721.
50. Testa JR, Tsichlis PN. AKT signaling in normal and malignant cells. Oncogene. 2005;24(50):7391-3. Epub 2005/11/17. doi: 10.1038/sj.onc.1209100. PubMed PMID: 16288285.
51. Datta SR, Dudek H, Tao X, Masters S, Fu H, Gotoh Y, et al. Akt phosphorylation of BAD couples survival signals to the cell-intrinsic death machinery. Cell. 1997;91(2):231-41. Epub 1997/11/05. doi: 10.1016/s0092-8674(00)80405-5. PubMed PMID: 9346240.
52. Yamaguchi H, Wang HG. The protein kinase PKB/Akt regulates cell survival and apoptosis by inhibiting Bax conformational change. Oncogene. 2001;20(53):7779-86. Epub 2001/12/26. doi: 10.1038/sj.onc.1204984. PubMed PMID: 11753656.
53. Zhou H, Li XM, Meinkoth J, Pittman RN. Akt regulates cell survival and apoptosis at a postmitochondrial level. The Journal of cell biology. 2000;151(3):483-94. Epub 2000/11/04. doi: 10.1083/jcb.151.3.483. PubMed PMID: 11062251; PubMed Central PMCID: PMCPMC2185587.
54. Fujita N, Sato S, Katayama K, Tsuruo T. Akt-dependent phosphorylation of p27Kip1 promotes binding to 14-3-3 and cytoplasmic localization. The Journal of biological chemistry. 2002;277(32):28706-13. Epub 2002/06/04. doi: 10.1074/jbc.M203668200. PubMed PMID: 12042314.
55. Song G, Ouyang G, Bao S. The activation of Akt/PKB signaling pathway and cell survival. Journal of cellular and molecular medicine. 2005;9(1):59-71. Epub 2005/03/24. doi: 10.1111/j.1582-4934.2005.tb00337.x. PubMed PMID: 15784165; PubMed Central PMCID: PMCPMC6741304.
56. Harada H, Itasaka S, Kizaka-Kondoh S, Shibuya K, Morinibu A, Shinomiya K, et al. The Akt/mTOR pathway assures the synthesis of HIF-1alpha protein in a glucose- and reoxygenation-dependent manner in irradiated tumors. The Journal of biological chemistry. 2009;284(8):5332-42. Epub 2008/12/23. doi: 10.1074/jbc.M806653200. PubMed PMID: 19098000.
57. Pore N, Jiang Z, Shu HK, Bernhard E, Kao GD, Maity A. Akt1 activation can augment hypoxia-inducible factor-1alpha expression by increasing protein translation through a mammalian target of rapamycin-independent pathway. Molecular cancer research : MCR. 2006;4(7):471-9. Epub 2006/07/20. doi: 10.1158/1541-7786.Mcr-05-0234. PubMed PMID: 16849522.
58. Diehl JA, Cheng M, Roussel MF, Sherr CJ. Glycogen synthase kinase-3beta regulates cyclin D1 proteolysis and subcellular localization. Genes & development. 1998;12(22):3499-511. Epub 1998/12/01. doi: 10.1101/gad.12.22.3499. PubMed PMID: 9832503; PubMed Central PMCID: PMCPMC317244.
59. Kohn AD, Summers SA, Birnbaum MJ, Roth RA. Expression of a constitutively active Akt Ser/Thr kinase in 3T3-L1 adipocytes stimulates glucose uptake and glucose transporter 4 translocation. The Journal of biological chemistry. 1996;271(49):31372-8. Epub 1996/12/06. doi: 10.1074/jbc.271.49.31372. PubMed PMID: 8940145.
60. Pap M, Cooper GM. Role of glycogen synthase kinase-3 in the phosphatidylinositol 3-Kinase/Akt cell survival pathway. The Journal of biological chemistry. 1998;273(32):19929-32. Epub 1998/08/01. doi: 10.1074/jbc.273.32.19929. PubMed PMID: 9685326.
61. Webb AE, Kundaje A, Brunet A. Characterization of the direct targets of FOXO transcription factors throughout evolution. Aging cell. 2016;15(4):673-85.

Epub 2016/04/12. doi: 10.1111/acel.12479. PubMed PMID: 27061590; PubMed Central PMCID: PMCPMC4933671.
62. Zhang X, Gan L, Pan H, Guo S, He X, Olson ST, et al. Phosphorylation of serine 256 suppresses transactivation by FKHR (FOXO1) by multiple mechanisms. Direct and indirect effects on nuclear/cytoplasmic shuttling and DNA binding. The Journal of biological chemistry. 2002;277(47):45276-84. Epub 2002/09/14. doi: 10.1074/jbc.M208063200. PubMed PMID: 12228231.
63. Tzivion G, Dobson M, Ramakrishnan G. FoxO transcription factors; Regulation by AKT and 14-3-3 proteins. Biochimica et biophysica acta. 2011;1813(11):1938-45. Epub 2011/06/29. doi: 10.1016/j.bbamcr.2011.06.002. PubMed PMID: 21708191.
64. Webb AE, Brunet A. FOXO transcription factors: key regulators of cellular quality control. Trends in biochemical sciences. 2014;39(4):159-69. Epub 2014/03/19. doi: 10.1016/j.tibs.2014.02.003. PubMed PMID: 24630600; PubMed Central PMCID: PMCPMC4021867.
65. Zhang X, Tang N, Hadden TJ, Rishi AK. Akt, FoxO and regulation of apoptosis. Biochimica et biophysica acta. 2011;1813(11):1978-86. Epub 2011/03/29. doi: 10.1016/j.bbamcr.2011.03.010. PubMed PMID: 21440011.
66. Moeller BJ, Cao Y, Li CY, Dewhirst MW. Radiation activates HIF-1 to regulate vascular radiosensitivity in tumors: role of reoxygenation, free radicals, and stress granules. Cancer cell. 2004;5(5):429-41. Epub 2004/05/18. doi: 10.1016/s1535-6108(04)00115-1. PubMed PMID: 15144951.
67. Niecknig H, Tug S, Reyes BD, Kirsch M, Fandrey J, Berchner-Pfannschmidt U. Role of reactive oxygen species in the regulation of HIF-1 by prolyl hydroxylase 2 under mild hypoxia. Free radical research. 2012;46(6):705-17. Epub 2012/03/01. doi: 10.3109/10715762.2012.669041. PubMed PMID: 22360728.
68. Lee YH, Bae HC, Noh KH, Song KH, Ye SK, Mao CP, et al. Gain of HIF-1α under normoxia in cancer mediates immune adaptation through the AKT/ERK and VEGFA axes. Clinical cancer research : an official journal of the American Association for Cancer Research. 2015;21(6):1438-46. Epub 2015/01/16. doi: 10.1158/1078-0432.Ccr-14-1979. PubMed PMID: 25589622; PubMed Central PMCID: PMCPMC4359944.
69. Krock BL, Skuli N, Simon MC. Hypoxia-induced angiogenesis: good and evil. Genes & cancer. 2011;2(12):1117-33. Epub 2012/08/07. doi: 10.1177/1947601911423654. PubMed PMID: 22866203; PubMed Central PMCID: PMCPMC3411127.
70. Santos CR, Schulze A. Lipid metabolism in cancer. The FEBS journal. 2012;279(15):2610-23. Epub 2012/05/25. doi: 10.1111/j.1742-4658.2012.08644.x. PubMed PMID: 22621751.
71. Huang J, Manning BD. The TSC1-TSC2 complex: a molecular switchboard controlling cell growth. The Biochemical journal. 2008;412(2):179-90. Epub 2008/05/10. doi: 10.1042/bj20080281. PubMed PMID: 18466115; PubMed Central PMCID: PMCPMC2735030.
72. Porstmann T, Santos CR, Griffiths B, Cully M, Wu M, Leevers S, et al. SREBP activity is regulated by mTORC1 and contributes to Akt-dependent cell growth. Cell metabolism. 2008;8(3):224-36. Epub 2008/09/03. doi: 10.1016/j.cmet.2008.07.007. PubMed PMID: 18762023; PubMed Central PMCID: PMCPMC2593919.
73. Krycer JR, Sharpe LJ, Luu W, Brown AJ. The Akt-SREBP nexus: cell signaling meets lipid metabolism. Trends in endocrinology and metabolism: TEM. 2010;21(5):268-76. Epub 2010/02/02. doi: 10.1016/j.tem.2010.01.001. PubMed PMID: 20117946.

74. Laplante M, Sabatini DM. An emerging role of mTOR in lipid biosynthesis. Current biology : CB. 2009;19(22):R1046-52. Epub 2009/12/02. doi: 10.1016/j.cub.2009.09.058. PubMed PMID: 19948145; PubMed Central PMCID: PMCPMC3390254.
75. Gingras AC, Kennedy SG, O'Leary MA, Sonenberg N, Hay N. 4E-BP1, a repressor of mRNA translation, is phosphorylated and inactivated by the Akt(PKB) signaling pathway. Genes & development. 1998;12(4):502-13. Epub 1998/03/21. doi: 10.1101/gad.12.4.502. PubMed PMID: 9472019; PubMed Central PMCID: PMCPMC316523.
76. Siddiqui N, Sonenberg N. Signalling to eIF4E in cancer. Biochemical Society transactions. 2015;43(5):763-72. Epub 2015/11/01. doi: 10.1042/bst20150126. PubMed PMID: 26517881; PubMed Central PMCID: PMCPMC4613458.
77. Lazaris-Karatzas A, Montine KS, Sonenberg N. Malignant transformation by a eukaryotic initiation factor subunit that binds to mRNA 5' cap. Nature. 1990;345(6275):544-7. Epub 1990/06/07. doi: 10.1038/345544a0. PubMed PMID: 2348862.
78. Wendel HG, Silva RL, Malina A, Mills JR, Zhu H, Ueda T, et al. Dissecting eIF4E action in tumorigenesis. Genes & development. 2007;21(24):3232-7. Epub 2007/12/07. doi: 10.1101/gad.1604407. PubMed PMID: 18055695; PubMed Central PMCID: PMCPMC2113024.
79. Cross DA, Alessi DR, Cohen P, Andjelkovich M, Hemmings BA. Inhibition of glycogen synthase kinase-3 by insulin mediated by protein kinase B. Nature. 1995;378(6559):785-9. Epub 1995/12/21. doi: 10.1038/378785a0. PubMed PMID: 8524413.
80. Jiang ZY, Zhou QL, Coleman KA, Chouinard M, Boese Q, Czech MP. Insulin signaling through Akt/protein kinase B analyzed by small interfering RNA-mediated gene silencing. Proceedings of the National Academy of Sciences of the United States of America. 2003;100(13):7569-74. Epub 2003/06/17. doi: 10.1073/pnas.1332633100. PubMed PMID: 12808134; PubMed Central PMCID: PMCPMC164627.
81. Maccario H, Perera NM, Davidson L, Downes CP, Leslie NR. PTEN is destabilized by phosphorylation on Thr366. The Biochemical journal. 2007;405(3):439-44. Epub 2007/04/21. doi: 10.1042/bj20061837. PubMed PMID: 17444818; PubMed Central PMCID: PMCPMC2267318.
82. Beurel E, Grieco SF, Jope RS. Glycogen synthase kinase-3 (GSK3): regulation, actions, and diseases. Pharmacology & therapeutics. 2015;148:114-31. Epub 2014/12/02. doi: 10.1016/j.pharmthera.2014.11.016. PubMed PMID: 25435019; PubMed Central PMCID: PMCPMC4340754.
83. Buller CL, Loberg RD, Fan MH, Zhu Q, Park JL, Vesely E, et al. A GSK-3/TSC2/mTOR pathway regulates glucose uptake and GLUT1 glucose transporter expression. American journal of physiology Cell physiology. 2008;295(3):C836-43. Epub 2008/07/25. doi: 10.1152/ajpcell.00554.2007. PubMed PMID: 18650261; PubMed Central PMCID: PMCPMC2544442.
84. Yost C, Torres M, Miller JR, Huang E, Kimelman D, Moon RT. The axis-inducing activity, stability, and subcellular distribution of beta-catenin is regulated in Xenopus embryos by glycogen synthase kinase 3. Genes & development. 1996;10(12):1443-54. Epub 1996/06/15. doi: 10.1101/gad.10.12.1443. PubMed PMID: 8666229.
85. Wu D, Pan W. GSK3: a multifaceted kinase in Wnt signaling. Trends in biochemical sciences. 2010;35(3):161-8. Epub 2009/11/04. doi: 10.1016/j.tibs.2009.10.002. PubMed PMID: 19884009; PubMed Central PMCID: PMCPMC2834833.

86. Elstrom RL, Bauer DE, Buzzai M, Karnauskas R, Harris MH, Plas DR, et al. Akt stimulates aerobic glycolysis in cancer cells. Cancer research. 2004;64(11):3892-9. Epub 2004/06/03. doi: 10.1158/0008-5472.Can-03-2904. PubMed PMID: 15172999.
87. Barthel A, Okino ST, Liao J, Nakatani K, Li J, Whitlock JP, Jr., et al. Regulation of GLUT1 gene transcription by the serine/threonine kinase Akt1. The Journal of biological chemistry. 1999;274(29):20281-6. Epub 1999/07/10. doi: 10.1074/jbc.274.29.20281. PubMed PMID: 10400647.
88. Buzzai M, Bauer DE, Jones RG, Deberardinis RJ, Hatzivassiliou G, Elstrom RL, et al. The glucose dependence of Akt-transformed cells can be reversed by pharmacologic activation of fatty acid beta-oxidation. Oncogene. 2005;24(26):4165-73. Epub 2005/04/05. doi: 10.1038/sj.onc.1208622. PubMed PMID: 15806154.
89. Staal SP, Hartley JW, Rowe WP. Isolation of transforming murine leukemia viruses from mice with a high incidence of spontaneous lymphoma. Proceedings of the National Academy of Sciences of the United States of America. 1977;74(7):3065-7. Epub 1977/07/01. doi: 10.1073/pnas.74.7.3065. PubMed PMID: 197531; PubMed Central PMCID: PMCPMC431413.
90. Manning BD, Cantley LC. AKT/PKB signaling: navigating downstream. Cell. 2007;129(7):1261-74. Epub 2007/07/03. doi: 10.1016/j.cell.2007.06.009. PubMed PMID: 17604717; PubMed Central PMCID: PMCPMC2756685.
91. Santi SA, Lee H. The Akt isoforms are present at distinct subcellular locations. American journal of physiology Cell physiology. 2010;298(3):C580-91. Epub 2009/12/19. doi: 10.1152/ajpcell.00375.2009. PubMed PMID: 20018949.
92. Cho H, Mu J, Kim JK, Thorvaldsen JL, Chu Q, Crenshaw EB, 3rd, et al. Insulin resistance and a diabetes mellitus-like syndrome in mice lacking the protein kinase Akt2 (PKB beta). Science (New York, NY). 2001;292(5522):1728-31. Epub 2001/06/02. doi: 10.1126/science.292.5522.1728. PubMed PMID: 11387480.
93. Chan CH, Jo U, Kohrman A, Rezaeian AH, Chou PC, Logothetis C, et al. Posttranslational regulation of Akt in human cancer. Cell & bioscience. 2014;4(1):59. Epub 2014/10/14. doi: 10.1186/2045-3701-4-59. PubMed PMID: 25309720; PubMed Central PMCID: PMCPMC4192732.
94. Yang ZZ, Tschopp O, Baudry A, Dümmler B, Hynx D, Hemmings BA. Physiological functions of protein kinase B/Akt. Biochemical Society transactions. 2004;32(Pt 2):350-4. Epub 2004/03/30. doi: 10.1042/bst0320350. PubMed PMID: 15046607.
95. Tschopp O, Yang ZZ, Brodbeck D, Dummler BA, Hemmings-Mieszczak M, Watanabe T, et al. Essential role of protein kinase B gamma (PKB gamma/Akt3) in postnatal brain development but not in glucose homeostasis. Development (Cambridge, England). 2005;132(13):2943-54. Epub 2005/06/03. doi: 10.1242/dev.01864. PubMed PMID: 15930105.
96. Riggio M, Perrone MC, Polo ML, Rodriguez MJ, May M, Abba M, et al. AKT1 and AKT2 isoforms play distinct roles during breast cancer progression through the regulation of specific downstream proteins. Scientific reports. 2017;7:44244. Epub 2017/03/14. doi: 10.1038/srep44244. PubMed PMID: 28287129; PubMed Central PMCID: PMCPMC5347151.
97. Linnerth-Petrik NM, Santry LA, Petrik JJ, Wootton SK. Opposing functions of Akt isoforms in lung tumor initiation and progression. PloS one. 2014;9(4):e94595. Epub 2014/04/12. doi: 10.1371/journal.pone.0094595. PubMed PMID: 24722238; PubMed Central PMCID: PMCPMC3983215.
98. Stockwell BR. Exploring biology with small organic molecules. Nature. 2004;432(7019):846-54. Epub 2004/12/17. doi: 10.1038/nature03196. PubMed PMID: 15602550; PubMed Central PMCID: PMCPMC3165172.

99. Alessi DR, Andjelkovic M, Caudwell B, Cron P, Morrice N, Cohen P, et al. Mechanism of activation of protein kinase B by insulin and IGF-1. Embo j. 1996;15(23):6541-51. Epub 1996/12/02. PubMed PMID: 8978681; PubMed Central PMCID: PMCPMC452479.
100. Masure S, Haefner B, Wesselink JJ, Hoefnagel E, Mortier E, Verhasselt P, et al. Molecular cloning, expression and characterization of the human serine/threonine kinase Akt-3. European journal of biochemistry. 1999;265(1):353-60. Epub 1999/09/22. doi: 10.1046/j.1432-1327.1999.00774.x. PubMed PMID: 10491192.
101. Scheffzek K, Welti S. Pleckstrin homology (PH) like domains - versatile modules in protein-protein interaction platforms. FEBS letters. 2012;586(17):2662-73. Epub 2012/06/26. doi: 10.1016/j.febslet.2012.06.006. PubMed PMID: 22728242.
102. Haslam RJ, Koide HB, Hemmings BA. Pleckstrin domain homology. Nature. 1993;363(6427):309-10. Epub 1993/05/27. doi: 10.1038/363309b0. PubMed PMID: 8497315.
103. Macias MJ, Musacchio A, Ponstingl H, Nilges M, Saraste M, Oschkinat H. Structure of the pleckstrin homology domain from beta-spectrin. Nature. 1994;369(6482):675-7. Epub 1994/06/23. doi: 10.1038/369675a0. PubMed PMID: 8208297.
104. Yoon HS, Hajduk PJ, Petros AM, Olejniczak ET, Meadows RP, Fesik SW. Solution structure of a pleckstrin-homology domain. Nature. 1994;369(6482):672-5. Epub 1994/06/23. doi: 10.1038/369672a0. PubMed PMID: 8208296.
105. Saraste M, Hyvönen M. Pleckstrin homology domains: a fact file. Current opinion in structural biology. 1995;5(3):403-8. Epub 1995/06/01. doi: 10.1016/0959-440x(95)80104-9. PubMed PMID: 7583640.
106. Chan TO, Zhang J, Rodeck U, Pascal JM, Armen RS, Spring M, et al. Resistance of Akt kinases to dephosphorylation through ATP-dependent conformational plasticity. Proceedings of the National Academy of Sciences of the United States of America. 2011;108(46):E1120-7. Epub 2011/10/28. doi: 10.1073/pnas.1109879108. PubMed PMID: 22031698; PubMed Central PMCID: PMCPMC3219155.
107. Ebner M, Lučić I, Leonard TA, Yudushkin I. PI(3,4,5)P(3) Engagement Restricts Akt Activity to Cellular Membranes. Molecular cell. 2017;65(3):416-31.e6. Epub 2017/02/06. doi: 10.1016/j.molcel.2016.12.028. PubMed PMID: 28157504.
108. Lucic I, Rathinaswamy MK, Truebestein L, Hamelin DJ, Burke JE, Leonard TA. Conformational sampling of membranes by Akt controls its activation and inactivation. Proceedings of the National Academy of Sciences of the United States of America. 2018;115(17):E3940-e9. Epub 2018/04/11. doi: 10.1073/pnas.1716109115. PubMed PMID: 29632185; PubMed Central PMCID: PMCPMC5924885.
109. Franke TF. Intracellular signaling by Akt: bound to be specific. Science signaling. 2008;1(24):pe29. Epub 2008/06/19. doi: 10.1126/scisignal.124pe29. PubMed PMID: 18560018.
110. Yap TA, Garrett MD, Walton MI, Raynaud F, de Bono JS, Workman P. Targeting the PI3K-AKT-mTOR pathway: progress, pitfalls, and promises. Current opinion in pharmacology. 2008;8(4):393-412. Epub 2008/08/30. doi: 10.1016/j.coph.2008.08.004. PubMed PMID: 18721898.
111. Cooray S. The pivotal role of phosphatidylinositol 3-kinase-Akt signal transduction in virus survival. The Journal of general virology. 2004;85(Pt 5):1065-76. Epub 2004/04/24. doi: 10.1099/vir.0.19771-0. PubMed PMID: 15105524.

112. Milburn CC, Deak M, Kelly SM, Price NC, Alessi DR, Van Aalten DM. Binding of phosphatidylinositol 3,4,5-trisphosphate to the pleckstrin homology domain of protein kinase B induces a conformational change. The Biochemical journal. 2003;375(Pt 3):531-8. Epub 2003/09/11. doi: 10.1042/bj20031229. PubMed PMID: 12964941; PubMed Central PMCID: PMCPMC1223737.
113. Deb TB, Coticchia CM, Dickson RB. Calmodulin-mediated activation of Akt regulates survival of c-Myc-overexpressing mouse mammary carcinoma cells. The Journal of biological chemistry. 2004;279(37):38903-11. Epub 2004/07/13. doi: 10.1074/jbc.M405314200. PubMed PMID: 15247222.
114. Powell DJ, Hajduch E, Kular G, Hundal HS. Ceramide disables 3-phosphoinositide binding to the pleckstrin homology domain of protein kinase B (PKB)/Akt by a PKCzeta-dependent mechanism. Molecular and cellular biology. 2003;23(21):7794-808. Epub 2003/10/16. doi: 10.1128/mcb.23.21.7794-7808.2003. PubMed PMID: 14560023; PubMed Central PMCID: PMCPMC207567.
115. Huang BX, Lee R, Akbar M, Kim HY. Threonine 34 phosphorylation by phosphoinositide-dependent protein kinase 1 facilitates dissociation of Akt from the plasma membrane. The international journal of biochemistry & cell biology. 2015;64:195-201. Epub 2015/04/29. doi: 10.1016/j.biocel.2015.04.007. PubMed PMID: 25912234; PubMed Central PMCID: PMCPMC4461485.
116. Várnai P, Bondeva T, Tamás P, Tóth B, Buday L, Hunyady L, et al. Selective cellular effects of overexpressed pleckstrin-homology domains that recognize PtdIns(3,4,5)P3 suggest their interaction with protein binding partners. Journal of cell science. 2005;118(Pt 20):4879-88. Epub 2005/10/13. doi: 10.1242/jcs.02606. PubMed PMID: 16219693.
117. Yudushkin I. Control of Akt activity and substrate phosphorylation in cells. IUBMB life. 2020;72(6):1115-25. Epub 2020/03/04. doi: 10.1002/iub.2264. PubMed PMID: 32125765; PubMed Central PMCID: PMCPMC7317883.
118. Humphrey SJ, Azimifar SB, Mann M. High-throughput phosphoproteomics reveals in vivo insulin signaling dynamics. Nature biotechnology. 2015;33(9):990-5. Epub 2015/08/19. doi: 10.1038/nbt.3327. PubMed PMID: 26280412.
119. Humphrey SJ, Yang G, Yang P, Fazakerley DJ, Stöckli J, Yang JY, et al. Dynamic adipocyte phosphoproteome reveals that Akt directly regulates mTORC2. Cell metabolism. 2013;17(6):1009-20. Epub 2013/05/21. doi: 10.1016/j.cmet.2013.04.010. PubMed PMID: 23684622; PubMed Central PMCID: PMCPMC3690479.
120. Kunkel MT, Ni Q, Tsien RY, Zhang J, Newton AC. Spatio-temporal dynamics of protein kinase B/Akt signaling revealed by a genetically encoded fluorescent reporter. The Journal of biological chemistry. 2005;280(7):5581-7. Epub 2004/12/08. doi: 10.1074/jbc.M411534200. PubMed PMID: 15583002; PubMed Central PMCID: PMCPMC2913970.
121. Vivanco I, Sawyers CL. The phosphatidylinositol 3-Kinase AKT pathway in human cancer. Nature reviews Cancer. 2002;2(7):489-501. Epub 2002/07/03. doi: 10.1038/nrc839. PubMed PMID: 12094235.
122. Garcia-Echeverria C, Sellers WR. Drug discovery approaches targeting the PI3K/Akt pathway in cancer. Oncogene. 2008;27(41):5511-26. Epub 2008/09/17. doi: 10.1038/onc.2008.246. PubMed PMID: 18794885.
123. Sun XF, Sun ZY, Pan B, Li L, Shen W. Alteration in methylation pattern of oncogene Akt1 promoter region in bladder cancer. Molecular biology reports. 2012;39(5):5631-6. Epub 2011/12/23. doi: 10.1007/s11033-011-1369-y. PubMed PMID: 22189542.
124. Heng J, Guo X, Wu W, Wang Y, Li G, Chen M, et al. Integrated analysis of promoter mutation, methylation and expression of AKT1 gene in Chinese breast

cancer patients. PloS one. 2017;12(3):e0174022. Epub 2017/03/17. doi: 10.1371/journal.pone.0174022. PubMed PMID: 28301567; PubMed Central PMCID: PMCPMC5354459 of Sanway Gene Technology Inc. This does not alter our adherence to PLOS ONE policies on sharing data and materials.
125. Sundaresan NR, Pillai VB, Wolfgeher D, Samant S, Vasudevan P, Parekh V, et al. The deacetylase SIRT1 promotes membrane localization and activation of Akt and PDK1 during tumorigenesis and cardiac hypertrophy. Science signaling. 2011;4(182):ra46. Epub 2011/07/22. doi: 10.1126/scisignal.2001465. PubMed PMID: 21775285.
126. Yang WL, Wu CY, Wu J, Lin HK. Regulation of Akt signaling activation by ubiquitination. Cell cycle (Georgetown, Tex). 2010;9(3):487-97. Epub 2010/01/19. doi: 10.4161/cc.9.3.10508. PubMed PMID: 20081374; PubMed Central PMCID: PMCPMC3077544.
127. Risso G, Pelisch F, Pozzi B, Mammi P, Blaustein M, Colman-Lerner A, et al. Modification of Akt by SUMO conjugation regulates alternative splicing and cell cycle. Cell cycle (Georgetown, Tex). 2013;12(19):3165-74. Epub 2013/09/10. doi: 10.4161/cc.26183. PubMed PMID: 24013425; PubMed Central PMCID: PMCPMC3865012.
128. de la Cruz-Herrera CF, Campagna M, Lang V, del Carmen González-Santamaría J, Marcos-Villar L, Rodríguez MS, et al. SUMOylation regulates AKT1 activity. Oncogene. 2015;34(11):1442-50. Epub 2014/04/08. doi: 10.1038/onc.2014.48. PubMed PMID: 24704831.
129. Li R, Wei J, Jiang C, Liu D, Deng L, Zhang K, et al. Akt SUMOylation regulates cell proliferation and tumorigenesis. Cancer research. 2013;73(18):5742-53. Epub 2013/07/26. doi: 10.1158/0008-5472.Can-13-0538. PubMed PMID: 23884910.
130. Lin CH, Liu SY, Lee EH. SUMO modification of Akt regulates global SUMOylation and substrate SUMOylation specificity through Akt phosphorylation of Ubc9 and SUMO1. Oncogene. 2016;35(5):595-607. Epub 2015/04/14. doi: 10.1038/onc.2015.115. PubMed PMID: 25867063.
131. Wang S, Huang X, Sun D, Xin X, Pan Q, Peng S, et al. Extensive crosstalk between O-GlcNAcylation and phosphorylation regulates Akt signaling. PloS one. 2012;7(5):e37427. Epub 2012/05/26. doi: 10.1371/journal.pone.0037427. PubMed PMID: 22629392; PubMed Central PMCID: PMCPMC3358304.
132. Costa C, Pereira S, Lima L, Peixoto A, Fernandes E, Neves D, et al. Abnormal Protein Glycosylation and Activated PI3K/Akt/mTOR Pathway: Role in Bladder Cancer Prognosis and Targeted Therapeutics. PloS one. 2015;10(11):e0141253. Epub 2015/11/17. doi: 10.1371/journal.pone.0141253. PubMed PMID: 26569621; PubMed Central PMCID: PMCPMC4646664.
133. Yi KH, Lauring J. Recurrent AKT mutations in human cancers: functional consequences and effects on drug sensitivity. Oncotarget. 2016;7(4):4241-51. Epub 2015/12/25. doi: 10.18632/oncotarget.6648. PubMed PMID: 26701849; PubMed Central PMCID: PMCPMC4826202.
134. Carpten JD, Faber AL, Horn C, Donoho GP, Briggs SL, Robbins CM, et al. A transforming mutation in the pleckstrin homology domain of AKT1 in cancer. Nature. 2007;448(7152):439-44. Epub 2007/07/06. doi: 10.1038/nature05933. PubMed PMID: 17611497.
135. Cerami E, Gao J, Dogrusoz U, Gross BE, Sumer SO, Aksoy BA, et al. The cBio cancer genomics portal: an open platform for exploring multidimensional cancer genomics data. Cancer discovery. 2012;2(5):401-4. Epub 2012/05/17. doi: 10.1158/2159-8290.Cd-12-0095. PubMed PMID: 22588877; PubMed Central PMCID: PMCPMC3956037.

136. Gao J, Aksoy BA, Dogrusoz U, Dresdner G, Gross B, Sumer SO, et al. Integrative analysis of complex cancer genomics and clinical profiles using the cBioPortal. Science signaling. 2013;6(269):pl1. Epub 2013/04/04. doi: 10.1126/scisignal.2004088. PubMed PMID: 23550210; PubMed Central PMCID: PMCPMC4160307.
137. Stephens PJ, Tarpey PS, Davies H, Van Loo P, Greenman C, Wedge DC, et al. The landscape of cancer genes and mutational processes in breast cancer. Nature. 2012;486(7403):400-4. Epub 2012/06/23. doi: 10.1038/nature11017. PubMed PMID: 22722201; PubMed Central PMCID: PMCPMC3428862.
138. Yi KH, Axtmayer J, Gustin JP, Rajpurohit A, Lauring J. Functional analysis of non-hotspot AKT1 mutants found in human breast cancers identifies novel driver mutations: implications for personalized medicine. Oncotarget. 2013;4(1):29-34. Epub 2012/12/15. doi: 10.18632/oncotarget.755. PubMed PMID: 23237847; PubMed Central PMCID: PMCPMC3702205 described in this article.
139. Cohen Y, Shalmon B, Korach J, Barshack I, Fridman E, Rechavi G. AKT1 pleckstrin homology domain E17K activating mutation in endometrial carcinoma. Gynecologic oncology. 2010;116(1):88-91. Epub 2009/10/27. doi: 10.1016/j.ygyno.2009.09.038. PubMed PMID: 19853286.
140. Boormans JL, Korsten H, Ziel-van der Made AC, van Leenders GJ, Verhagen PC, Trapman J. E17K substitution in AKT1 in prostate cancer. British journal of cancer. 2010;102(10):1491-4. Epub 2010/04/22. doi: 10.1038/sj.bjc.6605673. PubMed PMID: 20407443; PubMed Central PMCID: PMCPMC2869172.
141. Askham JM, Platt F, Chambers PA, Snowden H, Taylor CF, Knowles MA. AKT1 mutations in bladder cancer: identification of a novel oncogenic mutation that can co-operate with E17K. Oncogene. 2010;29(1):150-5. Epub 2009/10/06. doi: 10.1038/onc.2009.315. PubMed PMID: 19802009.
142. De Marco C, Malanga D, Rinaldo N, De Vita F, Scrima M, Lovisa S, et al. Mutant AKT1-E17K is oncogenic in lung epithelial cells. Oncotarget. 2015;6(37):39634-50. Epub 2015/06/09. doi: 10.18632/oncotarget.4022. PubMed PMID: 26053093; PubMed Central PMCID: PMCPMC4741851.
143. Davies MA, Stemke-Hale K, Tellez C, Calderone TL, Deng W, Prieto VG, et al. A novel AKT3 mutation in melanoma tumours and cell lines. British journal of cancer. 2008;99(8):1265-8. Epub 2008/09/25. doi: 10.1038/sj.bjc.6604637. PubMed PMID: 18813315; PubMed Central PMCID: PMCPMC2570525.
144. Kim MS, Jeong EG, Yoo NJ, Lee SH. Mutational analysis of oncogenic AKT E17K mutation in common solid cancers and acute leukaemias. British journal of cancer. 2008;98(9):1533-5. Epub 2008/04/09. doi: 10.1038/sj.bjc.6604212. PubMed PMID: 18392055; PubMed Central PMCID: PMCPMC2391109.
145. Ellis MJ, Ding L, Shen D, Luo J, Suman VJ, Wallis JW, et al. Whole-genome analysis informs breast cancer response to aromatase inhibition. Nature. 2012;486(7403):353-60. Epub 2012/06/23. doi: 10.1038/nature11143. PubMed PMID: 22722193; PubMed Central PMCID: PMCPMC3383766.
146. Zehir A, Benayed R, Shah RH, Syed A, Middha S, Kim HR, et al. Mutational landscape of metastatic cancer revealed from prospective clinical sequencing of 10,000 patients. Nature medicine. 2017;23(6):703-13. Epub 2017/05/10. doi: 10.1038/nm.4333. PubMed PMID: 28481359; PubMed Central PMCID: PMCPMC5461196.
147. Bessière L, Todeschini AL, Auguste A, Sarnacki S, Flatters D, Legois B, et al. A Hot-spot of In-frame Duplications Activates the Oncoprotein AKT1 in Juvenile Granulosa Cell Tumors. EBioMedicine. 2015;2(5):421-31. Epub 2015/07/03. doi: 10.1016/j.ebiom.2015.03.002. PubMed PMID: 26137586; PubMed Central PMCID: PMCPMC4485906.

148. Akbar M, Calderon F, Wen Z, Kim HY. Docosahexaenoic acid: a positive modulator of Akt signaling in neuronal survival. Proceedings of the National Academy of Sciences of the United States of America. 2005;102(31):10858-63. Epub 2005/07/26. doi: 10.1073/pnas.0502903102. PubMed PMID: 16040805; PubMed Central PMCID: PMCPMC1182431.
149. Nitulescu GM, Margina D, Juzenas P, Peng Q, Olaru OT, Saloustros E, et al. Akt inhibitors in cancer treatment: The long journey from drug discovery to clinical use (Review). International journal of oncology. 2016;48(3):869-85. Epub 2015/12/25. doi: 10.3892/ijo.2015.3306. PubMed PMID: 26698230; PubMed Central PMCID: PMCPMC4750533.
150. Yang J, Cron P, Good VM, Thompson V, Hemmings BA, Barford D. Crystal structure of an activated Akt/protein kinase B ternary complex with GSK3-peptide and AMP-PNP. Nature structural biology. 2002;9(12):940-4. Epub 2002/11/16. doi: 10.1038/nsb870. PubMed PMID: 12434148.
151. Okuzumi T, Fiedler D, Zhang C, Gray DC, Aizenstein B, Hoffman R, et al. Inhibitor hijacking of Akt activation. Nature chemical biology. 2009;5(7):484-93. Epub 2009/05/26. doi: 10.1038/nchembio.183. PubMed PMID: 19465931; PubMed Central PMCID: PMCPMC2783590.
152. Wu WI, Voegtli WC, Sturgis HL, Dizon FP, Vigers GP, Brandhuber BJ. Crystal structure of human AKT1 with an allosteric inhibitor reveals a new mode of kinase inhibition. PloS one. 2010;5(9):e12913. Epub 2010/10/05. doi: 10.1371/journal.pone.0012913. PubMed PMID: 20886116; PubMed Central PMCID: PMCPMC2944833 Wen-I Wu, Walter Voegtli, Hillary Sturgis, Guy Vigers, and Barbara Brandhuber are employees and stockholders of Array BioPharma Inc. Faith Dizon is a former employee of Array BioPharma Inc. Genentech, Inc. has products in development in this pathway. The authors agree to adhere to all the PLoS ONE policies on sharing data and materials, as detailed online in the PLoS ONE guide for authors. Array BioPharma Inc. and Genentech, Inc. approved this publication and adherence to the material and data sharing policies of the publishing journal.
153. Balog EM, Norton LE, Thomas DD, Fruen BR. Role of calmodulin methionine residues in mediating productive association with cardiac ryanodine receptors. American journal of physiology Heart and circulatory physiology. 2006;290(2):H794-9. Epub 2005/10/04. doi: 10.1152/ajpheart.00706.2005. PubMed PMID: 16199479.
154. Kumar CC, Madison V. AKT crystal structure and AKT-specific inhibitors. Oncogene. 2005;24(50):7493-501. Epub 2005/11/17. doi: 10.1038/sj.onc.1209087. PubMed PMID: 16288296.
155. Mundi PS, Sachdev J, McCourt C, Kalinsky K. AKT in cancer: new molecular insights and advances in drug development. British journal of clinical pharmacology. 2016;82(4):943-56. Epub 2016/05/28. doi: 10.1111/bcp.13021. PubMed PMID: 27232857; PubMed Central PMCID: PMCPMC5137819.
156. Xing Y, Lin NU, Maurer MA, Chen H, Mahvash A, Sahin A, et al. Phase II trial of AKT inhibitor MK-2206 in patients with advanced breast cancer who have tumors with PIK3CA or AKT mutations, and/or PTEN loss/PTEN mutation. Breast cancer research : BCR. 2019;21(1):78. Epub 2019/07/07. doi: 10.1186/s13058-019-1154-8. PubMed PMID: 31277699; PubMed Central PMCID: PMCPMC6612080.
157. Yu Y, Savage RE, Eathiraj S, Meade J, Wick MJ, Hall T, et al. Targeting AKT1-E17K and the PI3K/AKT Pathway with an Allosteric AKT Inhibitor, ARQ 092. PloS one. 2015;10(10):e0140479. Epub 2015/10/16. doi: 10.1371/journal.pone.0140479. PubMed PMID: 26469692; PubMed Central PMCID: PMCPMC4607407 TH, GA, and BS are employees of ArQule, Inc. JM and MJW have no competing financial

interests. This does not alter the authors' adherence to PLOS ONE policies on sharing data and materials.
158. Hyman DM, Smyth LM, Donoghue MTA, Westin SN, Bedard PL, Dean EJ, et al. AKT Inhibition in Solid Tumors With AKT1 Mutations. Journal of clinical oncology : official journal of the American Society of Clinical Oncology. 2017;35(20):2251-9. Epub 2017/05/11. doi: 10.1200/jco.2017.73.0143. PubMed PMID: 28489509; PubMed Central PMCID: PMCPMC5501365.
159. Leoni C, Gullo G, Resta N, Fagotti A, Onesimo R, Schwartz B, et al. First evidence of a therapeutic effect of miransertib in a teenager with Proteus syndrome and ovarian carcinoma. American journal of medical genetics Part A. 2019;179(7):1319-24. Epub 2019/05/07. doi: 10.1002/ajmg.a.61160. PubMed PMID: 31058421.
160. Landel I, Quambusch L, Depta L, Rauh D. Spotlight on AKT: Current Therapeutic Challenges. ACS medicinal chemistry letters. 2020;11(3):225-7. Epub 2020/03/19. doi: 10.1021/acsmedchemlett.9b00548. PubMed PMID: 32184947; PubMed Central PMCID: PMCPMC7073864.
161. Weisner J, Landel I, Reintjes C, Uhlenbrock N, Trajkovic-Arsic M, Dienstbier N, et al. Preclinical Efficacy of Covalent-Allosteric AKT Inhibitor Borussertib in Combination with Trametinib in KRAS-Mutant Pancreatic and Colorectal Cancer. Cancer research. 2019;79(9):2367-78. Epub 2019/03/13. doi: 10.1158/0008-5472.Can-18-2861. PubMed PMID: 30858154.
162. Uhlenbrock N, Smith S, Weisner J, Landel I, Lindemann M, Le TA, et al. Structural and chemical insights into the covalent-allosteric inhibition of the protein kinase Akt. Chemical science. 2019;10(12):3573-85. Epub 2019/04/19. doi: 10.1039/c8sc05212c. PubMed PMID: 30996949; PubMed Central PMCID: PMCPMC6430017.
163. Berman HM, Battistuz T, Bhat TN, Bluhm WF, Bourne PE, Burkhardt K, et al. The Protein Data Bank. Acta crystallographica Section D, Biological crystallography. 2002;58(Pt 6 No 1):899-907. Epub 2002/05/31. doi: 10.1107/s0907444902003451. PubMed PMID: 12037327.
164. BIOVIA DS. Discovery Studio Modelling Environment, Release 2017. Dassault Systeme, San Diego, CA 921212016.
165. Hubbard SJ, Thornton JM. NACCESS computer program version 2.1.1 Department of Biochemistry and Molecular Biology, University College, London, U.K.1993.
166. Baspinar A, Cukuroglu E, Nussinov R, Keskin O, Gursoy A. PRISM: a web server and repository for prediction of protein-protein interactions and modeling their 3D complexes. Nucleic acids research. 2014;42(Web Server issue):W285-9. Epub 2014/05/16. doi: 10.1093/nar/gku397. PubMed PMID: 24829450; PubMed Central PMCID: PMCPMC4086120.
167. DeLano WL. The PyMOL Molecular Graphics System. DeLano Scientific, San Carlos, CA 940802002.
168. Brooks BR, Brooks CL, 3rd, Mackerell AD, Jr., Nilsson L, Petrella RJ, Roux B, et al. CHARMM: the biomolecular simulation program. Journal of computational chemistry. 2009;30(10):1545-614. Epub 2009/05/16. doi: 10.1002/jcc.21287. PubMed PMID: 19444816; PubMed Central PMCID: PMCPMC2810661.
169. Chakrabarti M, Jang H, Nussinov R. Comparison of the Conformations of KRAS Isoforms, K-Ras4A and K-Ras4B, Points to Similarities and Significant Differences. The journal of physical chemistry B. 2016;120(4):667-79. Epub 2016/01/14. doi: 10.1021/acs.jpcb.5b11110. PubMed PMID: 26761128.
170. Jang H, Muratcioglu S, Gursoy A, Keskin O, Nussinov R. Membrane-associated Ras dimers are isoform-specific: K-Ras dimers differ from H-Ras dimers.

The Biochemical journal. 2016;473(12):1719-32. Epub 2016/04/09. doi: 10.1042/bcj20160031. PubMed PMID: 27057007.
171. Muratcioglu S, Jang H, Gursoy A, Keskin O, Nussinov R. PDEdelta Binding to Ras Isoforms Provides a Route to Proper Membrane Localization. The journal of physical chemistry B. 2017;121(24):5917-27. Epub 2017/05/26. doi: 10.1021/acs.jpcb.7b03035. PubMed PMID: 28540724.
172. Jang H, Banerjee A, Chavan T, Gaponenko V, Nussinov R. Flexible-body motions of calmodulin and the farnesylated hypervariable region yield a high-affinity interaction enabling K-Ras4B membrane extraction. The Journal of biological chemistry. 2017;292(30):12544-59. Epub 2017/06/18. doi: 10.1074/jbc.M117.785063. PubMed PMID: 28623230; PubMed Central PMCID: PMCPMC5535030.
173. Zhang M, Jang H, Gaponenko V, Nussinov R. Phosphorylated Calmodulin Promotes PI3K Activation by Binding to the SH2 Domains. Biophys J. 2017;113(9):1956-67. Epub 2017/11/09. doi: 10.1016/j.bpj.2017.09.008. PubMed PMID: 29117520; PubMed Central PMCID: PMCPMC5685777.
174. Ozdemir ES, Jang H, Gursoy A, Keskin O, Li Z, Sacks DB, et al. Unraveling the molecular mechanism of interactions of the Rho GTPases Cdc42 and Rac1 with the scaffolding protein IQGAP2. The Journal of biological chemistry. 2018;293(10):3685-99. Epub 2018/01/24. doi: 10.1074/jbc.RA117.001596. PubMed PMID: 29358323; PubMed Central PMCID: PMCPMC5846150.
175. Ozdemir ES, Jang H, Gursoy A, Keskin O, Nussinov R. Arl2-Mediated Allosteric Release of Farnesylated KRas4B from Shuttling Factor PDEdelta. The journal of physical chemistry B. 2018;122(30):7503-13. Epub 2018/07/03. doi: 10.1021/acs.jpcb.8b04347. PubMed PMID: 29961325.
176. Liao TJ, Jang H, Fushman D, Nussinov R. Allosteric KRas4B Can Modulate SOS1 Fast and Slow Ras Activation Cycles. Biophys J. 2018;115(4):629-41. Epub 2018/08/12. doi: 10.1016/j.bpj.2018.07.016. PubMed PMID: 30097175; PubMed Central PMCID: PMCPMC6103739.
177. Zhang M, Li Z, Wang G, Jang H, Sacks DB, Zhang J, et al. Calmodulin (CaM) Activates PI3Kalpha by Targeting the "Soft" CaM-Binding Motifs in Both the nSH2 and cSH2 Domains of p85alpha. The journal of physical chemistry B. 2018;122(49):11137-46. Epub 2018/07/27. doi: 10.1021/acs.jpcb.8b05982. PubMed PMID: 30047727; PubMed Central PMCID: PMCPMC6422767.
178. Jang H, Banerjee A, Marcus K, Makowski L, Mattos C, Gaponenko V, et al. The Structural Basis of the Farnesylated and Methylated KRas4B Interaction with Calmodulin. Structure. 2019;27(11):1647-59 e4. Epub 2019/09/10. doi: 10.1016/j.str.2019.08.009. PubMed PMID: 31495533.
179. Zhang M, Li Z, Jang H, Hedman AC, Sacks DB, Nussinov R. Ca(2+)-Dependent Switch of Calmodulin Interaction Mode with Tandem IQ Motifs in the Scaffolding Protein IQGAP1. Biochemistry. 2019;58(49):4903-11. Epub 2019/11/15. doi: 10.1021/acs.biochem.9b00854. PubMed PMID: 31724397.
180. Phillips JC, Braun R, Wang W, Gumbart J, Tajkhorshid E, Villa E, et al. Scalable molecular dynamics with NAMD. Journal of computational chemistry. 2005;26(16):1781-802. Epub 2005/10/14. doi: 10.1002/jcc.20289. PubMed PMID: 16222654; PubMed Central PMCID: PMCPMC2486339.
181. UniProt: the universal protein knowledgebase in 2021. Nucleic acids research. 2021;49(D1):D480-d9. Epub 2020/11/26. doi: 10.1093/nar/gkaa1100. PubMed PMID: 33237286; PubMed Central PMCID: PMCPMC7778908.
182. Klauda JB, Venable RM, Freites JA, O'Connor JW, Tobias DJ, Mondragon-Ramirez C, et al. Update of the CHARMM all-atom additive force field for lipids: validation on six lipid types. The journal of physical chemistry B.

2010;114(23):7830-43. Epub 2010/05/26. doi: 10.1021/jp101759q. PubMed PMID: 20496934; PubMed Central PMCID: PMCPMC2922408.
183. Huang J, Rauscher S, Nawrocki G, Ran T, Feig M, de Groot BL, et al. CHARMM36m: an improved force field for folded and intrinsically disordered proteins. Nature methods. 2017;14(1):71-3. Epub 2016/11/08. doi: 10.1038/nmeth.4067. PubMed PMID: 27819658; PubMed Central PMCID: PMCPMC5199616.
184. Pettersen EF, Goddard TD, Huang CC, Couch GS, Greenblatt DM, Meng EC, et al. UCSF Chimera--a visualization system for exploratory research and analysis. Journal of computational chemistry. 2004;25(13):1605-12. Epub 2004/07/21. doi: 10.1002/jcc.20084. PubMed PMID: 15264254.
185. Grant BJ, Rodrigues AP, ElSawy KM, McCammon JA, Caves LS. Bio3d: an R package for the comparative analysis of protein structures. Bioinformatics (Oxford, England). 2006;22(21):2695-6. Epub 2006/08/31. doi: 10.1093/bioinformatics/btl461. PubMed PMID: 16940322.
186. Han B, Liu Y, Ginzinger SW, Wishart DS. SHIFTX2: significantly improved protein chemical shift prediction. Journal of biomolecular NMR. 2011;50(1):43-57. Epub 2011/03/31. doi: 10.1007/s10858-011-9478-4. PubMed PMID: 21448735; PubMed Central PMCID: PMCPMC3085061.
187. Tuncbag N, Keskin O, Gursoy A. HotPoint: hot spot prediction server for protein interfaces. Nucleic acids research. 2010;38(Web Server issue):W402-6. Epub 2010/05/07. doi: 10.1093/nar/gkq323. PubMed PMID: 20444871; PubMed Central PMCID: PMCPMC2896123.
188. Vetter SW, Leclerc E. Novel aspects of calmodulin target recognition and activation. European journal of biochemistry. 2003;270(3):404-14. Epub 2003/01/25. doi: 10.1046/j.1432-1033.2003.03414.x. PubMed PMID: 12542690.
189. Villarroel A, Taglialatela M, Bernardo-Seisdedos G, Alaimo A, Agirre J, Alberdi A, et al. The ever changing moods of calmodulin: how structural plasticity entails transductional adaptability. Journal of molecular biology. 2014;426(15):2717-35. Epub 2014/05/27. doi: 10.1016/j.jmb.2014.05.016. PubMed PMID: 24857860.
190. Abdi H, Williams LJ. Principal component analysis. Wires Comput Stat. 2010;2(4):433-59. doi: 10.1002/wics.101. PubMed PMID: WOS:000214679600004.
191. Balsera MA, Wriggers W, Oono Y, Schulten K. Principal component analysis and long time protein dynamics. J Phys Chem-Us. 1996;100(7):2567-72. doi: DOI 10.1021/jp9536920. PubMed PMID: WOS:A1996TV69400015.
192. David CC, Jacobs DJ. Principal component analysis: a method for determining the essential dynamics of proteins. Methods Mol Biol. 2014;1084:193-226. Epub 2013/09/26. doi: 10.1007/978-1-62703-658-0_11. PubMed PMID: 24061923; PubMed Central PMCID: PMCPMC4676806.
193. Grant BJ, Skjaerven L, Yao XQ. The Bio3D packages for structural bioinformatics. Protein Sci. 2021;30(1):20-30. Epub 2020/08/01. doi: 10.1002/pro.3923. PubMed PMID: 32734663; PubMed Central PMCID: PMCPMC7737766.
194. Lemmon MA. Pleckstrin homology (PH) domains and phosphoinositides. Biochemical Society symposium. 2007;(74):81-93. Epub 2007/01/20. doi: 10.1042/bss0740081. PubMed PMID: 17233582; PubMed Central PMCID: PMCPMC3777418.
195. Xu Q, Bateman A, Finn RD, Abdubek P, Astakhova T, Axelrod HL, et al. Bacterial pleckstrin homology domains: a prokaryotic origin for the PH domain. Journal of molecular biology. 2010;396(1):31-46. Epub 2009/11/17. doi:

10.1016/j.jmb.2009.11.006. PubMed PMID: 19913036; PubMed Central PMCID: PMCPMC2817789.
196. Yu JW, Mendrola JM, Audhya A, Singh S, Keleti D, DeWald DB, et al. Genome-wide analysis of membrane targeting by S. cerevisiae pleckstrin homology domains. Molecular cell. 2004;13(5):677-88. Epub 2004/03/17. doi: 10.1016/s1097-2765(04)00083-8. PubMed PMID: 15023338.
197. Chin D, Means AR. Calmodulin: a prototypical calcium sensor. Trends in cell biology. 2000;10(8):322-8. Epub 2000/07/08. doi: 10.1016/s0962-8924(00)01800-6. PubMed PMID: 10884684.
198. Tidow H, Nissen P. Structural diversity of calmodulin binding to its target sites. FEBS J. 2013;280(21):5551-65. doi: 10.1111/febs.12296. PubMed PMID: 23601118.
199. Garrido E, Lázaro J, Jaumot M, Agell N, Rubio-Martinez J. Modeling and subtleties of K-Ras and Calmodulin interaction. PLoS computational biology. 2018;14(10):e1006552. Epub 2018/10/31. doi: 10.1371/journal.pcbi.1006552. PubMed PMID: 30376570; PubMed Central PMCID: PMCPMC6226203.
200. Ni D, Liu D, Zhang J, Lu S. Computational Insights into the Interactions between Calmodulin and the c/nSH2 Domains of p85alpha Regulatory Subunit of PI3Kalpha: Implication for PI3Kalpha Activation by Calmodulin. International journal of molecular sciences. 2018;19(1). doi: 10.3390/ijms19010151. PubMed PMID: 29300353; PubMed Central PMCID: PMCPMC5796100.
201. Aykut AO, Atilgan AR, Atilgan C. Designing molecular dynamics simulations to shift populations of the conformational states of calmodulin. PLoS Comput Biol. 2013;9(12):e1003366. doi: 10.1371/journal.pcbi.1003366. PubMed PMID: 24339763; PubMed Central PMCID: PMCPMC3854495.
202. Kurkcuoglu Z, Bahar I, Doruker P. ClustENM: ENM-Based Sampling of Essential Conformational Space at Full Atomic Resolution. J Chem Theory Comput. 2016;12(9):4549-62. doi: 10.1021/acs.jctc.6b00319. PubMed PMID: 27494296; PubMed Central PMCID: PMCPMC5088496.
203. Dong B, Valencia CA, Liu R. Ca(2+)/calmodulin directly interacts with the pleckstrin homology domain of AKT1. The Journal of biological chemistry. 2007;282(34):25131-40. Epub 2007/06/21. doi: 10.1074/jbc.M702123200. PubMed PMID: 17580302.
204. Ishida H, Vogel HJ. Protein-peptide interaction studies demonstrate the versatility of calmodulin target protein binding. Protein and peptide letters. 2006;13(5):455-65. Epub 2006/06/28. doi: 10.2174/092986606776819600. PubMed PMID: 16800798.
205. Wang X, Boyken SE, Hu J, Xu X, Rimer RP, Shea MA, et al. Calmodulin and PI(3,4,5)P3 cooperatively bind to the Itk pleckstrin homology domain to promote efficient calcium signaling and IL-17A production. Science signaling. 2014;7(337):ra74. Epub 2014/08/07. doi: 10.1126/scisignal.2005147. PubMed PMID: 25097034; PubMed Central PMCID: PMCPMC4269470.
206. Watson GM, Wilce JA. Direct Interaction between Calmodulin and the Grb7 RA-PH Domain. International journal of molecular sciences. 2020;21(4). Epub 2020/02/23. doi: 10.3390/ijms21041336. PubMed PMID: 32079204; PubMed Central PMCID: PMCPMC7073000.
207. Nussinov R, Zhang M, Tsai CJ, Liao TJ, Fushman D, Jang H. Autoinhibition in Ras effectors Raf, PI3Kα, and RASSF5: a comprehensive review underscoring the challenges in pharmacological intervention. Biophysical reviews. 2018;10(5):1263-82. Epub 2018/10/01. doi: 10.1007/s12551-018-0461-0. PubMed PMID: 30269291; PubMed Central PMCID: PMCPMC6233353.

208. Pufall MA, Graves BJ. Autoinhibitory domains: modular effectors of cellular regulation. Annual review of cell and developmental biology. 2002;18:421-62. Epub 2002/07/27. doi: 10.1146/annurev.cellbio.18.031502.133614. PubMed PMID: 12142282.
209. Risso G, Blaustein M, Pozzi B, Mammi P, Srebrow A. Akt/PKB: one kinase, many modifications. The Biochemical journal. 2015;468(2):203-14. Epub 2015/05/23. doi: 10.1042/bj20150041. PubMed PMID: 25997832.
210. Yang J, Cron P, Thompson V, Good VM, Hess D, Hemmings BA, et al. Molecular mechanism for the regulation of protein kinase B/Akt by hydrophobic motif phosphorylation. Molecular cell. 2002;9(6):1227-40. Epub 2002/06/28. doi: 10.1016/s1097-2765(02)00550-6. PubMed PMID: 12086620.
211. Truebestein L, Hornegger H, Anrather D, Hartl M, Fleming KD, Stariha JTB, et al. Structure of autoinhibited Akt1 reveals mechanism of PIP(3)-mediated activation. Proceedings of the National Academy of Sciences of the United States of America. 2021;118(33). Epub 2021/08/14. doi: 10.1073/pnas.2101496118. PubMed PMID: 34385319; PubMed Central PMCID: PMCPMC8379990.
212. Lučić I, Rathinaswamy MK, Truebestein L, Hamelin DJ, Burke JE, Leonard TA. Conformational sampling of membranes by Akt controls its activation and inactivation. Proceedings of the National Academy of Sciences of the United States of America. 2018;115(17):E3940-e9. Epub 2018/04/11. doi: 10.1073/pnas.1716109115. PubMed PMID: 29632185; PubMed Central PMCID: PMCPMC5924885.
213. Landgraf KE, Pilling C, Falke JJ. Molecular mechanism of an oncogenic mutation that alters membrane targeting: Glu17Lys modifies the PIP lipid specificity of the AKT1 PH domain. Biochemistry. 2008;47(47):12260-9. Epub 2008/10/29. doi: 10.1021/bi801683k. PubMed PMID: 18954143; PubMed Central PMCID: PMCPMC2919500.
214. Barnett SF, Defeo-Jones D, Fu S, Hancock PJ, Haskell KM, Jones RE, et al. Identification and characterization of pleckstrin-homology-domain-dependent and isoenzyme-specific Akt inhibitors. The Biochemical journal. 2005;385(Pt 2):399-408. Epub 2004/10/01. doi: 10.1042/bj20041140. PubMed PMID: 15456405; PubMed Central PMCID: PMCPMC1134710.
215. Chennubhotla C, Bahar I. Markov propagation of allosteric effects in biomolecular systems: application to GroEL-GroES. Molecular systems biology. 2006;2:36. Epub 2006/07/06. doi: 10.1038/msb4100075. PubMed PMID: 16820777; PubMed Central PMCID: PMCPMC1681507.
216. Oh WJ, Wu CC, Kim SJ, Facchinetti V, Julien LA, Finlan M, et al. mTORC2 can associate with ribosomes to promote cotranslational phosphorylation and stability of nascent Akt polypeptide. Embo j. 2010;29(23):3939-51. Epub 2010/11/04. doi: 10.1038/emboj.2010.271. PubMed PMID: 21045808; PubMed Central PMCID: PMCPMC3020639.
217. Facchinetti V, Ouyang W, Wei H, Soto N, Lazorchak A, Gould C, et al. The mammalian target of rapamycin complex 2 controls folding and stability of Akt and protein kinase C. Embo j. 2008;27(14):1932-43. Epub 2008/06/21. doi: 10.1038/emboj.2008.120. PubMed PMID: 18566586; PubMed Central PMCID: PMCPMC2486276.
218. Chu N, Viennet T, Bae H, Salguero A, Boeszoermenyi A, Arthanari H, et al. The structural determinants of PH domain-mediated regulation of Akt revealed by segmental labeling. eLife. 2020;9. Epub 2020/08/04. doi: 10.7554/eLife.59151. PubMed PMID: 32744507; PubMed Central PMCID: PMCPMC7438110.

Appendix A

A sample CHARMM-generated input file

```
 * File: cam1phd_mod2_gen_coor.inp
* Generate initial coordinates for CHARMM & NAMD
*

!!!!!!!!!!!!!!!!!!!!!!!!!!!!!!!!!!!!!!!!!!!!!!!!!!!!!!!
! set directory
set type cam1phd_mod2
set dir data/weakoj2/@type
!!!!!!!!!!!!!!!!!!!!!!!!!!!!!!!!!!!!!!!!!!!!!!!!!!!!!!!

bomlev -2

! read topology
open read card unit 10 name
/data/weakoj2/charmm_input/top_all36_phd_c39b2_hbj.inp
read rtf card unit 10
close unit 10

! read parameters
open read card unit 10 name
/data/weakoj2/charmm_input/par_all36_phd_c39b2_hbj.inp
read param card unit 10
close unit 10

!!!!!!!!!!!!!!!!!!!!!!!!!!!!!!!!!!!!!!!!!!!!!!!!!!!!!!!

! Get PH domain of Akt
read sequence card
* The sequence is PHD Akt 1 to 117
*
117
MET SER ASP VAL ALA ILE VAL LYS GLU GLY TRP LEU HSD
LYS ARG GLY GLU TYR ILE LYS THR TRP ARG PRO ARG TYR
PHE LEU LEU LYS ASN ASP GLY THR PHE ILE GLY TYR LYS
GLU ARG PRO GLN ASP VAL ASP GLN ARG GLU ALA PRO LEU
ASN ASN PHE SER VAL ALA GLN CYS GLN LEU MET LYS THR
GLU ARG PRO ARG PRO ASN THR PHE ILE ILE ARG CYS LEU
GLN TRP THR THR VAL ILE GLU ARG THR PHE HSD VAL GLU
THR PRO GLU GLU ARG GLU GLU TRP THR THR ALA ILE GLN
THR VAL ALA ASP GLY LEU LYS LYS GLN GLU GLU GLU GLU

generate PHDO first NTER last CTER setup

! Fill internal coordinates with IC PARA
IC PARA
```

```
open read card unit 1 name /@dir/coor/phd.crd
read coor card unit 1
close unit 1

! Fill IC with input coordinates, but preserve those not available from
coordinates
IC FILL PREServe
! Rebulit whole IC
IC BUILD
! Build and Rebuild Hydrogens
HBUILD SELEct (hydrogen) END

!!!!!!!!!!!!!!!

set N ?nres

! Get Calmodulin
read sequence card
* The sequence is CaM 1 to 148
*
148
ALA ASP GLN LEU THR GLU GLU GLN ILE ALA GLU PHE LYS
GLU ALA PHE SER LEU PHE ASP LYS ASP GLY ASP GLY THR
ILE THR THR LYS GLU LEU GLY THR VAL MET ARG SER LEU
GLY GLN ASN PRO THR GLU ALA GLU LEU GLN ASP MET ILE
ASN GLU VAL ASP ALA ASP GLY ASN GLY THR ILE ASP PHE
PRO GLU PHE LEU THR MET MET ALA ARG LYS MET LYS ASP
THR ASP SER GLU GLU GLU ILE ARG GLU ALA PHE ARG VAL
PHE ASP LYS ASP GLY ASN GLY TYR ILE SER ALA ALA GLU
LEU ARG HSD VAL MET THR ASN LEU GLY GLU LYS LEU THR
ASP GLU GLU VAL ASP GLU MET ILE ARG GLU ALA ASP ILE
ASP GLY ASP GLY GLN VAL ASN TYR GLU GLU PHE VAL GLN
MET MET THR ALA LYS

generate CAMD first NTER last CTER setup

! Fill internal coordinates with IC PARA
IC PARA

open read card unit 1 name /@dir/coor/cam.crd
read coor card unit 1 offset @N
close unit 1

! Fill IC with input coordinates, but preserve those not available from
coordinates
IC FILL PREServe
! Rebulit whole IC
IC BUILD
! Build and Rebuild Hydrogens
HBUILD SELEct (hydrogen) END

!!!!!!!!!!!!!!!
```

```
set N ?nres

! Get Cal
read sequence CAL 4
generate CALS noangle nodihedral

open read card unit 1 name /@dir/coor/cal.crd
read coor card unit 1 offset @N
close unit 1

!!!!!!!!!!!!!!!!!!!!!!!!!!!!!!!!!!!!!!!!!!!!!!!!!!!!!!!

! Get the initial coordinate

open write card unit 1 name /@dir/coor/@type_ini_coor.crd
write coor card unit 1
* crd file of protein
*

!!!!!!!!!!!!!!!!!

Stop
```

A sample CHARMM-generated input file

```
* File: cam1phd_mod2_ini_config.inp
* Translocate the N-term of HVR to remove clash
*

!!!!!!!!!!!!!!!!!!!!!!!!!!!!!!!!!!!!!!!!!!!!!!!!!!!!!!!
! set directory
set type cam1phd_mod2
set dir data/weakoj2/@type
!!!!!!!!!!!!!!!!!!!!!!!!!!!!!!!!!!!!!!!!!!!!!!!!!!!!!!!

bomlev -2

! read topology
open read card unit 10 name
/data/weakoj2/charmm_input/top_all36_phd_c39b2_hbj.inp
read rtf card unit 10
close unit 10

! read parameters
open read card unit 10 name
/data/weakoj2/charmm_input/par_all36_phd_c39b2_hbj.inp
read param card unit 10
close unit 10

!!!!!!!!!!!!!!!!!!!!!!!!!!!!!!!!!!!!!!!!!!!!!!!!!!!!!!!
```

```
! Get PH domain of Akt
read sequence card
* The sequence is PHD Akt 1 to 117
*
117
MET SER ASP VAL ALA ILE VAL LYS GLU GLY TRP LEU HSD
LYS ARG GLY GLU TYR ILE LYS THR TRP ARG PRO ARG TYR
PHE LEU LEU LYS ASN ASP GLY THR PHE ILE GLY TYR LYS
GLU ARG PRO GLN ASP VAL ASP GLN ARG GLU ALA PRO LEU
ASN ASN PHE SER VAL ALA GLN CYS GLN LEU MET LYS THR
GLU ARG PRO ARG PRO ASN THR PHE ILE ILE ARG CYS LEU
GLN TRP THR THR VAL ILE GLU ARG THR PHE HSD VAL GLU
THR PRO GLU GLU ARG GLU GLU TRP THR THR ALA ILE GLN
THR VAL ALA ASP GLY LEU LYS LYS GLN GLU GLU GLU GLU

generate PHDO first NTER last CTER setup

! Get Calmodulin
read sequence card
* The sequence is CaM 1 to 148
*
148
ALA ASP GLN LEU THR GLU GLU GLN ILE ALA GLU PHE LYS
GLU ALA PHE SER LEU PHE ASP LYS ASP GLY ASP GLY THR
ILE THR THR LYS GLU LEU GLY THR VAL MET ARG SER LEU
GLY GLN ASN PRO THR GLU ALA GLU LEU GLN ASP MET ILE
ASN GLU VAL ASP ALA ASP GLY ASN GLY THR ILE ASP PHE
PRO GLU PHE LEU THR MET MET ALA ARG LYS MET LYS ASP
THR ASP SER GLU GLU GLU ILE ARG GLU ALA PHE ARG VAL
PHE ASP LYS ASP GLY ASN GLY TYR ILE SER ALA ALA GLU
LEU ARG HSD VAL MET THR ASN LEU GLY GLU LYS LEU THR
ASP GLU GLU VAL ASP GLU MET ILE ARG GLU ALA ASP ILE
ASP GLY ASP GLY GLN VAL ASN TYR GLU GLU PHE VAL GLN
MET MET THR ALA LYS

generate CAMD first NTER last CTER setup

! Get Cal
read sequence CAL 4
generate CALS noangle nodihedral

open read card unit 1 name /@dir/coor/@type_ini_coor.crd
read coor card unit 1
close unit 1

!!!!!!!!!!!!!!!!!!!!!!!!!!!!!!!!!!!!!!!!!!!!!!!!!!!!!!!

define BACKBONE sele (segid PHDO .and. resid 2:117 .and. (type N .or. type CA
.or. type C .or. type O)) .or. -
                (segid CAMD .and. resid 3:147 .and. (type N .or. type CA .or. type C
.or. type O)) end
```

```
cons fix sele BACKBONE end

mini sd nstep 200
mini sd nstep 200
mini sd nstep 200
mini sd nstep 200
mini abnr nstep 100
mini abnr nstep 100
mini abnr nstep 100
mini abnr nstep 100

!!!!!!!!!!!!!!!!!!!!!!!!!!!!!!!!!!!!!!!!!!!!!!!!!!!!

! Move to center
coor stat sele all end
coor trans xdir -?XAVE ydir -?YAVE zdir -?ZAVE sele all end
coor stat sele all end

!!!!!!!!!!!!!!!!!!!!!!!!!!!!!!!!!!!!!!!!!!!!!!!!!!!!

open write card unit 1 name /@dir/coor/@type_ini_config.crd
write coor card unit 1
* crd file of protein
*

!!!!!!!!!!!!!!!!!

Stop
```

A sample CHARMM-generated input file

```
* File: cam1phd_mod2_water_overlay_1st.inp
* Generates the bulk overlay of water for the system
* Use simplified method for water addition
*

!!!!!!!!!!!!!!!!!!!!!!!!!!!!!!!!!!!!!!!!!!!!!!!!!!!!
! set directory
set type cam1phd_mod2
set dir data/weakoj2/@type
!!!!!!!!!!!!!!!!!!!!!!!!!!!!!!!!!!!!!!!!!!!!!!!!!!!!
! set initial numbers of system
set bs 100.0          ! cell dimension
! set number of water; read from water directory
set nwt1 8682
set nwt2 8681
set nwt3 8578
set nwt4 8578
!!!!!!!!!!!!!!!!!!!!!!!!!!!!!!!!!!!!!!!!!!!!!!!!!!!!

bomlev -2
```

```
! read topology
open read card unit 10 name
/data/weakoj2/charmm_input/top_all36_phd_c39b2_hbj.inp
read rtf card unit 10
close unit 10

! read parameters
open read card unit 10 name
/data/weakoj2/charmm_input/par_all36_phd_c39b2_hbj.inp
read param card unit 10
close unit 10

!!!!!!!!!!!!!!!!!!!!!!!!!!!!!!!!!!!!!!!!!!!!!!!!!!!!

open read card unit 1 name /@dir/coor/@type_ini_config.crd
read sequence coor unit 1
generate JANG setup noangle nodihedrals first none last none
close unit 1
open read card unit 1 name /@dir/coor/@type_ini_config.crd
read coor card unit 1
close unit 1

delete atom sele .not. INIT end
scalar charge set 0.0

set N ?nres

read sequence TIP3 @nwt1
generage OV11 noangle nodihedral
read sequence TIP3 @nwt2
generage OV12 noangle nodihedral

open read card unit 1 name /@dir/water/water_large_box_@bs_1.crd
read coor card unit 1 offset @N
close unit 1

set N ?nres

read sequence TIP3 @nwt3
generage OV21 noangle nodihedral
read sequence TIP3 @nwt4
generage OV22 noangle nodihedral

open read card unit 1 name /@dir/water/water_large_box_@bs_2.crd
read coor card unit 1 offset @N
close unit 1

!!!!!!!!!!!!!!!!!!!!!!!!!!!!!!!!!!!!!!!!!!!!!!!!!!!!

! Initial overlay of each water box

! Lower layer
```

```
coor stat sele segid OV1* end
define COUNT1 sele ((type OH2 .and. segid OV1*) .and. (segid JANG .around.
2.6)) end
delete atoms sele .byres. COUNT1 end

! Upper layer
coor stat sele segid OV2* end
define COUNT2 sele ((type OH2 .and. segid OV2*) .and. (segid JANG .around.
2.6)) end
delete atoms sele .byres. COUNT2 end

!!!!!!!!!!!!!!!!!!!!!!!!!!!!!!!!!!!!!!!!!!!!!!!!!!!

delete atoms sele segid JANG end

!!!!!!!!!!!!!!!!!!!!!!!!!!!!!!!!!!!!!!!!!!!!!!!!!!!

! Write water coordinates

open write card unit 1 name /@dir/coor/temp_water_ov11.crd
write coor sele segid OV11 end card unit 1
* overlay of waters
*

delete atoms sele segid OV11 end

open write card unit 1 name /@dir/coor/temp_water_ov12.crd
write coor sele segid OV12 end card unit 1
* overlay of waters
*

delete atoms sele segid OV12 end


! Write water coordinates
open write card unit 1 name /@dir/coor/temp_water_ov21.crd
write coor sele segid OV21 end card unit 1
* overlay of waters
*

delete atoms sele segid OV21 end

! Write water coordinates
open write card unit 1 name /@dir/coor/temp_water_ov22.crd
write coor sele segid OV22 end card unit 1
* overlay of waters
*

stop
```

A sample CHARMM-generated input file for water box

```
* File: cam1phd_mod2_water_overlay_2nd.inp
* Generates the bulk overlay of water for the system
* Use simplified method for water addition
*

!!!!!!!!!!!!!!!!!!!!!!!!!!!!!!!!!!!!!!!!!!!!!!!!!!!!!!!
! set directory
set type cam1phd_mod2
set dir data/weakoj2/@type
!!!!!!!!!!!!!!!!!!!!!!!!!!!!!!!!!!!!!!!!!!!!!!!!!!!!!!!
! set initial numbers of system
set bs 100.0           ! cell dimension
!!!!!!!!!!!!!!!!!!!!!!!!!!!!!!!!!!!!!!!!!!!!!!!!!!!!!!!

bomlev -2

! read topology
open read card unit 10 name
/data/weakoj2/charmm_input/top_all36_phd_c39b2_hbj.inp
read rtf card unit 10
close unit 10

! read parameters
open read card unit 10 name
/data/weakoj2/charmm_input/par_all36_phd_c39b2_hbj.inp
read param card unit 10
close unit 10

!!!!!!!!!!!!!!!!!!!!!!!!!!!!!!!!!!!!!!!!!!!!!!!!!!!!!!!

! Get PH domain of Akt
read sequence card
* The sequence is PHD Akt 1 to 117
*
117
MET SER ASP VAL ALA ILE VAL LYS GLU GLY TRP LEU HSD
LYS ARG GLY GLU TYR ILE LYS THR TRP ARG PRO ARG TYR
PHE LEU LEU LYS ASN ASP GLY THR PHE ILE GLY TYR LYS
GLU ARG PRO GLN ASP VAL ASP GLN ARG GLU ALA PRO LEU
ASN ASN PHE SER VAL ALA GLN CYS GLN LEU MET LYS THR
GLU ARG PRO ARG PRO ASN THR PHE ILE ILE ARG CYS LEU
GLN TRP THR THR VAL ILE GLU ARG THR PHE HSD VAL GLU
THR PRO GLU GLU ARG GLU GLU TRP THR THR ALA ILE GLN
THR VAL ALA ASP GLY LEU LYS LYS GLN GLU GLU GLU GLU

generate PHDO first NTER last CTER setup

! Get Calmodulin
read sequence card
* The sequence is CaM 1 to 148
*
148
```

```
ALA ASP GLN LEU THR GLU GLU GLN ILE ALA GLU PHE LYS
GLU ALA PHE SER LEU PHE ASP LYS ASP GLY ASP GLY THR
ILE THR THR LYS GLU LEU GLY THR VAL MET ARG SER LEU
GLY GLN ASN PRO THR GLU ALA GLU LEU GLN ASP MET ILE
ASN GLU VAL ASP ALA ASP GLY ASN GLY THR ILE ASP PHE
PRO GLU PHE LEU THR MET MET ALA ARG LYS MET LYS ASP
THR ASP SER GLU GLU GLU ILE ARG GLU ALA PHE ARG VAL
PHE ASP LYS ASP GLY ASN GLY TYR ILE SER ALA ALA GLU
LEU ARG HSD VAL MET THR ASN LEU GLY GLU LYS LEU THR
ASP GLU GLU VAL ASP GLU MET ILE ARG GLU ALA ASP ILE
ASP GLY ASP GLY GLN VAL ASN TYR GLU GLU PHE VAL GLN
MET MET THR ALA LYS

generate CAMD first NTER last CTER setup

! Get Cal
read sequence CAL 4
generate CALS noangle nodihedral

open read card unit 1 name /@dir/coor/@type_ini_config.crd
read coor card unit 1
close unit 1

set N ?nres

open read card unit 1 name /@dir/coor/temp_water_ov11.crd
read sequence coor unit 1
generate BLK1 nodihedrals noangles first none last none
close unit 1
open read card unit 1 name /@dir/coor/temp_water_ov11.crd
read coor card unit 1 offset @N
close unit 1

set N ?nres

open read card unit 1 name /@dir/coor/temp_water_ov12.crd
read sequence coor unit 1
generate BLK2 nodihedrals noangles first none last none
close unit 1
open read card unit 1 name /@dir/coor/temp_water_ov12.crd
read coor card unit 1 offset @N
close unit 1

set N ?nres

open read card unit 1 name /@dir/coor/temp_water_ov21.crd
read sequence coor unit 1
generate BLK3 nodihedrals noangles first none last none
close unit 1
open read card unit 1 name /@dir/coor/temp_water_ov21.crd
read coor card unit 1 offset @N
close unit 1
```

```
set N ?nres

open read card unit 1 name /@dir/coor/temp_water_ov22.crd
read sequence coor unit 1
generate BLK4 nodihedrals noangles first none last none
close unit 1
open read card unit 1 name /@dir/coor/temp_water_ov22.crd
read coor card unit 1 offset @N
close unit 1

!!!!!!!!!!!!!!!!!!!!!!!!!!!!!!!!!!!!!!!!!!!!!!!!!!!!!!!

! Delete waters beyond cell dimension
! xdirection
calc hbx = @bs/2.0
set XCUT1 -@hbx
set XCUT2 @hbx
delete atom sele .byres. (type OH2 .and. (prop x .lt. @XCUT1)) end
delete atom sele .byres. (type OH2 .and. (prop x .gt. @XCUT2)) end
! y direction
calc hby = @bs/2.0
set YCUT1 -@hby
set YCUT2 @hby
delete atom sele .byres. (type OH2 .and. (prop y .lt. @YCUT1)) end
delete atom sele .byres. (type OH2 .and. (prop y .gt. @YCUT2)) end
! z direction
calc hbz = @bs/2.0
set ZCUT1 -@hbz
set ZCUT2 @hbz
delete atom sele .byres. (type OH2 .and. (prop z .lt. @ZCUT1)) end
delete atom sele .byres. (type OH2 .and. (prop z .gt. @ZCUT2)) end

!!!!!!!!!!!!!!!!!!!!!!!!!!!!!!!!!!!!!!!!!!!!!!!!!!!!!!!

! Write coordinates

open write card unit 1 name
/@dir/coor/@type_water_overlay_system_protein.crd
write coor sele segid PHDO .or. segid CAMD .or. segid CALS end card unit 1
* proteins
*

dele atom sele segid PHDO .or. segid CAMD .or. segid CALS end

open write card unit 1 name
/@dir/coor/@type_water_overlay_system_bulk_1.crd
write coor sele segid BLK1 end card unit 1
* water
*

dele atom sele segid BLK1 end
```

```
open write card unit 1 name
/@dir/coor/@type_water_overlay_system_bulk_2.crd
write coor sele segid BLK2 end card unit 1
* water
*

dele atom sele segid BLK2 end

open write card unit 1 name
/@dir/coor/@type_water_overlay_system_bulk_3.crd
write coor sele segid BLK3 end card unit 1
* water
*

dele atom sele segid BLK3 end

open write card unit 1 name
/@dir/coor/@type_water_overlay_system_bulk_4.crd
write coor sele segid BLK4 end card unit 1
* water
*

stop
```

A sample CHARMM-generated input file for salt

```
 * File: model_2_apo_water_add_salt_mk_coor.inp
* Add salts and make coordinates
*

!!!!!!!!!!!!!!!!!!!!!!!!!!!!!!!!!!!!!!!!!!!!!!!!!!!!
! set directory
set type model_2_apo
set dir data/weakoj2/@type
!!!!!!!!!!!!!!!!!!!!!!!!!!!!!!!!!!!!!!!!!!!!!!!!!!!!
! set initial numbers of system
set nna 105          ! number of Na+
set ncl 94           ! number of Cl-
!!!!!!!!!!!!!!!!!!!!!!!!!!!!!!!!!!!!!!!!!!!!!!!!!!!!

bomlev -2

! read topology
open read card unit 10 name
/data/weakoj2/charmm_input/top_all36_phd_c39b2_hbj.inp
read rtf card unit 10
close unit 10
```

```
! read parameters
open read card unit 10 name
/data/weakoj2/charmm_input/par_all36_phd_c39b2_hbj.inp
read param card unit 10
close unit 10

!!!!!!!!!!!!!!!!!!!!!!!!!!!!!!!!!!!!!!!!!!!!!!!!!!!!!!!

! Get Akt
read sequence card
* The sequence is Akt 1 to 480
480
MET SER ASP VAL ALA ILE VAL LYS GLU GLY TRP LEU HSD LYS ARG GLY
GLU TYR ILE LYS
THR TRP ARG PRO ARG TYR PHE LEU LEU LYS ASN ASP GLY THR PHE ILE
GLY TYR LYS GLU
ARG PRO GLN ASP VAL ASP GLN ARG GLU ALA PRO LEU ASN ASN PHE
SER VAL ALA GLN CYS
GLN LEU MET LYS THR GLU ARG PRO ARG PRO ASN THR PHE ILE ILE
ARG CYS LEU GLN TRP
THR THR VAL ILE GLU ARG THR PHE HSD VAL GLU THR PRO GLU GLU
ARG GLU GLU TRP THR
THR ALA ILE GLN THR VAL ALA ASP GLY LEU LYS LYS GLN GLU GLU GLU
GLU MET ASP PHE
ARG SER GLY SER PRO SER ASP ASN SER GLY ALA GLU GLU MET GLU VAL
SER LEU ALA LYS
PRO LYS HSD ARG VAL THR MET ASN GLU PHE GLU TYR LEU LYS LEU
LEU GLY LYS GLY THR
PHE GLY LYS VAL ILE LEU VAL LYS GLU LYS ALA THR GLY ARG TYR TYR
ALA MET LYS ILE
LEU LYS LYS GLU VAL ILE VAL ALA LYS ASP GLU VAL ALA HSD THR LEU
THR GLU ASN ARG
VAL LEU GLN ASN SER ARG HSD PRO PHE LEU THR ALA LEU LYS TYR
SER PHE GLN THR HSD
ASP ARG LEU CYS PHE VAL MET GLU TYR ALA ASN GLY GLY GLU LEU
PHE PHE HSD LEU SER
ARG GLU ARG VAL PHE SER GLU ASP ARG ALA ARG PHE TYR GLY ALA
GLU ILE VAL SER ALA
LEU ASP TYR LEU HSD SER GLU LYS ASN VAL VAL TYR ARG ASP LEU LYS
LEU GLU ASN LEU
MET LEU ASP LYS ASP GLY HSD ILE LYS ILE THR ASP PHE GLY LEU CYS
LYS GLU GLY ILE
LYS ASP GLY ALA THR MET LYS THR PHE CYS GLY THR PRO GLU TYR LEU
ALA PRO GLU VAL
LEU GLU ASP ASN ASP TYR GLY ARG ALA VAL ASP TRP TRP GLY LEU GLY
VAL VAL MET TYR
GLU MET MET CYS GLY ARG LEU PRO PHE TYR ASN GLN ASP HSD GLU
LYS LEU PHE GLU LEU
ILE LEU MET GLU GLU ILE ARG PHE PRO ARG THR LEU GLY PRO GLU
ALA LYS SER LEU LEU
SER GLY LEU LEU LYS LYS ASP PRO LYS GLN ARG LEU GLY GLY GLY SER
```

```
GLU ASP ALA LYS
GLU ILE MET GLN HSD ARG PHE PHE ALA GLY ILE VAL TRP GLN HSD
VAL TYR GLU LYS LYS
LEU SER PRO PRO PHE LYS PRO GLN VAL THR SER GLU THR ASP THR
ARG TYR PHE ASP GLU
GLU PHE THR ALA GLN MET ILE THR ILE THR PRO PRO ASP GLN ASP ASP
SER MET GLU CYS
VAL ASP SER GLU ARG ARG PRO HSD PHE PRO GLN PHE SER TYR SER
ALA SER GLY THR ALA

generate AKTT first NTER last CTER setup

open read card unit 1 name /@dir/coor/@type_water_overlay_system_prot.crd
read coor card unit 1
close unit 1

set N ?nres

open read card unit 1 name
/@dir/coor/@type_water_overlay_system_bulk_1.crd
read sequence coor unit 1
generate BLK1 nodihedrals noangles first none last none
close unit 1
open read card unit 1 name
/@dir/coor/@type_water_overlay_system_bulk_1.crd
read coor card unit 1 offset @N
close unit 1

set N ?nres

open read card unit 1 name
/@dir/coor/@type_water_overlay_system_bulk_2.crd
read sequence coor unit 1
generate BLK2 nodihedrals noangles first none last none
close unit 1
open read card unit 1 name
/@dir/coor/@type_water_overlay_system_bulk_2.crd
read coor card unit 1 offset @N
close unit 1

set N ?nres

open read card unit 1 name
/@dir/coor/@type_water_overlay_system_bulk_3.crd
read sequence coor unit 1
generate BLK3 nodihedrals noangles first none last none
close unit 1
open read card unit 1 name
/@dir/coor/@type_water_overlay_system_bulk_3.crd
read coor card unit 1 offset @N
close unit 1
```

```
set N ?nres

open read card unit 1 name
/@dir/coor/@type_water_overlay_system_bulk_4.crd
read sequence coor unit 1
generate BLK4 nodihedrals noangles first none last none
close unit 1
open read card unit 1 name
/@dir/coor/@type_water_overlay_system_bulk_4.crd
read coor card unit 1 offset @N
close unit 1

!!!!!!!!!!!!!!!!!!!!!!!!!!!!!!!!!!!!!!!!!!!!!!!!!!!!

! Stat for protein
coor stat sele segid AKTT end
coor stat sele segid AKTT .and. type CA end
!coor stat sele segid IP4 end

! Stat for water
coor stat sele resname TIP3 .and. type OH2 end
coor stat sele resname TIP3 .and. type OH2 .and. segid BLK1 end
coor stat sele resname TIP3 .and. type OH2 .and. segid BLK2 end
coor stat sele resname TIP3 .and. type OH2 .and. segid BLK3 end
coor stat sele resname TIP3 .and. type OH2 .and. segid BLK4 end

!!!!!!!!!!!!!!!!!!!!!!!!!!!!!!!!!!!!!!!!!!!!!!!!!!!!

! Write protein coordinates
define JANG sele segid AKTT end

open write card unit 1 name /@dir/coor/@type_add_salt_system.crd
write coor sele JANG end card unit 1
* full system for protein
*

dele atom sele JANG end

!!!!!!!!!!!!!!!!!!!!!!!!!!!!!!!!!!!!!!!!!!!!!!!!!!!!

! Stat waters

coor stat sele resn TIP3 .and. type OH2  end

coor stat sele segid BLK1 .and. type OH2 end
set nt1 ?nsel
coor stat sele segid BLK2 .and. type OH2 end
set nt2 ?nsel
coor stat sele segid BLK3 .and. type OH2 end
set nt3 ?nsel
coor stat sele segid BLK4 .and. type OH2 end
set nt4 ?nsel
```

```
!!!!!!!!!!!!!!!!!!!!!!!!!!!!!!!!!!!!!!!!!!!!!!!!!!!!!

! Randomly choose waters for replacing salts

! random number generation
RAND UNIF ISEED 318098

!!!!!!!!!!!!!!!!!!!!!!!!!!!!!!!!!!!!!!!!!!!!!!!!!!!!!

! Na+ selection, nsod = total # of Na

set nsod @nna

label loop_sod1

    set r ?RAND
    if r gt 0.0   set NAME BLK1
    if r gt 0.50  set NAME BLK2
    if r gt 0.25  set NAME BLK2
    if r gt 0.50  set NAME BLK3
    if r gt 0.75  set NAME BLK4

    set n ?RAND
    if @NAME eq BLK1  mult n by @nt1
    if @NAME eq BLK2  mult n by @nt2
    if @NAME eq BLK3  mult n by @nt3
    if @NAME eq BLK4  mult n by @nt4
    if n lt 10000  trim n to 4
    if n lt 1000  trim n to 3
    if n lt 100  trim n to 2
    if n lt 10  trim n to 1
    if n eq 0  set n 1
!   salt selection
    print coor sele segid @NAME .and. resid @n .and. type OH2 end
    if ?nsel eq 0 goto loop_sod1
!   no salts around 4A each other
    define temp sele (type CLA .or. type SOD .or. type MG) .and. (segid @NAME
.and. resid @n .and. type OH2) .around. 4.0 end
    if ?nsel gt 0 goto loop_sod1
!   replace water to salt
    dele atom sele segid @NAME .and. type H* .and. resi @n end
    rena atom SOD sele segid @NAME .and. type OH2 .and. resi @n end
    coor stat sele type SOD end

if ?nsel lt @nsod goto loop_sod1

!!!!!!!!!!!!!!!!!!!!!!!!!!!!!!!!!!!!!!!!!!!!!!!!!!!!!!!

! Cl- selection, ncla = total # of Cl

set ncla @ncl
```

```
label loop_cla1

    set r ?RAND
    if r gt 0.0   set NAME BLK1
    if r gt 0.50  set NAME BLK2
    if r gt 0.25  set NAME BLK2
    if r gt 0.50  set NAME BLK3
    if r gt 0.75  set NAME BLK4

    set n ?RAND
    if @NAME eq BLK1  mult n by @nt1
    if @NAME eq BLK2  mult n by @nt2
    if @NAME eq BLK3  mult n by @nt3
    if @NAME eq BLK4  mult n by @nt4
    if n lt 10000  trim n to 4
    if n lt 1000  trim n to 3
    if n lt 100  trim n to 2
    if n lt 10  trim n to 1
    if n eq 0  set n 1
!   salt selection
    print coor sele segid @NAME .and. resid @n .and. type OH2 end
    if ?nsel eq 0 goto loop_cla1
!   no salts around 4A each other
    define temp sele (type CLA .or. type SOD .or. type MG) .and. (segid @NAME
.and. resid @n .and. type OH2) .around. 4.0 end
    if ?nsel gt 0 goto loop_cla1
!   replace water to salt
    dele atom sele segid @NAME .and. type H* .and. resi @n end
    rena atom CLA sele segid @NAME .and. type OH2 .and. resi @n end
    coor stat sele type CLA end

if ?nsel lt @ncla goto loop_cla1

!!!!!!!!!!!!!!!!!!!!!!!!!!!!!!!!!!!!!!!!!!!!!!!!!!!!!!!!!!!!!!!!!!!

! Write salt coordinates

open write card unit 1 name /@dir/coor/temp_sod.crd
write coor card unit 1 sele type SOD end
* temp salt coordinates
*

dele atoms sele type SOD end

open write card unit 1 name /@dir/coor/temp_cla.crd
write coor card unit 1 sele type CLA end
* temp salt coordinates
*

dele atoms sele type CLA end
```

```
!!!!!!!!!!!!!!!!!

! Write water coordinates

open write card unit 1 name /@dir/coor/temp_blk1.crd
write coor sele segid BLK1 end card unit 1
* water coor
*

dele atom sele segid BLK1 end

open write card unit 1 name /@dir/coor/temp_blk2.crd
write coor sele segid BLK2 end card unit 1
* water coor
*

dele atom sele segid BLK2 end

open write card unit 1 name /@dir/coor/temp_blk3.crd
write coor sele segid BLK3 end card unit 1
* water coor
*

dele atom sele segid BLK3 end

open write card unit 1 name /@dir/coor/temp_blk4.crd
write coor sele segid BLK4 end card unit 1
* water coor
*

Stop
```

A sample CHARMM-generated input file for psf

```
 * File: model_2_apo_mk_psf_salt.inp
* Generate combined coordinates for NMAD simulation
*

!!!!!!!!!!!!!!!!!!!!!!!!!!!!!!!!!!!!!!!!!!!!!!!!!!!!
! set directory
set type model_2_apo
set dir data/weakoj2/@type
!!!!!!!!!!!!!!!!!!!!!!!!!!!!!!!!!!!!!!!!!!!!!!!!!!!!

bomlev -2

! read topology
open read card unit 10 name
/data/weakoj2/charmm_input/top_all36_phd_c39b2_hbj.inp
read rtf card unit 10
close unit 10
```

```
! read parameters
open read card unit 10 name
/data/weakoj2/charmm_input/par_all36_phd_c39b2_hbj.inp
read param card unit 10
close unit 10

!!!!!!!!!!!!!!!!!!!!!!!!!!!!!!!!!!!!!!!!!!!!!!!!!!!!!!!

! Get PHD-Akt
read sequence card
* The sequence is AKTT 1 to 480
*
480
MET SER ASP VAL ALA ILE VAL LYS GLU GLY TRP LEU HSD LYS ARG GLY
GLU TYR ILE LYS
THR TRP ARG PRO ARG TYR PHE LEU LEU LYS ASN ASP GLY THR PHE ILE
GLY TYR LYS GLU
ARG PRO GLN ASP VAL ASP GLN ARG GLU ALA PRO LEU ASN ASN PHE
SER VAL ALA GLN CYS
GLN LEU MET LYS THR GLU ARG PRO ARG PRO ASN THR PHE ILE ILE
ARG CYS LEU GLN TRP
THR THR VAL ILE GLU ARG THR PHE HSD VAL GLU THR PRO GLU GLU
ARG GLU GLU TRP THR
THR ALA ILE GLN THR VAL ALA ASP GLY LEU LYS LYS GLN GLU GLU GLU
GLU MET ASP PHE
ARG SER GLY SER PRO SER ASP ASN SER GLY ALA GLU GLU MET GLU VAL
SER LEU ALA LYS
PRO LYS HSD ARG VAL THR MET ASN GLU PHE GLU TYR LEU LYS LEU
LEU GLY LYS GLY THR
PHE GLY LYS VAL ILE LEU VAL LYS GLU LYS ALA THR GLY ARG TYR TYR
ALA MET LYS ILE
LEU LYS LYS GLU VAL ILE VAL ALA LYS ASP GLU VAL ALA HSD THR LEU
THR GLU ASN ARG
VAL LEU GLN ASN SER ARG HSD PRO PHE LEU THR ALA LEU LYS TYR
SER PHE GLN THR HSD
ASP ARG LEU CYS PHE VAL MET GLU TYR ALA ASN GLY GLY GLU LEU
PHE PHE HSD LEU SER
ARG GLU ARG VAL PHE SER GLU ASP ARG ALA ARG PHE TYR GLY ALA
GLU ILE VAL SER ALA
LEU ASP TYR LEU HSD SER GLU LYS ASN VAL VAL TYR ARG ASP LEU LYS
LEU GLU ASN LEU
MET LEU ASP LYS ASP GLY HSD ILE LYS ILE THR ASP PHE GLY LEU CYS
LYS GLU GLY ILE
LYS ASP GLY ALA THR MET LYS THR PHE CYS GLY THR PRO GLU TYR LEU
ALA PRO GLU VAL
LEU GLU ASP ASN ASP TYR GLY ARG ALA VAL ASP TRP TRP GLY LEU GLY
VAL VAL MET TYR
GLU MET MET CYS GLY ARG LEU PRO PHE TYR ASN GLN ASP HSD GLU
LYS LEU PHE GLU LEU
ILE LEU MET GLU GLU ILE ARG PHE PRO ARG THR LEU GLY PRO GLU
ALA LYS SER LEU LEU
```

```
SER GLY LEU LEU LYS LYS ASP PRO LYS GLN ARG LEU GLY GLY GLY SER
GLU ASP ALA LYS
GLU ILE MET GLN HSD ARG PHE PHE ALA GLY ILE VAL TRP GLN HSD
VAL TYR GLU LYS LYS
LEU SER PRO PRO PHE LYS PRO GLN VAL THR SER GLU THR ASP THR
ARG TYR PHE ASP GLU
GLU PHE THR ALA GLN MET ILE THR ILE THR PRO PRO ASP GLN ASP ASP
SER MET GLU CYS
VAL ASP SER GLU ARG ARG PRO HSD PHE PRO GLN PHE SER TYR SER
ALA SER GLY THR ALA

generate AKTT first NTER last CTER setup

open read card unit 1 name /@dir/coor/@type_add_salt_system.crd
read coor card unit 1
close unit 1

set N ?nres

open read card unit 1 name /@dir/coor/temp_blk1.crd
read sequence coor unit 1
generate BLK1 nodihedrals noangles first none last none
close unit 1
open read card unit 1 name /@dir/coor/temp_blk1.crd
read coor card unit 1 offset @N
close unit 1

set N ?nres

open read card unit 1 name /@dir/coor/temp_blk2.crd
read sequence coor unit 1
generate BLK2 nodihedrals noangles first none last none
close unit 1
open read card unit 1 name /@dir/coor/temp_blk2.crd
read coor card unit 1 offset @N
close unit 1

set N ?nres

open read card unit 1 name /@dir/coor/temp_blk3.crd
read sequence coor unit 1
generate BLK3 nodihedrals noangles first none last none
close unit 1
open read card unit 1 name /@dir/coor/temp_blk3.crd
read coor card unit 1 offset @N
close unit 1

set N ?nres

open read card unit 1 name /@dir/coor/temp_blk4.crd
read sequence coor unit 1
generate BLK4 nodihedrals noangles first none last none
```

```
close unit 1
open read card unit 1 name /@dir/coor/temp_blk4.crd
read coor card unit 1 offset @N
close unit 1

set N ?nres

open read card unit 1 name /@dir/coor/temp_sod.crd_mod
read sequence coor unit 1
generate SODI noangle nodihedral
close unit 1
open read card unit 1 name /@dir/coor/temp_sod.crd_mod
read coor card unit 1 offset @N
close unit 1

set N ?nres

open read card unit 1 name /@dir/coor/temp_cla.crd_mod
read sequence coor unit 1
generate CHLO noangle nodihedral
close unit 1
open read card unit 1 name /@dir/coor/temp_cla.crd_mod
read coor card unit 1 offset @N
close unit 1

!!!!!!!!!!!!!!!!!

! Stat for protein
coor stat sele segid AKTT end
coor stat sele segid AKTT .and. type CA end
!coor stat sele segid IP4 end

! Stat for salt
coor stat sele resn SOD end
coor stat sele resn CLA end

! Stat for water
coor stat sele segid BLK1 .and. type OH2 end
coor stat sele segid BLK2 .and. type OH2 end
coor stat sele segid BLK3 .and. type OH2 end
coor stat sele segid BLK4 .and. type OH2 end

!!!!!!!!!!!!!!!!!
!IOFOrmat NOEXtended
!!!!!!!!!!!!!!!!!

! Write psf file in charmm format
open write card unit 1 name /@dir/psf/@type_namd_salt_charmm.psf
write psf card unit 1
close unit 1

! Write psf file in charmm format
```

```
open write card unit 1 name /@dir/psf/@type_namd_salt_xplor.psf
write psf card xplor unit 1
close unit 1

!!!!!!!!!!!!!!!!!!

! Get the final coordinates in pdb
open write form unit 1 name /@dir/coor/@type_namd_salt_charmm.pdb
write coor pdb unit 1
close unit 1

stop
```

A sample minimization configuration file suitable for CHARMM-generated psf file

```
#%%%%%%%%%%%%%%%%%%%%%%%%%%%%%%%%%%%%%%%%%%%%%%%%%%%%%%%%%%%%%%%%%%%%%%%%%%%%%%%%# %%%%%%# %%%%%%# %%%%
#   FILE: cam1phd_mod2_namd_preequ_mini.cnfg                   #
#   Minimization of solvent with protein fix                   #
#%%%%%%%%%%%%%%%%%%%%%%%%%%%%%%%%%%%%%%%%%%%%%%%%%%%%%%%%%%%%%%%%%%%%%%%%%%%%%%%%#

#%%%%%%%%%%%%%%%%%%%%%%%%%%%%%%%%%%%%%%%%%%%%%%%%%%%%%%%%%%%%%%%%%%%%%%%%%%%%%%%%#
#   Set variable values                                        #
#%%%%%%%%%%%%%%%%%%%%%%%%%%%%%%%%%%%%%%%%%%%%%%%%%%%%%%%%%%%%%%%%%%%%%%%%%%%%%%%%#
set temp              310
set dir              /data/weakoj2/cam1phd_mod2
set type              cam1phd_mod2

#%%%%%%%%%%%%%%%%%%%%%%%%%%%%%%%%%%%%%%%%%%%%%%%%%%%%%%%%%%%%%%%%%%%%%%%%%%%%%%%%#
#   Parameters                                                 #
#%%%%%%%%%%%%%%%%%%%%%%%%%%%%%%%%%%%%%%%%%%%%%%%%%%%%%%%%%%%%%%%%%%%%%%%%%%%%%%%%#
paraTypeCharmm        on
parameters            /data/weakoj2/charmm_input/par_all36_phd_c39b2_hbj.inp

#%%%%%%%%%%%%%%%%%%%%%%%%%%%%%%%%%%%%%%%%%%%%%%%%%%%%%%%%%%%%%%%%%%%%%%%%%%%%%%%%#
#   Input files                                                #
#%%%%%%%%%%%%%%%%%%%%%%%%%%%%%%%%%%%%%%%%%%%%%%%%%%%%%%%%%%%%%%%%%%%%%%%%%%%%%%%%#
structure             ${dir}/psf/${type}_namd_salt_xplor.psf       ;# Name of structure file
coordinates           ${dir}/coor/${type}_namd_salt_charmm.pdb     ;# Name of input pdb
file

#%%%%%%%%%%%%%%%%%%%%%%%%%%%%%%%%%%%%%%%%%%%%%%%%%%%%%%%%%%%%%%%%%%%%%%%%%%%%%%%%#
```

```
#   Restart files                                    #
#%%%%%%%%%%%%%%%%%%%%%%%%%%%%%%%%%%%%%%%%%%%%%%%
%%%%%%%%%%%%%%%%%%%%%%%%%%%#
# NOTE: Do not set the initial restart velocity if you have also specified a temperature!
if {0} {
velocities          ${dir}/vel/                          ;# Initial velocies in pdb file
binVelocities        ${dir}/vel/                          ;# Initial velocies in binary format
                                                          ;# Remove the "temperature" entry if you use
this!
binCoordinates       ${dir}/coor/                         ;# Initial coor in binary format
extendedSystem       ${dir}/xsc/                          ;# Input periodic cell para read
from
}

#%%%%%%%%%%%%%%%%%%%%%%%%%%%%%%%%%%%%%%%%%%%%%%%
%%%%%%%%%%%%%%%%%%%%%%%%%%%#
#   Simulation temperature                              #
#%%%%%%%%%%%%%%%%%%%%%%%%%%%%%%%%%%%%%%%%%%%%%%%
%%%%%%%%%%%%%%%%%%%%%%%%%%%#
# NOTE: Do not set the initial velocity temperature if you have also specified a .vel
restart file!
temperature          $temp

#%%%%%%%%%%%%%%%%%%%%%%%%%%%%%%%%%%%%%%%%%%%%%%%
%%%%%%%%%%%%%%%%%%%%%%%%%%%#
#   Output files                                     #
#%%%%%%%%%%%%%%%%%%%%%%%%%%%%%%%%%%%%%%%%%%%%%%%
%%%%%%%%%%%%%%%%%%%%%%%%%%%#
outputName           ${dir}/coor/${type}_namd_preequ_mini_pdb    ;# Name of final
output coor file
binaryoutput         no                                   ;# Save final coor in binary format
restartname          ${dir}/coor/${type}_namd_preequ_mini        ;# Name of
output(restart) coor & vel file
binaryrestart        yes                                  ;# Save restart file in binary format
restartfreq          10000                                ;# Freq saving coor & vel (1000 steps =
every 1ps)
restartsave          yes                                  ;# Append time step at end of file name
dcdfile              ${dir}/trj/${type}_namd_preequ_mini.dcd     ;# Name of trajectory file
dcdfreq              100                                  ;# Freq saving trajectory
dcdUnitCell          yes                                  ;# Write unit cell data to dcd file
#veldcdfile     ${dir}/vel/${type}_namd_preequ_mini_vel.dcd     ;# Name of vel
trajectory file
#veldcdfreq          500                                  ;# Freq saving vel trajectory

#%%%%%%%%%%%%%%%%%%%%%%%%%%%%%%%%%%%%%%%%%%%%%%%
%%%%%%%%%%%%%%%%%%%%%%%%%%%#
#   Output configurations                            #
#%%%%%%%%%%%%%%%%%%%%%%%%%%%%%%%%%%%%%%%%%%%%%%%
%%%%%%%%%%%%%%%%%%%%%%%%%%%#
outputEnergies       100                                  ;# Freq for printing Energies
outputTiming         100                                  ;# Freq for printing Timing info
```

```
outputPressure       100                                    ;# Freq for printing Pressure

#%%%%%%%%%%%%%%%%%%%%%%%%%%%%%%%%%%%%%%%%%%%%%%%%
%%%%%%%%%%%%%%%%%%%%%%%%%%%#
#   Periodic Boundary conditions                              #
#%%%%%%%%%%%%%%%%%%%%%%%%%%%%%%%%%%%%%%%%%%%%%%%%
%%%%%%%%%%%%%%%%%%%%%%%%%%%#
# NOTE: Do not set the periodic cell basis if you have specified an .xsc restart file!
if {1} {
cellBasisVector1     100.0  0.   0.
cellBasisVector2       0. 100.0  0.
cellBasisVector3       0.   0. 100.0
cellOrigin             0.   0.   0.
}
#xstFile             ${dir}/xsc/${type}_namd_preequ_mini.xst     ;# Name of cell param
trajectory file
#xstfreq             100                                    ;# Freq for writing cell param trajectory
wrapWater            on                                     ;# Wrap water around periodic boundary
wrapAll              on                                     ;# Wrap all atoms around periodic
boundary

#%%%%%%%%%%%%%%%%%%%%%%%%%%%%%%%%%%%%%%%%%%%%%%%%
%%%%%%%%%%%%%%%%%%%%%%%%%%%#
#   Force-field parameters                                    #
#%%%%%%%%%%%%%%%%%%%%%%%%%%%%%%%%%%%%%%%%%%%%%%%%
%%%%%%%%%%%%%%%%%%%%%%%%%%%#
cutoff               12.                                    ;# Local interaction dist to elec & VdW
calculation
switching            on                                     ;# Smoothing func for cutoff, otherwise
truncated
switchdist           10.                                    ;# Should be less than or equal to cutoff
value
pairlistdist         14.                                    ;# Cutoff for generating pair list,larger than
cutoff
exclude              scaled1-4                              ;# Exclude pairs in nonbonding
interactions
1-4scaling           1.0                                    ;# Scaling factor for 1-4 interaction
COMmotion            no                                     ;# No center of mass motion for entire
system
splitPatch           hydrogen                               ;# Set hydrogen to allow faster distance
check
hgroupCutoff         2.5                                    ;# Use for group-based distance testing

#%%%%%%%%%%%%%%%%%%%%%%%%%%%%%%%%%%%%%%%%%%%%%%%%
%%%%%%%%%%%%%%%%%%%%%%%%%%%#
#   Time step parameters                                      #
#%%%%%%%%%%%%%%%%%%%%%%%%%%%%%%%%%%%%%%%%%%%%%%%%
%%%%%%%%%%%%%%%%%%%%%%%%%%%#
timestep             2.                                     ;# 2 fs/step
firsttimestep        0                                      ;# Starting time step value
stepspercycle        20                                     ;# Freq updating nonbond list
```

```
#%%%%%%%%%%%%%%%%%%%%%%%%%%%%%%%%%%%%%%%%%%
%%%%%%%%%%%%%%%%%%%%%%%%#
#   Multiple time step parameters for long range elec             #
#%%%%%%%%%%%%%%%%%%%%%%%%%%%%%%%%%%%%%%%%%%
%%%%%%%%%%%%%%%%%%%%%%%%#
fullElectFrequency    1                                  ;# Calc long range elec stat every time
step
nonbondedFreq         1                                  ;# Freq for calc short range nonbond
interac
MTSAlgorithm          impulse                            ;# Integr method for long range elec
longsplitting         c1                                 ;# Method for split elec forces between
long and short

#%%%%%%%%%%%%%%%%%%%%%%%%%%%%%%%%%%%%%%%%%%
%%%%%%%%%%%%%%%%%%%%%%%%#
#   PME parameters                                #
#%%%%%%%%%%%%%%%%%%%%%%%%%%%%%%%%%%%%%%%%%%
%%%%%%%%%%%%%%%%%%%%%%%%#
if {0} {
PME                   no                                 ;# Use particle mesh Ewald for
electrostatics
PMETolerance          1.0e-6                             ;# Affect value of Ewald coefficient
PMEInterpOrder        4                                  ;# For cubic 4
PMEGridSizeX          92                                 ;# Number of grid ponts in x
PMEGridSizeY          92                                 ;# Number of grid ponts in y
PMEGridSizeZ          92                                 ;# Number of grid ponts in z
}

#%%%%%%%%%%%%%%%%%%%%%%%%%%%%%%%%%%%%%%%%%%
%%%%%%%%%%%%%%%%%%%%%%%%#
#   Constant temperature control                          #
#%%%%%%%%%%%%%%%%%%%%%%%%%%%%%%%%%%%%%%%%%%
%%%%%%%%%%%%%%%%%%%%%%%%#
if {0} {
langevin              on                                 ;# Use langeving dynam for temp control
langevinTemp          $temp
langevinDamping       2.5                                ;# Friction coeff (gamma) (1/ps), use
a small value
langevinHydrogen      off                                ;# Don't couple langevin bath to
hydrogens
}

#%%%%%%%%%%%%%%%%%%%%%%%%%%%%%%%%%%%%%%%%%%
%%%%%%%%%%%%%%%%%%%%%%%%#
#  Temperature control for heating or cooling                   #
#%%%%%%%%%%%%%%%%%%%%%%%%%%%%%%%%%%%%%%%%%%
%%%%%%%%%%%%%%%%%%%%%%%%#
if {0} {
reassignFreq          50000                              ;# Frequency to reassign temperature
reassignTemp          10.0                               ;# Initial temperature
```

```
reassignIncr         30.0                              ;# Temperature increment or decrement
reassignHold          $temp                              ;# Target temperature
}

#%%%%%%%%%%%%%%%%%%%%%%%%%%%%%%%%%%%%%%%%%%%%%
%%%%%%%%%%%%%%%%%%%%%%%%%%%%#
#   Constant pressure control                            #
#%%%%%%%%%%%%%%%%%%%%%%%%%%%%%%%%%%%%%%%%%%%%%
%%%%%%%%%%%%%%%%%%%%%%%%%%%%#
useGroupPressure      yes                              ;# Should use w/SHAKE, needed for
2fs steps
useFlexibleCell       no                               ;# Allows dimensions of cell to
fluctuate
                                                  ;# no for water box, yes for membrane
useConstantArea       no                               ;# x-y fixed and z dim can vary
                                                  ;# no for water box, yes for membrane
if {1} {
LangevinPiston        on                               ;# Use Nose-Hoover Langeving Piston
Algorithm
LangevinPistonTarget  1.01325                          ;# Target pressure to run simu at
(bars)
LangevinPistonPeriod  200                              ;# Oscillation period
LangevinPistonDecay   100                              ;# Damping time scale
LangevinPistonTemp    $temp                            ;# Should be set equal to the
target temperature
SurfaceTensionTarget  0.0                              ;# Apply suface tension in xy plane
(dyn/cm)
}

#%%%%%%%%%%%%%%%%%%%%%%%%%%%%%%%%%%%%%%%%%%%%%
%%%%%%%%%%%%%%%%%%%%%%%%%%%%#
#   Fix hydrogens                                   #
#%%%%%%%%%%%%%%%%%%%%%%%%%%%%%%%%%%%%%%%%%%%%%
%%%%%%%%%%%%%%%%%%%%%%%%%%%%#
if {1} {
rigidBonds           all                               ;# Fix h-bonds to none, water, or all h-
atoms
rigidTolerance        1.0e-8                           ;# Allowable bond-length error for
ShakeH
rigidIterations       100                              ;# Maximum ShakeH iterations
rigidDieOnError       on                               ;# Exit and report an error
useSettle            off                               ;# Keep waters rigid
}

#%%%%%%%%%%%%%%%%%%%%%%%%%%%%%%%%%%%%%%%%%%%%%
%%%%%%%%%%%%%%%%%%%%%%%%%%%%#
#   Harmonic constraints : constraint protein backbone with k=5    #
#%%%%%%%%%%%%%%%%%%%%%%%%%%%%%%%%%%%%%%%%%%%%%
%%%%%%%%%%%%%%%%%%%%%%%%%%%%#
if {1} {
constraints          on                                ;# Turn on the use of contraints
```

```
consexp          2                              ;# Exponent to be use in harmonic
constraint energy
consref      ${dir}/cons/${type}_preequ_constr_atoms_ref_5.pdb    ;# A pdb file to use
for reference positions
conskfile    ${dir}/cons/${type}_preequ_constr_atoms_kfile_5.pdb  ;# A pdb file to use
for k values
conskcol         B                              ;# Column of pdb file to use for harmonic
constraint
}

#%%%%%%%%%%%%%%%%%%%%%%%%%%%%%%%%%%%%%%%%%%%%%%%%%%%%%%%%%%%%%%%%%%%%%%%%%%%%%%%#
#   Fixed atoms constraint : fix protein                    #
#%%%%%%%%%%%%%%%%%%%%%%%%%%%%%%%%%%%%%%%%%%%%%%%%%%%%%%%%%%%%%%%%%%%%%%%%%%%%%%%#
if {1} {
fixedAtoms       on                             ;# Turn on the use of contraints
fixedAtomsForces     on                         ;# Calculate forces between fixed
atoms
fixedAtomsFile       ${dir}/cons/${type}_preequ_fix_protein.pdb     ;# A pdb file to use
for reference positions
fixedAtomsCol        O                          ;# Set O to read occupancy column in
pdb file
}

#%%%%%%%%%%%%%%%%%%%%%%%%%%%%%%%%%%%%%%%%%%%%%%%%%%%%%%%%%%%%%%%%%%%%%%%%%%%%%%%#
#   Minimization parameters                             #
#%%%%%%%%%%%%%%%%%%%%%%%%%%%%%%%%%%%%%%%%%%%%%%%%%%%%%%%%%%%%%%%%%%%%%%%%%%%%%%%#
if {1} {
minimization         on                         ;# Perform conjugate gradient energy
minimization
minTinyStep          1.0e-8                     ;# First initial step for line minimizer
minBabyStep          1.0e-2                     ;# Max initial step for line minimizer
minLineGoal          1.0e-4                     ;# Gradient reduction factor for line
minimizer
}

#%%%%%%%%%%%%%%%%%%%%%%%%%%%%%%%%%%%%%%%%%%%%%%%%%%%%%%%%%%%%%%%%%%%%%%%%%%%%%%%#
#   Extra parameters                                    #
#%%%%%%%%%%%%%%%%%%%%%%%%%%%%%%%%%%%%%%%%%%%%%%%%%%%%%%%%%%%%%%%%%%%%%%%%%%%%%%%#
# Put here any custom parameters that are specific to this job

#%%%%%%%%%%%%%%%%%%%%%%%%%%%%%%%%%%%%%%%%%%%%%%%%%%%%%%%%%%%%%%%%%%%%%%%%%%%%%%%#
#   Execution script                                    #
#%%%%%%%%%%%%%%%%%%%%%%%%%%%%%%%%%%%%%%%%%%%%%%%%%%%%%%%%%%%%%%%%%%%%%%%%%%%%%%%#
```

```
#----------------------------#
minimize             10000                          ;# Minimization step
#----------------------------#
#----------------------------#
#run                 10000                          ;# Dynamics step
#----------------------------#
#%%%%%%%%%%%%%%%%%%%%%%%%%%%%%%%%%%%%%%%%%%%%%%%%%%%%%%%%%%%%%%%%%%%%%%%%%%%%%%%#
#   End of script
#%%%%%%%%%%%%%%%%%%%%%%%%%%%%%%%%%%%%%%%%%%%%%%%%%%%%%%%%%%%%%%%%%%%%%%%%%%%%%%%#
```

A sample production run configuration file (suitable for CHARMM-generated psf fil.

```
#%%%%%%%%%%%%%%%%%%%%%%%%%%%%%%%%%%%%%%%%%%%%%%%%%%%%%%%%%%%%%%%%%%%%%%%%%%%%%%%#
#   FILE: cam1phd_mod2_namd_prod_50_ns.cnfg                    #
#   50 ns dynamics and production                          #
#%%%%%%%%%%%%%%%%%%%%%%%%%%%%%%%%%%%%%%%%%%%%%%%%%%%%%%%%%%%%%%%%%%%%%%%%%%%%%%%#

#%%%%%%%%%%%%%%%%%%%%%%%%%%%%%%%%%%%%%%%%%%%%%%%%%%%%%%%%%%%%%%%%%%%%%%%%%%%%%%%#
#   Set variable values                                    #
#%%%%%%%%%%%%%%%%%%%%%%%%%%%%%%%%%%%%%%%%%%%%%%%%%%%%%%%%%%%%%%%%%%%%%%%%%%%%%%%#
set temp            310
set dir             /data/weakoj2/cam1phd_mod2
set type            cam1phd_mod2

#%%%%%%%%%%%%%%%%%%%%%%%%%%%%%%%%%%%%%%%%%%%%%%%%%%%%%%%%%%%%%%%%%%%%%%%%%%%%%%%#
#   Parameters                                             #
#%%%%%%%%%%%%%%%%%%%%%%%%%%%%%%%%%%%%%%%%%%%%%%%%%%%%%%%%%%%%%%%%%%%%%%%%%%%%%%%#
paraTypeCharmm      on
parameters          /data/weakoj2/charmm_input/par_all36_phd_c39b2_hbj.inp

#%%%%%%%%%%%%%%%%%%%%%%%%%%%%%%%%%%%%%%%%%%%%%%%%%%%%%%%%%%%%%%%%%%%%%%%%%%%%%%%#
#   Input files                                            #
#%%%%%%%%%%%%%%%%%%%%%%%%%%%%%%%%%%%%%%%%%%%%%%%%%%%%%%%%%%%%%%%%%%%%%%%%%%%%%%%#
structure           ${dir}/psf/${type}_namd_salt_xplor.psf      ;# Name of structure file
coordinates    ${dir}/coor/${type}_namd_preequ_ewald_last_pdb.coor ;# Name of input
pdb file

#%%%%%%%%%%%%%%%%%%%%%%%%%%%%%%%%%%%%%%%%%%%%%%%%%%%%%%%%%%%%%%%%%%%%%%%%%%%%%%%#
```

```
#   Restart files                                    #
#%%%%%%%%%%%%%%%%%%%%%%%%%%%%%%%%%%%%%%%%
%%%%%%%%%%%%%%%%%%%%%%%%#
# NOTE: Do not set the initial restart velocity if you have also specified a temperature!
if {1} {
#velocities          ${dir}/vel/                          ;# Initial velocies in pdb file
binVelocities  ${dir}/vel/${type}_namd_preequ_ewald_last.50000.vel   ;# Initial
velocies in binary format
                                                    ;# Remove the "temperature" entry if you use
this!
binCoordinates ${dir}/coor/${type}_namd_preequ_ewald_last.50000.coor ;# Initial coor
in binary format
extendedSystem ${dir}/xsc/${type}_namd_preequ_ewald_last.50000.xsc   ;# Input
periodic cell para read from
}

#%%%%%%%%%%%%%%%%%%%%%%%%%%%%%%%%%%%%%%%%
%%%%%%%%%%%%%%%%%%%%%%%%#
#   Simulation temperature                               #
#%%%%%%%%%%%%%%%%%%%%%%%%%%%%%%%%%%%%%%%%
%%%%%%%%%%%%%%%%%%%%%%%%#
# NOTE: Do not set the initial velocity temperature if you have also specified a .vel
restart file!
#temperature          $temp

#%%%%%%%%%%%%%%%%%%%%%%%%%%%%%%%%%%%%%%%%
%%%%%%%%%%%%%%%%%%%%%%%%#
#   Output files                                     #
#%%%%%%%%%%%%%%%%%%%%%%%%%%%%%%%%%%%%%%%%
%%%%%%%%%%%%%%%%%%%%%%%%#
outputName           ${dir}/coor/${type}_namd_prod_50_ns_pdb     ;# Name of final
output coor file
binaryoutput          no                                 ;# Save final coor in binary format
restartname          ${dir}/coor/${type}_namd_prod_50_ns        ;# Name of
output(restart) coor & vel file
binaryrestart         yes                                ;# Save restart file in binary format
restartfreq          5000000                               ;# Freq saving coor & vel (1000 steps
= every 1ps)
restartsave          yes                                ;# Append time step at end of file name
dcdfile             ${dir}/trj/${type}_namd_prod_merged_50_ns.dcd       ;# Name of
trajectory file
dcdfreq             50000                                ;# Freq saving trajectory
dcdUnitCell          yes                                ;# Write unit cell data to dcd file
#veldcdfile          ${dir}/vel/${type}_namd_prod_50_ns_vel.dcd  ;# Name of vel
trajectory file
#veldcdfreq           1000                                ;# Freq saving vel trajectory

#%%%%%%%%%%%%%%%%%%%%%%%%%%%%%%%%%%%%%%%%
%%%%%%%%%%%%%%%%%%%%%%%%#
#   Output configurations                                #
#%%%%%%%%%%%%%%%%%%%%%%%%%%%%%%%%%%%%%%%%
```

```
%%%%%%%%%%%%%%%%%%%%%%%%#
outputEnergies       50000                    ;# Freq for printing Energies
outputTiming         50000                    ;# Freq for printing Timing info
outputPressure       50000                    ;# Freq for printing Pressure

#%%%%%%%%%%%%%%%%%%%%%%%%%%%%%%%%%%%%%%%%%%%%%%%%%%%%%%%%%%%%%%%%%%%%%%%%%%%#
#   Periodic Boundary conditions                                               #
#%%%%%%%%%%%%%%%%%%%%%%%%%%%%%%%%%%%%%%%%%%%%%%%%%%%%%%%%%%%%%%%%%%%%%%%%%%%#
# NOTE: Do not set the periodic cell basis if you have specified an .xsc restart file!
if {0} {
cellBasisVector1     100.0  0.   0.
cellBasisVector2      0. 100.0  0.
cellBasisVector3      0.   0. 100.0
cellOrigin            0.   0.   0.
}
xstFile              ${dir}/xsc/${type}_namd_prod_50_ns.xst     ;# Name of cell param
trajectory file
xstfreq              50000                    ;# Freq for writing cell param trajectory
wrapWater            on                       ;# Wrap water around periodic boundary
wrapAll              on                       ;# Wrap all atoms around periodic
boundary

#%%%%%%%%%%%%%%%%%%%%%%%%%%%%%%%%%%%%%%%%%%%%%%%%%%%%%%%%%%%%%%%%%%%%%%%%%%%#
#   Force-field parameters                                                     #
#%%%%%%%%%%%%%%%%%%%%%%%%%%%%%%%%%%%%%%%%%%%%%%%%%%%%%%%%%%%%%%%%%%%%%%%%%%%#
cutoff               12.                      ;# Local interaction dist to elec & VdW
calculation
switching            on                       ;# Smoothing func for cutoff, otherwise
truncated
switchdist           10.                      ;# Should be less than or equal to cutoff
value
pairlistdist         14.                      ;# Cutoff for generating pair list,larger than
cutoff
exclude              scaled1-4                ;# Exclude pairs in nonbonding
interactions
1-4scaling           1.0                      ;# Scaling factor for 1-4 interaction
COMmotion            no                       ;# No center of mass motion for entire
system
splitPatch           hydrogen                 ;# Set hydrogen to allow faster distance
check
hgroupCutoff         2.5                      ;# Use for group-based distance testing

#%%%%%%%%%%%%%%%%%%%%%%%%%%%%%%%%%%%%%%%%%%%%%%%%%%%%%%%%%%%%%%%%%%%%%%%%%%%#
#   Time step parameters                                                       #
#%%%%%%%%%%%%%%%%%%%%%%%%%%%%%%%%%%%%%%%%%%%%%%%%%%%%%%%%%%%%%%%%%%%%%%%%%%%#
```

```
timestep            2.                      ;# 2 fs/step
firsttimestep       0                       ;# Starting time step value
stepspercycle       20                      ;# Freq updating nonbond list

#%%%%%%%%%%%%%%%%%%%%%%%%%%%%%%%%%%%%%%%%%%%%%%%%%%%%%%%%%%%%%%%%%%%%%%%%%%%#
#   Multiple time step parameters for long range elec           #
#%%%%%%%%%%%%%%%%%%%%%%%%%%%%%%%%%%%%%%%%%%%%%%%%%%%%%%%%%%%%%%%%%%%%%%%%%%%#
fullElectFrequency  1                       ;# Calc long range elec stat every time
step
nonbondedFreq       1                       ;# Freq for calc short range nonbond
interac
MTSAlgorithm        impulse                 ;# Integr method for long range elec
longsplitting       c1                      ;# Method for split elec forces between
long and short

#%%%%%%%%%%%%%%%%%%%%%%%%%%%%%%%%%%%%%%%%%%%%%%%%%%%%%%%%%%%%%%%%%%%%%%%%%%%#
#   PME parameters                                              #
#%%%%%%%%%%%%%%%%%%%%%%%%%%%%%%%%%%%%%%%%%%%%%%%%%%%%%%%%%%%%%%%%%%%%%%%%%%%#
if {1} {
PME                 yes                     ;# Use particle mesh Ewald for
electrostatics
PMEGridSpacing      1.0                     ;# NAMD assigns automatically the
grid space
#PMETolerance       1.0e-6                  ;# Affect value of Ewald coefficient
#PMEInterpOrder     4                       ;# For cubic 4
#PMEGridSizeX       92                      ;# Number of grid ponts in x
#PMEGridSizeY       92                      ;# Number of grid ponts in y
#PMEGridSizeZ       92                      ;# Number of grid ponts in z
}

#%%%%%%%%%%%%%%%%%%%%%%%%%%%%%%%%%%%%%%%%%%%%%%%%%%%%%%%%%%%%%%%%%%%%%%%%%%%#
#   Constant temperature control                                #
#%%%%%%%%%%%%%%%%%%%%%%%%%%%%%%%%%%%%%%%%%%%%%%%%%%%%%%%%%%%%%%%%%%%%%%%%%%%#
if {1} {
langevin            on                      ;# Use langeving dynam for temp control
langevinTemp        $temp
langevinDamping     2.5                     ;# Friction coeff (gamma) (1/ps), use
a small value
langevinHydrogen    off                     ;# Don't couple langevin bath to
hydrogens
}

#%%%%%%%%%%%%%%%%%%%%%%%%%%%%%%%%%%%%%%%%%%%%%%%%%%%%%%%%%%%%%%%%%%%%%%%%%%%#
#  Temperature control for heating or cooling                   #
```

```
#%%%%%%%%%%%%%%%%%%%%%%%%%%%%%%%%%%%%%%%%%%%%%%%
%%%%%%%%%%%%%%%%%%%%%%%%%%%#
if {0} {
reassignFreq          50000                                ;# Frequency to reassign temperature
reassignTemp            10.0                               ;# Initial temperature
reassignIncr          30.0                               ;# Temperature increment or decrement
reassignHold           $temp                              ;# Target temperature
}

#%%%%%%%%%%%%%%%%%%%%%%%%%%%%%%%%%%%%%%%%%%%%%%%
%%%%%%%%%%%%%%%%%%%%%%%%%%%#
#   Constant pressure control                              #
#%%%%%%%%%%%%%%%%%%%%%%%%%%%%%%%%%%%%%%%%%%%%%%%
%%%%%%%%%%%%%%%%%%%%%%%%%%%#
useGroupPressure      yes                                  ;# Should use w/SHAKE, needed for
2fs steps
useFlexibleCell       no                                  ;# Allows dimensions of cell to
fluctuate
                                                    ;# no for water box, yes for membrane
useConstantArea       no                                   ;# x-y fixed and z dim can vary
                                                    ;# no for water box, yes for membrane
if {1} {
LangevinPiston        on                                   ;# Use Nose-Hoover Langeving Piston
Algorithm
LangevinPistonTarget  1.01325                                   ;# Target pressure to run simu at
(bars)
LangevinPistonPeriod  200                                    ;# Oscillation period
LangevinPistonDecay   100                                    ;# Damping time scale
LangevinPistonTemp    $temp                                     ;# Should be set equal to the
target temperature
SurfaceTensionTarget  0.0                                   ;# Apply suface tension in xy plane
(dyn/cm)
}

#%%%%%%%%%%%%%%%%%%%%%%%%%%%%%%%%%%%%%%%%%%%%%%%
%%%%%%%%%%%%%%%%%%%%%%%%%%%#
#   Fix hydrogens                                    #
#%%%%%%%%%%%%%%%%%%%%%%%%%%%%%%%%%%%%%%%%%%%%%%%
%%%%%%%%%%%%%%%%%%%%%%%%%%%#
if {1} {
rigidBonds            all                                ;# Fix h-bonds to none, water, or all h-
atoms
rigidTolerance         1.0e-8                              ;# Allowable bond-length error for
ShakeH
rigidIterations       100                                 ;# Maximum ShakeH iterations
rigidDieOnError       on                                   ;# Exit and report an error
useSettle            off                               ;# Keep waters rigid
}

#%%%%%%%%%%%%%%%%%%%%%%%%%%%%%%%%%%%%%%%%%%%%%%%
%%%%%%%%%%%%%%%%%%%%%%%%%%%#
```

```
#   Harmonic constraints                                  #
#%%%%%%%%%%%%%%%%%%%%%%%%%%%%%%%%%%%%%%%%%%%%%%%%%%%%%%%%%%%%%%%%#
if {0} {
constraints          on                          ;# Turn on the use of contraints
consexp              2                           ;# Exponent to be use in harmonic
constraint energy
consref              ${dir}/cons/                ;# A pdb file to use for reference
positions
conskfile            ${dir}/cons/                ;# A pdb file to use for k values
conskcol             B                           ;# Column of pdb file to use for harmonic
constraint
}

#%%%%%%%%%%%%%%%%%%%%%%%%%%%%%%%%%%%%%%%%%%%%%%%%%%%%%%%%%%%%%%%%#
#   Fixed atoms constraint                                #
#%%%%%%%%%%%%%%%%%%%%%%%%%%%%%%%%%%%%%%%%%%%%%%%%%%%%%%%%%%%%%%%%#
if {0} {
fixedAtoms           on                          ;# Turn on the use of contraints
fixedAtomsForces     off                         ;# Calculate forces between fixed
atoms
fixedAtomsFile       ${dir}/coor/                ;# A pdb file to use for reference
positions
fixedAtomsCol        O                           ;# Set O to read occupancy column in
pdb file
}

#%%%%%%%%%%%%%%%%%%%%%%%%%%%%%%%%%%%%%%%%%%%%%%%%%%%%%%%%%%%%%%%%#
#   Minimization parameters                               #
#%%%%%%%%%%%%%%%%%%%%%%%%%%%%%%%%%%%%%%%%%%%%%%%%%%%%%%%%%%%%%%%%#
if {0} {
minimization         on                          ;# Perform conjugate gradient energy
minimization
minTinyStep          1.0e-8                      ;# First initial step for line minimizer
minBabyStep          1.0e-2                      ;# Max initial step for line minimizer
minLineGoal          1.0e-4                      ;# Gradient reduction factor for line
minimizer
}

#%%%%%%%%%%%%%%%%%%%%%%%%%%%%%%%%%%%%%%%%%%%%%%%%%%%%%%%%%%%%%%%%#
#   Extra parameters                                      #
#%%%%%%%%%%%%%%%%%%%%%%%%%%%%%%%%%%%%%%%%%%%%%%%%%%%%%%%%%%%%%%%%#
# Put here any custom parameters that are specific to this job

#%%%%%%%%%%%%%%%%%%%%%%%%%%%%%%%%%%%%%%%%%%%%%%%%%%%%%%%%%%%%%%%%
```

```
%%%%%%%%%%%%%%%%%%%%%%%%%%%#
#   Execution script                              #
#%%%%%%%%%%%%%%%%%%%%%%%%%%%%%%%%%%%%%%%%%%%%%%%
%%%%%%%%%%%%%%%%%%%%%%%%%%%#
#----------------------------#
#minimize              5000                              ;# Minimization step
#----------------------------#
#----------------------------#
run                 25000000                              ;# Dynamics step
#----------------------------#
#%%%%%%%%%%%%%%%%%%%%%%%%%%%%%%%%%%%%%%%%%%%%%%%
%%%%%%%%%%%%%%%%%%%%%%%%%%%#
#   End of script
#%%%%%%%%%%%%%%%%%%%%%%%%%%%%%%%%%%%%%%%%%%%%%%%
%%%%%%%%%%%%%%%%%%%%%%%%%%%#
```

Appendix B

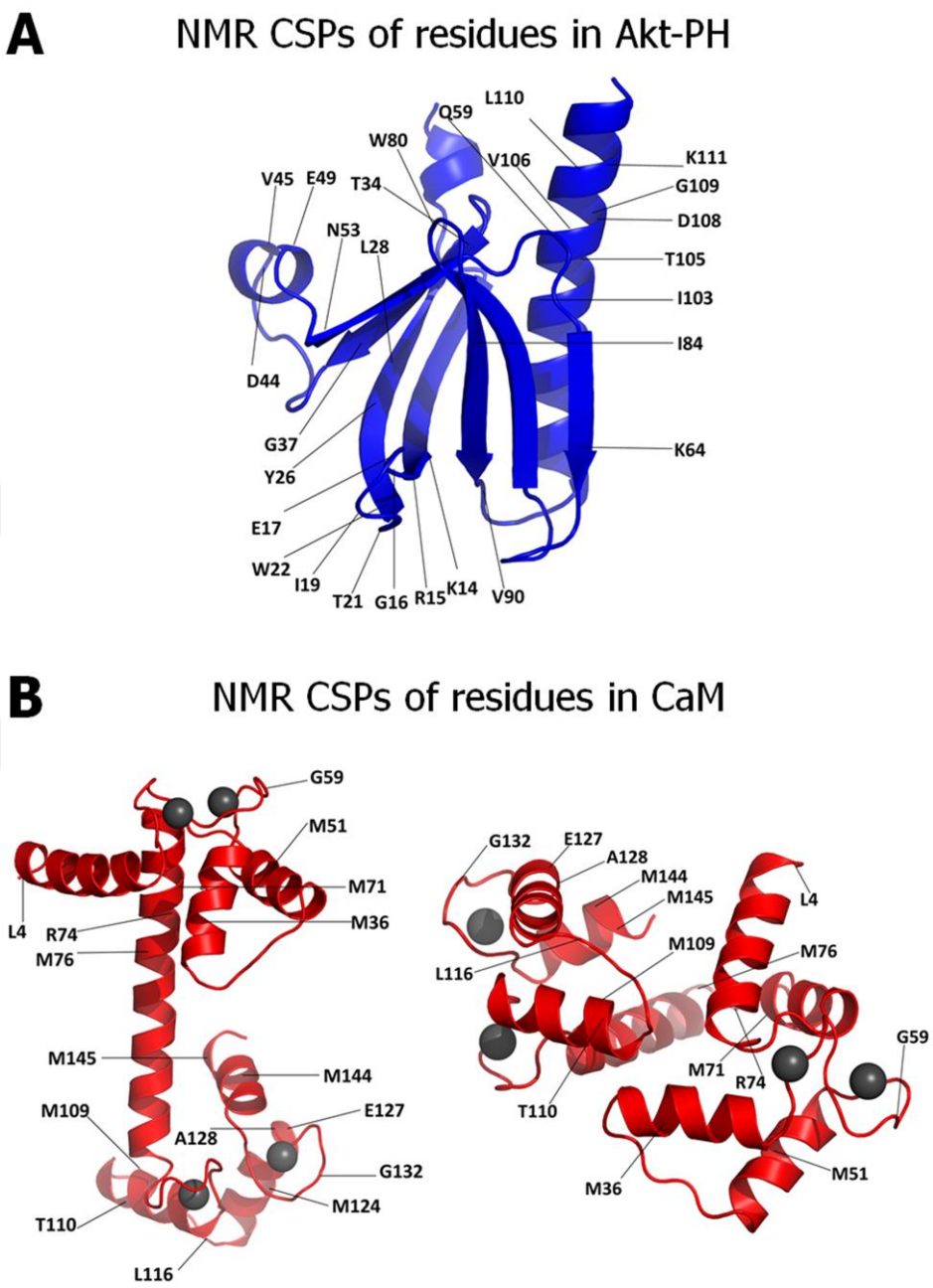

FIGURE B.1. NMR chemical shift perturbation (CSP). NMR CSP residues that exhibited high chemical shift as reported by NMR data (23,31) mapped onto the crystal structures of (A) Akt-PHD (PDB ID: 1H10) and (B) CaM with extended (left, PDB ID:1CLL) and collapsed (right, PDB ID:1CDL) linkers.

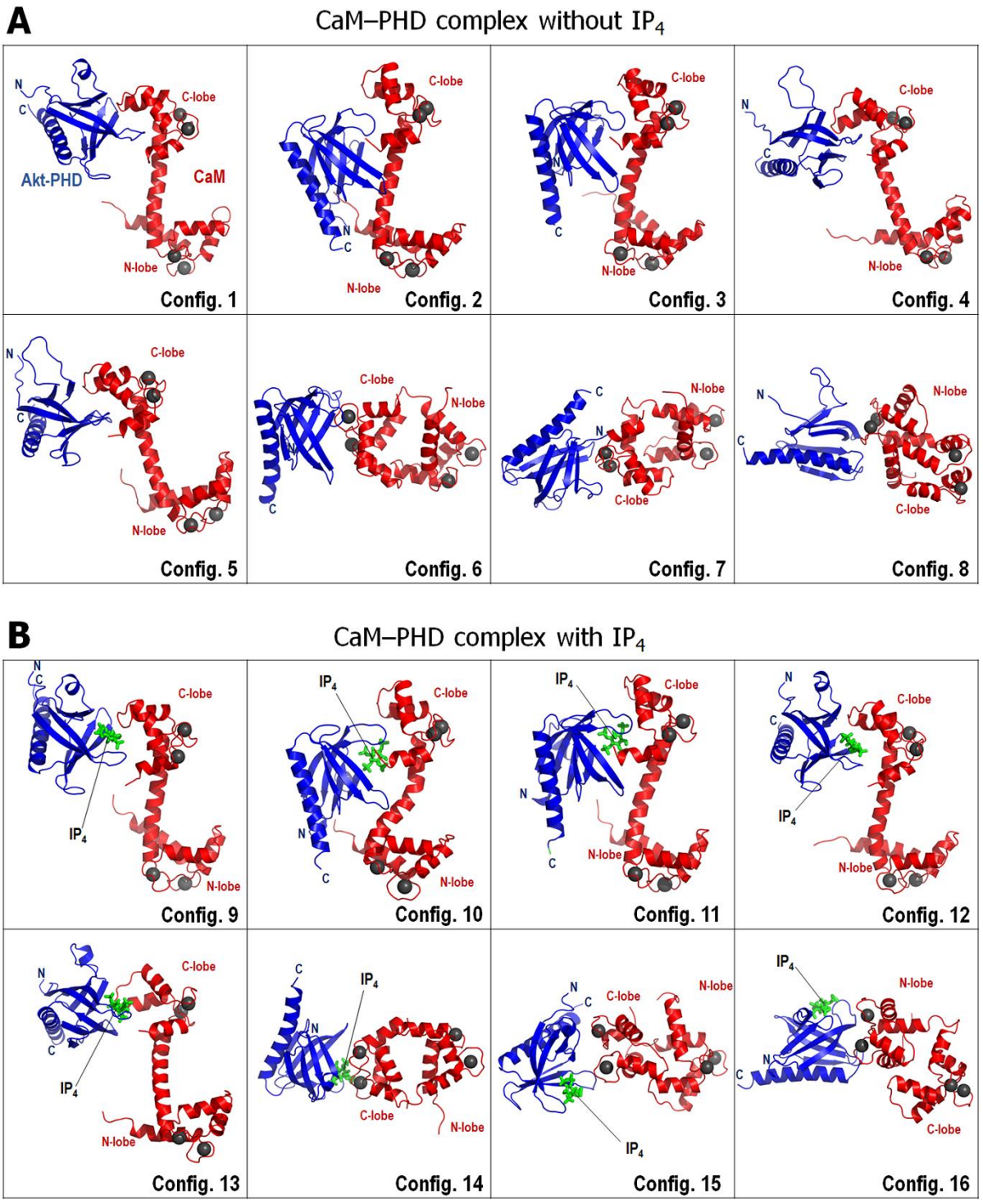

FIGURE B.2. Initial structures of the CaM–PHD complex. Cartoon representatives of the CaM–PHD complex for (A) Configs. 1-8 without IP_4 and (B) Configs. 9 -16 with IP_4.

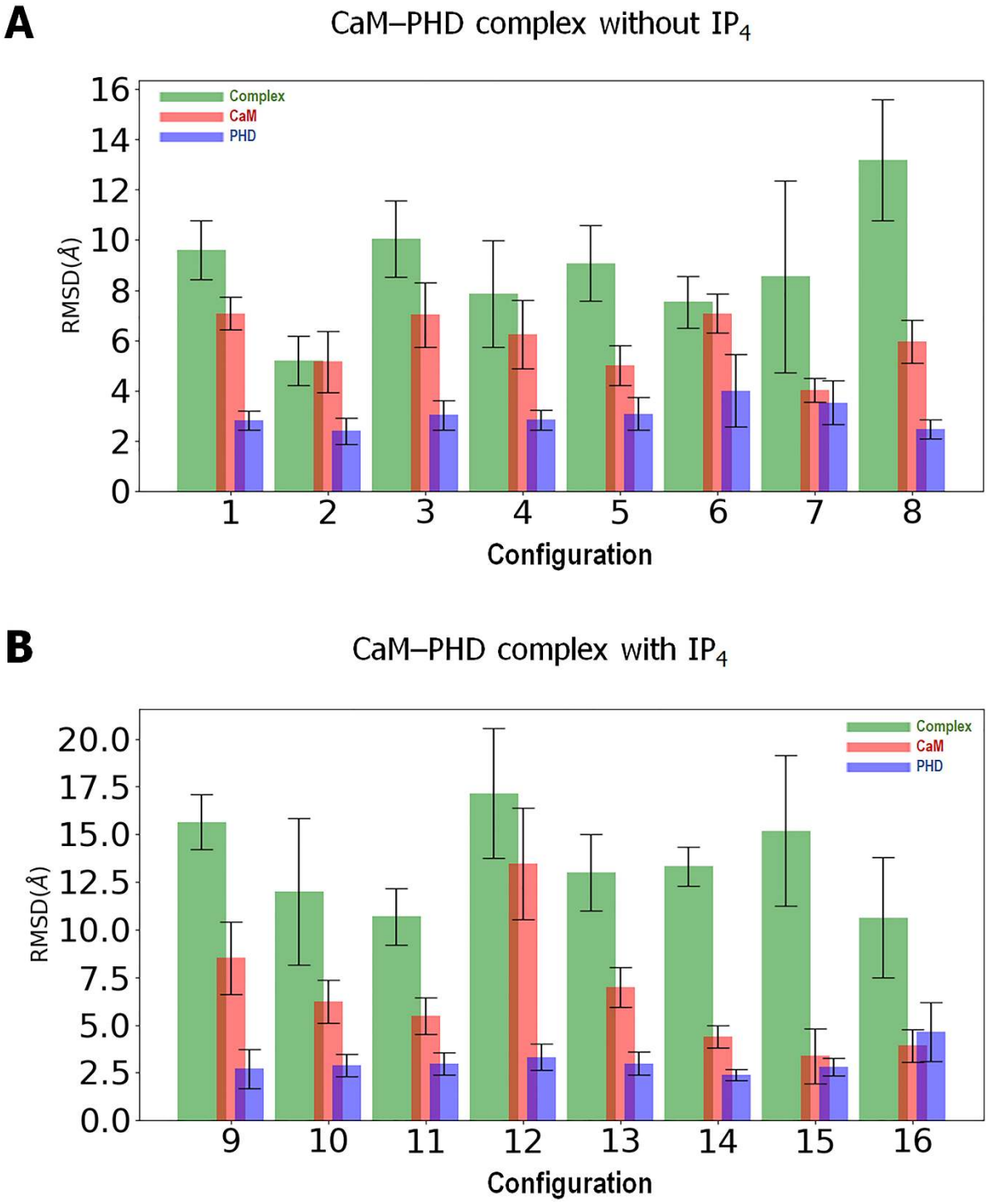

FIGURE B.3. The root-mean-square deviation (RMSD) profiles. Averaged RMSDs of CaM and PHD for (A) Configs. 1-8 without IP_4 and (B) Configs. 9 -16 with IP_4. Color code: CaM–PHD complex (green bar), CaM (red bar), and PHD (blue bar).

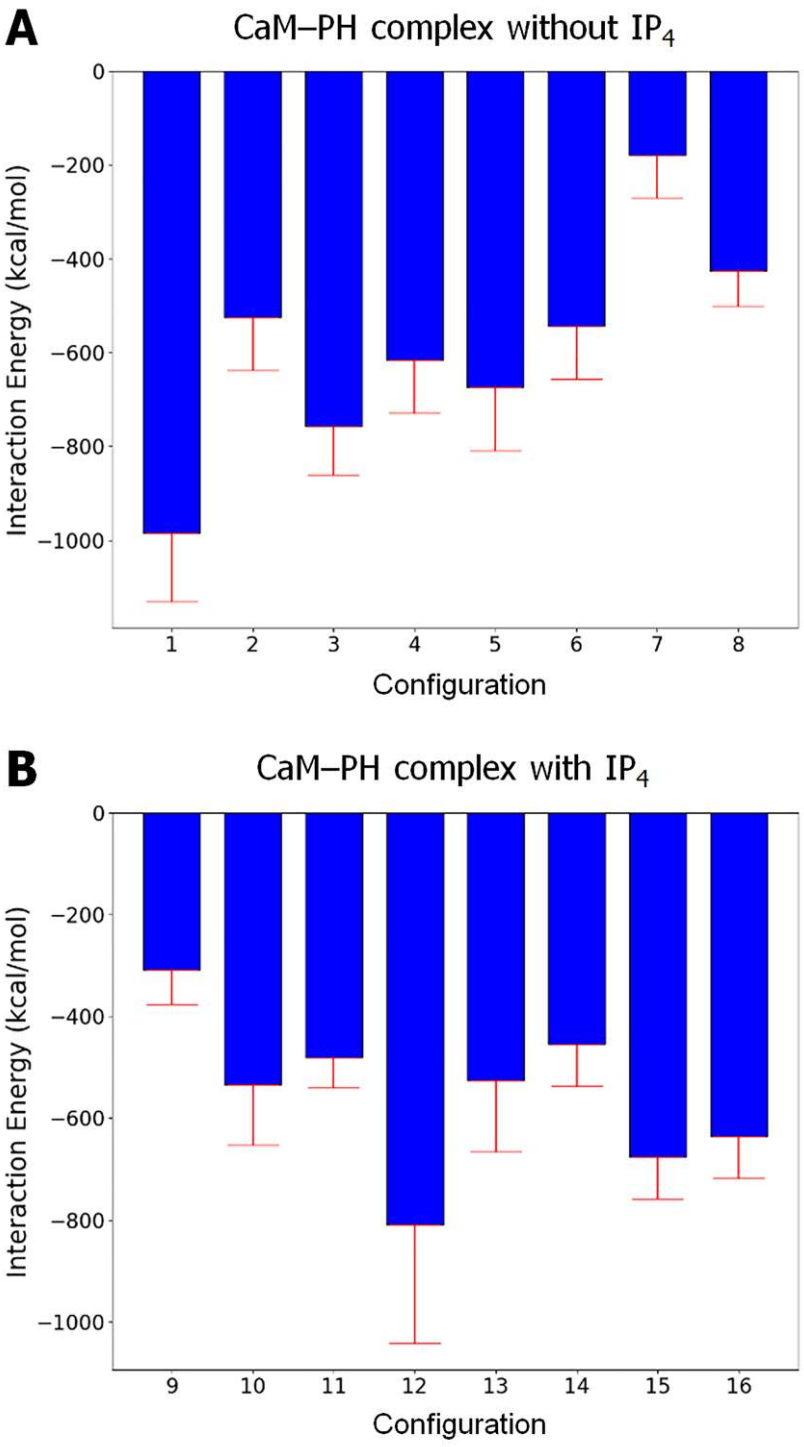

FIGURE B. 4. Interaction of CaM–PHD. Averaged interaction energy, contributions from electrostatic and van der Waals (vdW) interactions gauging the CaM–PHD association after 500 ns simulation for (A) Configs. 1-8 without IP_4 and (B) Configs. 9 -16 with IP_4.

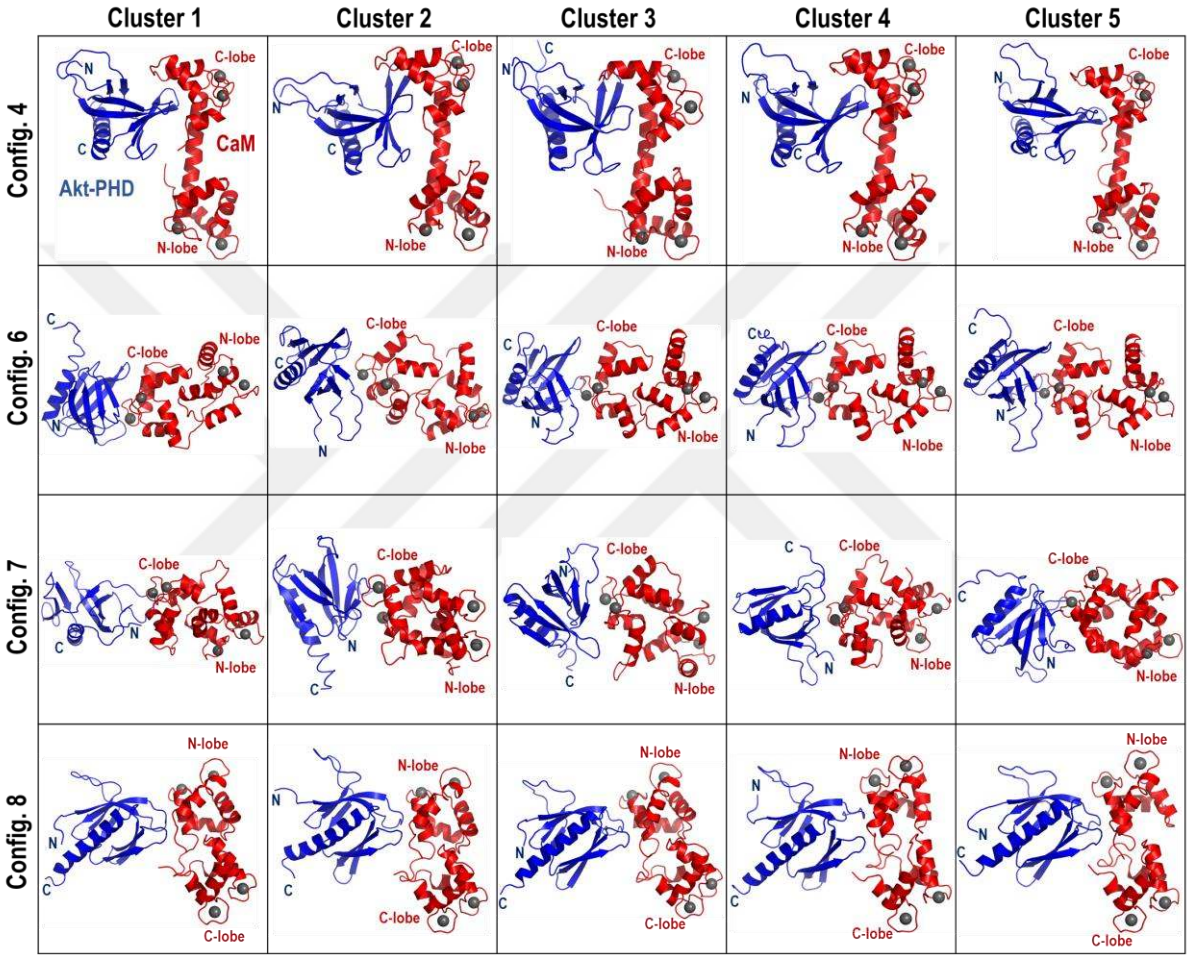

FIGURE B.5. The best approximated representative clusters for the other models (Configs. 4, 6, 7, and 8) of CaM–PHD complex. Conformation of the best approximated representative clusters of each model. The top five cluster representatives for Config. 4 were defined with probabilities, p = 0.082, 0.081, 0.044, 0.043, and 0.039 for clusters 1-5, respectively. For Config. 6, p = 0.09, 0.066, 0.061, 0.059, and 0.04; for Config. 7, p = 0.105, 0.095, 0.093, 0.050, and 0.050; for Config. 8, p = 0.163, 0.118, 0.062, 0.053, and 0.048 for clusters 1-5, respectively. The ensemble clustering was based on pairwise best-fit RSMD values, which returns the clusters, their sizes, and their conformational representatives.

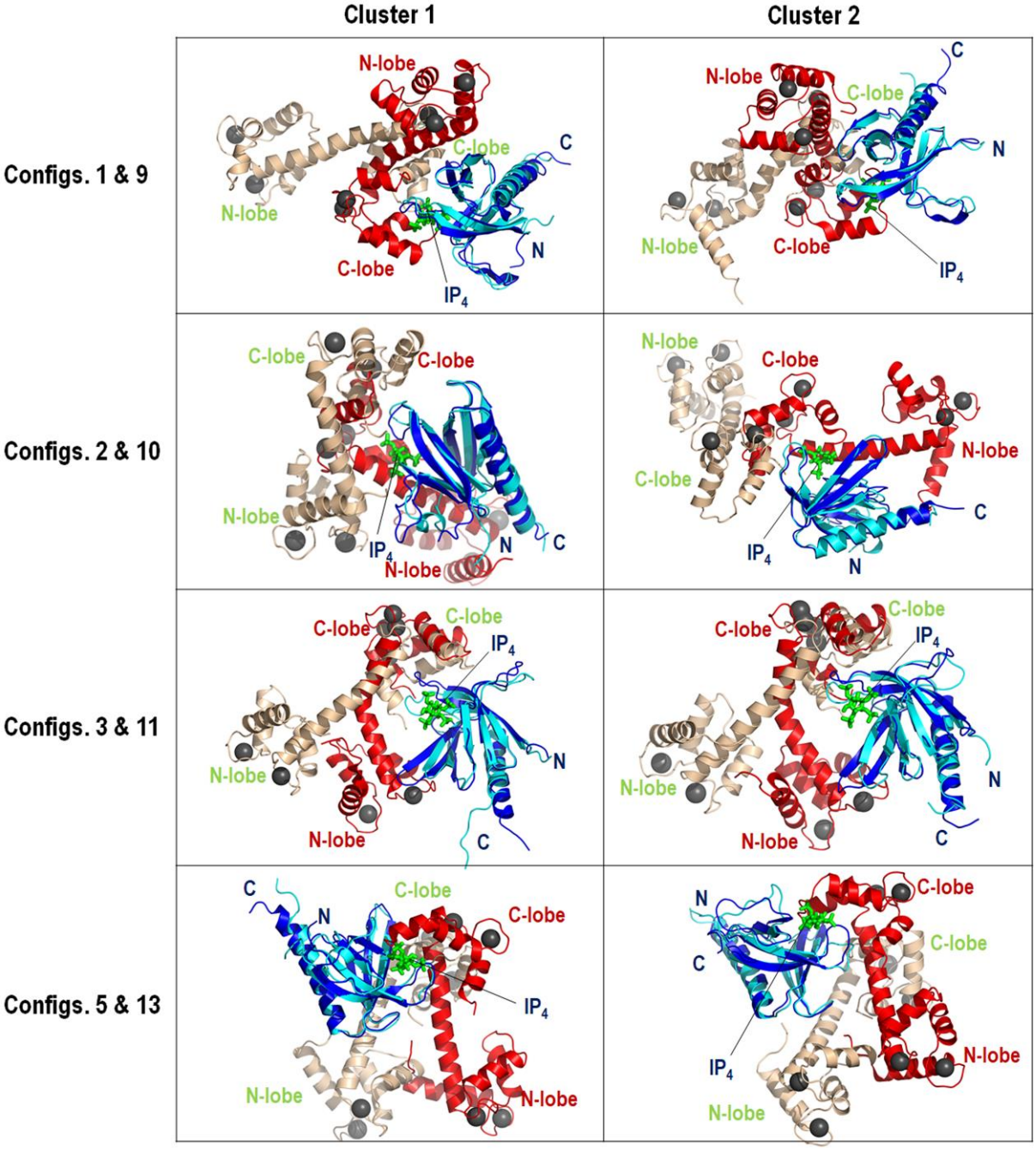

FIGURE B.6. Superimposition of clusters from Chimera. Top two clusters' representations of the best model for both with and without IP_4 were superimposed with respect to Akt-PHD. In the cartoons, configurations without IP_4 are colored red for CaM and blue for PHD, and configurations with IP_4 are colored wheat for CaM and cyan for PHD. For Configs. 1 & 9, RMSDs are 2.01 Å and 1.93 Å for clusters 1 and 2, respectively. For Configs. 2 & 10, RMSDs are 1.42 Å and 1.43 Å for clusters 1 and 2, respectively. For Configs. 3 & 11, RMSDs are 1.64 Å and 1.85 Å for clusters 1 and 2, respectively. For Configs. 5 & 13, RMSDs are 1.13 Å and 1.23 Å for clusters 1 and 2, respectively. RMSDs were computed only for the PHD.

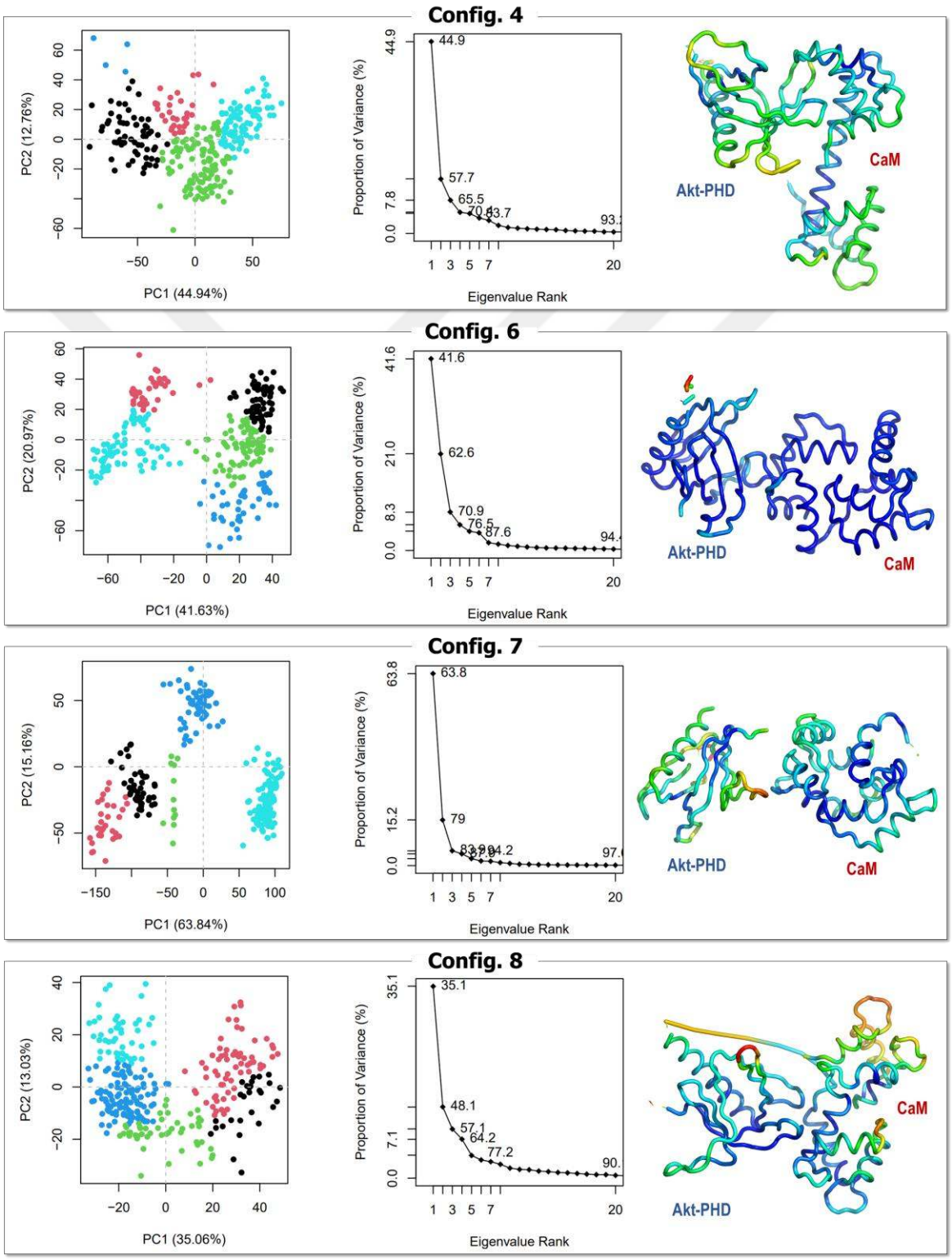

FIGURE B.7. Principal component analysis (PCA) for less favorable models. PC1 versus PC2 conformer plot for Configs. 4, 6, 7, and 8 shows five distinct clusters obtained via hierarchical clustering (hc, $k = 5$, left panels),

the eigenvalue scree plot (middle panels), and the collective motion for CaM–PHD complex defined by PC1 representing the structure colored by *B*-factor or temperature factor (right panels). In the B-factor structure, blue and red denote atoms with low and high-temperature values, respectively, while light blue, white, and pink denote intermediate temperature values.

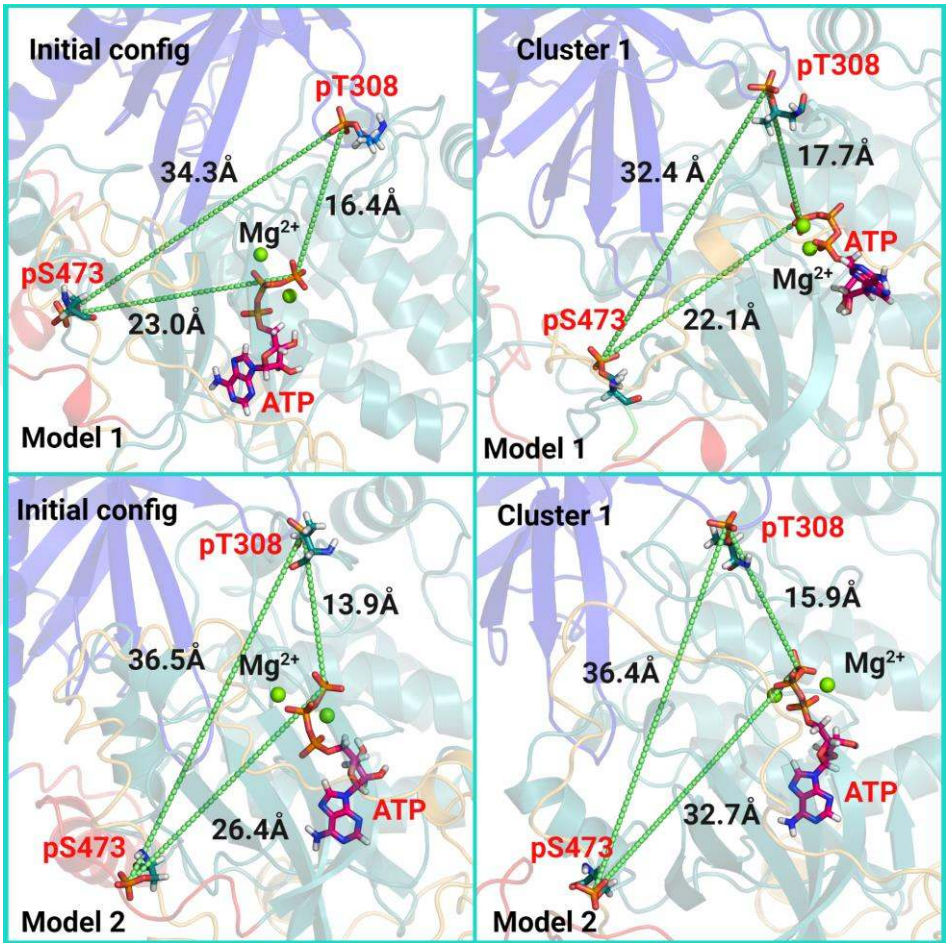

FIGURE B.8 Distance measurement of ATP in the binding cavity from pThr 308 and pS473. The ATP and the phosphorylated threonine and serine are shown as sticks

Appendix C

TABLE C.1. Accessible surface area (ASA) for Configs. 1-8 for initial docked structures. The ASA for each predicted configuration was calculated using Naccess standalone version. Here, to calculate the accessible area buried between CaM and Akt-PHD, we ran three separate calculations. Once for CaM (chain A), once for PHD (chain B), and a third time for the CaM–PHD (AB) complex. We then subtracted the AB surface from the (A+B) surfaces to obtain the buried surface in the CaM–PHD complex.

CaM–PHD complex	Accessible surface area (Å^2)				
	CaM (chain A)	PHD (chain B)	CaM–PH (A+B)	CaM–PH (AB)	(A+B) - AB
Configs. 1	11129.8	8231.8	19361.6	18039.5	1322.1
Configs. 2	10821.9	8283.0	19104.9	16877.0	2227.9
Configs. 3	10866.1	8385.2	19251.3	17386.8	1864.5
Configs. 4	10845.2	8348.1	19193.3	17578.0	1615.3
Configs. 5	10870.2	8361.3	19231.5	17948.2	1283.3
Configs. 6	10372.9	8459.0	18831.9	17664.2	1167.7
Configs. 7	10447.6	8321.2	18768.8	17686.9	1081.9
Configs. 8	10316.4	8414.1	18730.5	17421.1	1309.4

TABLE C.2 Initial configurations of CaM–PHD complex.

CaM–PHD complex	CaM conformation (PDB)	IP_4 binding to PHD
Configs. 1-5	Extended (1CLL)	Yes
Configs. 6-8	Collapsed (1CDL)	
Configs. 9-13	Extended (1CLL)	No
Configs. 14-16	Collapsed (1CDL)	

TABLE C.3. The decomposition of the binding free energy, ΔG_b, into the enthalpy (ΔH) and entropy ($T\Delta S$) contributions.

CaM–PHD complex	ΔH (kcal/mol)	$T\Delta S$ (kcal/mol)	$\Delta G_b = \Delta H - T\Delta S$ (kcal/mol)
Config. 1	-123.47	66.00	-57.46
Config. 2	-98.89	59.52	-39.37
Config. 3	-96.45	63.01	-33.44
Config. 4	-85.49	61.90	-23.58
Config. 5	-96.785	59.63	-37.14
Config. 6	-48.49	59.32	10.83
Config. 7	-45.57	55.83	10.25
Config. 8	-74.92	58.38	-16.53
Config. 9	-48.64	62.31	13.66
Config. 10	-62.76	54.02	-8.73
Config. 11	-63.96	57.77	-6.192
Config. 12	-110.21	62.75	-47.46
Config. 13	-62.29	57.91	-4.38
Config. 14	-88.97	56.19	-32.77
Config. 15	-62.06	56.27	-5.78
Config. 16	-77.57	57.82	-19.74

TABLE C.4. The types of intermolecular interactions including salt bridge, nonpolar, and H-bond interactions in the CaM–PHD association without IP_4. The atomic residues pairs are interface residues, and the pairs are considered effective and counted if and only if, the residue pairs have at least 50% occurrence rate. To determine these intermolecular interactions - salt bridge, nonpolar, polar, and H-bond interactions we set some criteria using CHARMM scripts. For the salt bridge, we defined the position of both positive and negative charged amino acids (Arg, Lys, Asp and Glu) in CaM and PHD respectively and observe their occurrences in the interface at 4Å distance. Similarly, for the polar and nonpolar interactions, we specified the polar (Ser, Thr, Cys, Asn, Gln, Tyr, and HSD) and nonpolar (Gly, Ala, Leu, Met, Ile, Pro, Trp, and Phe) residues in both CaM and PHD and checked the probability of a pair (polar-polar and nonpolar-nonpolar) occurring in the CaM-PHD interface at 5Å distance. Finally, for the H-bond we set 2.4Å threshold distance for all residues except Arg, Lys, Asp and Glu.

CaM–PHD complex	Salt bridge	Hydrophobic	Polar	H-bond
Config. 1	R74-E85, D58-R67, E114-K14, E114-R25, E120-R25, E123-R23, K77-E85, D2-R76, E84-R76, E120-R23	I9-M63, A73-M63, M124-I19, A128-I19, M144-I19, L112-I84, F92-I84, G113-F55, M71-P68, L4-M63	T5-Q61, T70-T65, Q143-Y18, Q3-Q61	A128-Y18
Config. 2	E84-R86, E114-R23, E127-K20	V55-W80, M71-W80, F92-I19, L105-I19, V108-I19, M109-I19, L112-I19, M124-I19, A147-I84, A88-L52, M51-W80	T5-Q113, S81-N54	M124-Y18
Config. 3	K115-E40, R74-E85, D50-R67, E114-R23, E114-R25, E127-R69, E54-R67, E120-R23, E84-K20	G59-M63, F92-I19, L105-I19, V108-I19, M109-I19, L112-I19, F141-I19, M144-I19, M145-I19, A57-V83, P66-L78, P66-V83, M124-I19, A73-V83, L116-I19, L4-W80, I9-L78, A73-L78, F12-W80, L69-W80, M72-W80, M76-W80	T70-T82	T70-V83
Config. 4	R74-E66, E114-R86, E84-R76, E54-R69, D78-R67	V91-W80, V108-W80, L112-W80, M124-I19, L112-I84, F92-I84, M145-I19, V91-I84, A147-P68	NA	NA
Config. 5	R90-E85, D2-R67, D80-R67, E84-R15, E114-R25, E114-K14, D2-R69, E84-K20, E84-R69	L112-F55, L112-I84, G113-F55, M144-I19, M145-I19, V91-I84	N111-Q79, N111-T82	L112-N53, G113-N54, M124-Y18
Config. 6	D131-R25, D133-K14, D133-R86, E139-R23, E139-K39	G98-A50, A102-W80, A103-W80, V121-W80, I130-G16, G132-G16, G134-F55, I130-I19	Y99-N53, Y99-N54, Q135-N53, Q135-N54, Q135-Q79, Q137-N53, N97-N54	Q135-N54, N137-L52
Config. 7	R106-D3, K94-D46, R126-E117, D133-R48	G96-W80, A102-M1, A103-M1, V121-M1	N97-N54, Y99-N54, Y99-N53, Q135-N54, Y99-S56, N97-S56, Y99-T34, H107-Y38, T110-Q47	NA
Config. 8	D2-R67, E54-K20, D58-R23, D78-R67	L4-P68, L4P70, A57-P24, A73-P68, V55-I19, A57-I19, P66-W22	T70-T21, N53-Y18,	L4-P68, V55-T21, T70-T21

TABLE C.5. The types of intermolecular interactions including salt bridge, nonpolar, and H-bond interactions in the CaM–PHD association with IP_4. The atomic residues pairs are interface residues, and the pairs are considered effective and counted if and only if, the residue pairs have at least 50% occurrence rate. To determine these intermolecular interactions - salt bridge, nonpolar, polar, and H-bond interactions we set some criteria using CHARMM scripts. For the salt bridge, we defined the position of both positive and negative charged amino acids (Arg, Lys, Asp and Glu) in CaM and PHD respectively and observe their occurrences in the interface at 4Å distance. Similarly, for the polar and nonpolar interactions, we specified the polar (Ser, Thr, Cys, Asn, Gln, Tyr, and HSD) and nonpolar (Gly, Ala, Leu, Met, Ile, Pro, Trp, and Phe) residues in both CaM and PHD and checked the probability of a pair (polar-polar and nonpolar-nonpolar) occurring in the CaM-PHD interface at 5Å distance. Finally, for the H-bond we set 2.4Å threshold distance for all residues except Arg, Lys, Asp and Glu.

CaM–PHD complex	Salt bridge	Hydrophobic	Polar	H-bond
Config. 9	NA	A103-V83, I125-W80, A103-W80	H107-T82, T110-Y18, S101-T81, H107-T82	A103-V83
Config. 10	E127-R69, E119-R67, E123-R15, E127-R15, E123-R67, D2-K39	A128-I19, I130-I19, M144-I19, A147-I19	Q143-Y18, Q3-Y38, Q3-Q47, Q143-T21	NA
Config. 11	K115-E40, E114-R25, E114-K39, E127-R69	A88-I19, F92-I19, L116-P24, M124-W22, F141-I19, M144-I19, M145-I19, V91-I19, A147-P68	NA	NA
Config. 12	R106-E115, E45-R86	F92-W80, F141-W80, M145-W80, P43-W80, V108-W80, A46-I19, G113-M1, L112-W80, L112-F55	N42-T82, Q49-Y18, H107-Q59, N111-S56, H107-Q79, N111-Q59, N111-Q79, Y138-T81, N53-Y18, N42-T81, T44-T82, T146-N53, Q49-T21	N111-Q79, N111-S56
Config. 13	K115-E85, D2-K64, E47-R67, E54-R69, D78-R67, E84-R76, E114-K20, E114-R76, E82-R67, E127-R76	L112-M63, G113-L78, M144-M63, M145-M63, M145-I74, A147-P68, A147-I74	S81-T65, N11-Q61, T146-T65	M144-M63, M145-I74, A147-I74, A147-P68??
Config. 14	K21-E116, K94-D32, R90-D3, R90-D46, K94-D	M36-M1, G40-V4, P43-M1, L48-M1, M51-M1, G92-A50, G92-P51, A102-W80, A103-W80, V121-W80, G96-A50, G96-P51, V91-M1, L39-M1	S38-Q113, Q41-S2, N42-S2, H107-S56, N111-S56, T34-Q113, H107-T34, N97-Q47	G40-V4, N42-S2
Config. 15	R86-E85, R90-E85, E87-K20, E47-R23, E87- R15, D80-R67, E83-R67, E84-K20, D80-K20	G96-V83, G96-W80, G40-I19	Q41-Y18, N97-T82, N97-T81, Q41-T21, N111-Y18, H107-Y18	Q41-Y18
Config. 16	K77-E91, E6-R41, D80-R67, D78-R69	L4-W11, I9-W11, A57-I19, P66-P24, L69-W22, A73-W22, A147-P70, L4-P24, P66-W11, L69-P24, L69-W11, A73-P24	Q3-Y26, T70-T21, Q3-T92	Q3-W11, V55-T21, T70-W22, Q3-T92

TABLE C.6 The interaction of Akt with ADP, ATP, and ATP D323H in the model 1

Mode 1	Type of interactions	Interacting residues
ADP	Conventional H-bond	Lys 158, Asn 279, Arg 436
	Van der Waals	Gly 157, Leu 295, Phe 293, Leu 165, Lys 154, Gly 294
	Salt bridge	Arg 436
	Attractive charge	Arg 436
	Metal accepter	$PO4^-$
	Pi-Akyl	Val 164
ATP	Conventional H-bond	Glu 298, Leu 295, Lys 301
	Van der Waals	Tyr 315, Gly 157, Thr 448, Gly 159, Asp 274, Glu 314
	Attractive charge	Lys 276, Lys 297, Lys 301
	Metal accepter	PO4-
	Pi-Akyl	Val 164
	Amide-pi Stacked	Phe 293
	Carbon hydrogen bond	Leu 156
ATP D323H	Conventional H-bond	Arg 69, Arg 15
	Van der Waals	Thr 21, Pro 68, His 89
	Salt bridge	Lys 20, Arg 67
	Attractive charge	Lys 20, Arg 67
	Metal accepter	PO4-
	Carbon hydrogen bond	Trp 22, Lys 20, His 13
	Pi-donor hydrogen bond	His 13

TABLE C.7. The interaction of Akt with ADP, ATP, and ATP D323H in the model 2

Mode 2	Type of interactions	Interacting residues
ADP	Conventional H-bond	Lys 179, Lys 301
	Van der Waals	Met 227, Tyr 229, Glu 234, Ala 304, Thr 312, Lys 138, Cys 296, Gly 159,
	Salt bridge	Lys 276, Lys 310
	Attractive charge	Lys 276, Lys 310
	Metal accepter	Gamma phosphate group
	Pi-Akyl	Ala 177, Leu 156
	Pi-sigma	Val 164,
	Pipi stacked	Phe 293
	Unfavorable acceptor	Glu 278
ATP	Conventional H-bond	Phe 293, Cys 296, Gly 294, Lys 276
	Van der Waals	Leu 156, Gly 159, Leu 295, Lys 158, Cys 310, Gly 311, Glu 278, Glu 314
	Attractive charge	Lys 301, Lys 276
	Metal accepter	Phosphate groups
	Pi-Akyl	Val 164
	Pi-pi stacked	Phe 293
	Amide-pi stacked	Phe 293, Gly 157
	Pi-sulfur	Cys 296
ATP D323H	Van der Waals	Glu 314, Thr 160, Phe 293, Glu 441
	Salt bridge	Lys 276
	Attractive charge	Lys 276
	Metal accepter	Phosphate groups
	Pi-sigma	Gly 159
	Pi-cation	Mg^{2+}
	Unfavorable Acceptor	Glu 278

TABLE C. 8 The interacting interface residue of autoinhibited state of Akt, where the former and latter residues denote residue from the PH domain and kinase domain, respectively for the most populated apo state of model 1 & 2.

Mode	Interacting residues
Model 1 apo cluster 1	K14-D323, K20-D302, R23-E322, E17-R273, Y18-R273, Y18-K297, Y18, L316, Y18-V320
Mode 2 apo cluster 1	K20-D302, R23-D323, K39-E322, R76-D190, R86-D325, K112 -E198, K14-D325, R25-D323, E17-D323, Y18-D323, R23-D323, R25-E332